5-14-2020

Source Apportionment of Ozone and Its Health Effects in North China Plain and Southeast U.S.

Kaiyu Chen

Louisiana State University and Agricultural and Mechanical College

SOURCE APPORTIONMENT OF OZONE AND ITS HEALTH EFFECTS IN NORTH CHINA PLAIN AND SOUTHEAST U.S.

A Dissertation

Submitted to the Graduate Faculty of the
Louisiana State University and
Agricultural and Mechanical College
in partial fulfillment of the
requirements for the degree of
Doctor of Philosophy

in

The Department of Civil and Environmental Engineering

by
Kaiyu Chen
B.S., China University of Mining and Technology, Beijing, 2014
M.S., China University of Mining and Technology, Beijing, 2017
May 2020

ACKNOWLEDGEMENTS

I would like to thank my advisors, Dr. Hongliang Zhang and Xiuping Zhu, for their supports on the projects and guiding me on my academic career. This dissertation would not have been accomplished without their help.

Then, I want to show appreciation to my committee members (in the alphabetic order), Dr. Eurico J D'Sa, Dr. Nina Lam and Dr. John Pardue for providing valuable suggestions on this dissertation.

I also want to express my gratitude to all the instructors I have had courses with. Thanks to my colleagues, my friends, our department and LSU for giving me an unforgettable 3 years' experience in Baton Rouge. Especially, I would like to thank LSU HPC for providing great computational resources for this work. I also want to thank Dr. Feng Chen, who is the LSU IT Consultant, for his help in using LSU HPC resources.

Finally, I want to thank my parents and my families for their support and understanding for my decisions. Their love always accompanies me and inspires me when difficulties come to me. Without their understanding and love, I would never become what I am now.

TABLE OF CONTENTS

ACKNOWLEDGEMENTS ii

LIST OF TABLES v

LIST OF FIGURES vii

LIST OF ABBREVIATIONS x

ABSTRACT xiv

CHAPTER 1. INTRODUCTION 1

CHAPTER 2. OVERVIEW OF OZONE SOURCE APPORTIONMENT TECHNIQUES 8
- 2.1 Introduction 8
- 2.2 DDM 10
- 2.3 BFM 13
- 2.4 OSAT 14
- 2.5 Source-oriented methods 17
- 2.6 O_3 regime schemes 19
- 2.7 O_3 source apportionment in China 20
- 2.8 Conclusions 23

CHAPTER 3. IMPROVING OZONE SIMULATION IN THE NCP 25
- 3.1 Introduction 25
- 3.2 Methods 27
- 3.4 Results and discussions 32
- 3.5 Conclusions 48

CHAPTER 4. OZONE SOURCE APPORTIONMENT IN THE NCP 49
- 4.1 Introduction 49
- 4.2 Methods 51
- 4.3 Results and discussions 55
- 4.4 Conclusions 70

CHAPTER 5. OZONE SOURCE APPORTIONMENT IN SOUTHEAST U.S. 72
- 5.1 Introduction 72
- 5.2 Methods 73
- 5.3 Results and discussions 76
- 5.4 Conclusions 83

CHAPTER 6. OZONE ASSOCIATED HEALTH RISK ANALYSIS 85
6.1 Introduction 85
6.2 Methods 87
6.3 Results and discussions 89
6.4 Conclusions 101

CHAPTER 7. CONCLUSIONS 103

REFERENCES 108

VITA 124

LIST OF TABLES

1. Summarization of studies using DDM in O_3 source apportionment......................................11

2. Summarization of studies using BFM in O_3 source apportionment.......................................13

3. Summarization of studies using OSAT in O_3 source apportionment.....................................16

4. Summary of studies using 2R scheme in O_3 source apportionment 19

5. Scaling factors for VOCs emissions in NCP 29

6. Scaling factor for NO_x emissions in NCP 30

7. NO_x emission from each source for different inventory in NCP 2017 summer. 31

8. VOCs emission from each source for different inventory in 2017 summer. 31

9. Summertime model performances of meteorological conditions in NCP for temperature (T), wind speed (WS), wind direction (WD) and relative humidity (RH). 32

10. Model performances in 11 major cities in NCP for 8h-O_3 simulation using EDGAR+ (E) and MEIC (M). Units are ppb for OBS and PRE. Bold represents the statistical result exceeds criteria...33

11. Summertime 8h-O_3 contribution from background and emissions. Units are ppb. 68

12. 8h-O_3 concentration and its contribution from background and emissions in peak episodes. Units are ppb..68

13. Scaling factor for NO_x emissions for major states in SUS. 74

14. Scaling factor for VOCs emissions for major states in SUS 74

15. Model performances in 9 states in SUS for 8h-O_3 simulation. Units are ppb for OBS and PRE. Bold represents the statistical result exceeds criteria. 78

16. Provincial health risk analysis results within the NCP. Units for health endpoints are cases. 89

17. Provincial health risk analysis results within the NCP. Units for health endpoints are cases. 92

8. Comparison of health outcome with previous studies 95

19. Incidence of mortality of respiratory (RDM) and cardiovascular (CDM) diseases. Units are cases per 100,000 people. 101

LIST OF FIGURES

1. Simulation domains. Coarse domain (36km by 36km) covers mainland China and part of surrounding countries. NCP (d02) is included as the finer domain (12km by 12km). 28

2. Averaged NO_x and VOCs emission rates from MEIC and EDGAR+ and their differences (subtracting EDGAR+ by MEIC) in summer 2017. Units are tons/month. 31

3. Model performance statistics on average daily 8h-O_3 concentration. Summertime average concentration (top), MFB, MFE, NME and NMB for 11 major cities are shown. Red lines represent suggested criteria by US EPA for each index...35

4. Average daily 8h-O_3 concentration in major cities. Results from EDGAR+ (E) and MEIC (M),observation (Obs) and statistical results (NMB) are shown in each row. Units for O_3 concentrations are ppb..37

5. Diurnal variations of 8h-O_3 from EDGAR+, MEIC and observation (Obs), temperature (T) and relative humidity (RH) in major cities, Units for O_3 concentration are ppb, for T are ˚C, for RH are %. 39

6. 8h-O_3 concentrations in NCP for 2017 summer predicted by EDGAR+ and MEIC, and their differences (subtracting EDGAR+ by MEIC). Units are ppb. 41

7. Hourly 8h-O_3 concentration at major cities for peak episodes. Units are ppb. 43

8. Spatial distribution of 8h-O_3 concentrations in 3 peak concentration episodes predicted by EDGAR+ and MEIC, and their differences (subtracting EDGAR+ by MEIC). Units are ppb. ...45

9. Meteorological conditions in NCP during 3 peak episodes. T represents temperature, RH represents relative humidity, WS represents wind speed, red arrows in the third row represent wind direction, arrow length represents wind speed. 46

10. Averaged sources of NO_x emissions in NCP 2017 summer. Units are tons/month................52

11. Averaged sources of VOCs emissions in NCP 2017 summer. Units are tons/month. 52

12. Simulation domains and regional classifications for emissions. Coarse domain (36km by 36km) covers mainland China and part of surrounding countries. NCP (d02) is included as the finer domain (12km by 12km). 55

13. Summertime 8h-O_3 concentration in China and their contribution from background (BG) and emissions (EM). Units are ppb. 56

14. Summer 8h-O_3 contribution from regional emission sources in China. Units are ppb. 57

15. Summer 8h-O_3 contribution from sectoral emission sources in China. Units are ppb...........57

16. Summertime 8h-O_3 concentration in NCP and their contribution from background (BG) and emissions (EM). Units are ppb. 58

17. Summertime 8h-O_3 contribution from sectoral emissions in NCP. Units are ppb. 59

18. Summertime 8h-O_3 contribution from regional emissions in NCP. Units are ppb. 60

19. summer 8h-O_3 contribution from NO_x (8h-O_3N) and VOCs (8h-O_3V) in NCP. Units are ppb. 61

20. Summertime NO_x and VOCs regional contributions to 8h-O_3 concentration. Units are ppb..62

21. Summertime NO_x and VOCs sectoral contributions to 8h-O_3 concentration. Units are ppb. .64

22. 8h-O_3 contributions from NO_x (O_3N), VOCs (O_3V) and background (O_3-BG) in the 3R scenario (first row) and differences with 2R, NO_x-limited and VOC-limited scenarios (subtracting 3R by the results from each case). Units are ppb. 65

23. 8h-O_3 contributions from sectoral emissions in major city in summertime (left column) and peak episodes (right column). Units are ppb. 69

24. 8h-O_3 contributions from regional emissions in major city in summertime (left column) and peak episodes (right column). Units are ppb. 70

25. Domain setting of SUS. Outer domain represents parent domain (36km by 36km) covered the United State except Alaska, Hawaii etc. Nested 12km by 12km domain (d02) cover SUS in this study. 76

26. Summertime 8h-O_3 concentration in U.S. and its contribution from background (BG) and emissions (EM). Units are ppb. 77

27. Summertime 8h-O_3 concentration in SUS and its contribution from background (BG) and emissions (EM). Units are ppm. 78

28. 8h-O_3 contributions from emissions of NO_x and VOCs. Units are ppb. 79

29. 8h-O_3 contributions from emission sectors. Units are ppb. 80

30. Summertime NO_x and VOCs contributions to 8h-O_3 by sectors. Units are ppb. 81

31. Summertime average monthly emissions of NO_x and VOCs and contribution from anthropogenic sources in SUS. Units are tons/month. 82

32. Health end point results of five O_3-associated diseases. Total shows the total mortality due to O_3-related diseases including RDM, CDM COPD, IHD and STK. Units are cases/grid. 93

33. Difference of health endpoints between EDGAR+ and MEIC (subtracting EDGAR+ by MEIC). Units are cases/grid. 94

34. Spatial contributions from NO_x and VOCs emissions to premature mortality. Units are cases/grid cell...97

35. Regional (left) and sectoral (right) emission contribution ratios to total premature mortality. 97

36. Spatial contribution of health impacts from regional (left) and sectoral (right) emission sources. Units are cases/grid cell. 98

37. O_3-related health risk in SUS. First row represents the estimated premature mortality, bottom row refers to the estimated impacts cases for ER visits and HA. Units are cases/grid. 99

38. All-cause mortality contributions from BG and emission sources. Right panel shows the contribution of emission related impacts from emission sources. 100

39. Population in SUS (left) and NCP (right). Population data are both for 2015. 101

LIST OF ABBREVIATIONS

AERO6	Aerosol module version 6
AQI	Air Quality index
AQM	Air Quality Models
BC	Boundary conditions
BenMAP	Benefits Mapping and Analysis Program
BFM	Brute force method
BTH	Beijing-Tianjin-Hebei region
BVOC	Biogenic VOCs
CAMx	Comprehensive Air Quality Models with Extensions
CDM	Cardiovascular diseases mortality
CIESIN	Center for International Earth Science Information Network
CMAQ	Community Multi-scale Air Quality models
CNEMC	China National Environmental Monitoring Center
COPD	Chronic obstructive pulmonary diseases
CRF	Concentration response function
CTMs	Chemical transport models
DDM	Decoupled Direct Method

EDGAR	Emission Database for Global Atmospheric Research
EPA	Environmental Protect Agency
ER	Emergency room
FINN	Fire INventory from NCAR
GE	Gross error
GEOS-Chem	Goddard Earth Observing System chemical transport model
HA	Hospital admission
HDDM	High-order DDM
IC	Initial condition
IHD	Ischemic heart disease
MB	Mean Bias
MCIP	Meteorology-Chemistry Interface Processor
MEGAN	Model for Emissions of Gases and Aerosols from Nature
MEIC	Multi-resolution Emission Inventory for China
MFB	Mean fractional bias
MFE	Mean fractional error
NAQPMS	Nested Air Quality Prediction Modeling System
NCAR	National Center for Atmospheric Research

NCL	NCAR Command Language
NCP	North China Plain
NMB	Normalized mean bias
NME	Normalized mean error
NO_x	Nitrogen oxides
O_3	Ozone
O_3N	NO_x-related O_3
O_3V	VOCs-related O_3
O_3-BG	O_3 from background
O_3-EM	O_3 from emissions
OMI	Ozone monitoring Instrument
OSAT	Ozone source apportionment technology
PRD	Pearl River Delta
REAS	Regional Emission Inventory in ASia
REAM	Regional Chemical Transport Model
RH	Relative humidity
RDM	Respiratory diseases mortality
RMSE	Root mean squared error

RR	Relative risk
SUS	Southeast U.S.
STK	Strokes, including both ischemic and hemorrhagic strokes
T	Temperature
VOCs	Volatile organic compounds
WD	Wind direction
WHO	World Health Organization
WRF	Weather Research and Forecasting model
WPS	WRF Preprocessing System
WS	Wind speed
YRD	Yellow River Delta
8h-O3	Maximum daily 8 hourly O_3
2R	O_3 two regime scheme
3R	O_3 three regime scheme

ABSTRACT

Ground-level ozone (O_3), as one of six common air pollutants set by National Ambient Air Quality Standards from the U.S. Environmental Protection Agency (EPA), is of great interest due to its health and economical effects. However, O_3 contributions from different emission sources are not well understood due to its complicated nonlinear reactions. In this study, O_3 source apportionment methods and the applications are firstly reviewed to provide a comprehensive understanding for O_3 formations. Application of High-order Decoupled Direct Method (HDDM), brute force method (BFM), O_3 source apportionment technology (OSAT) and source-oriented method in O_3 simulations are discussed in detail. And applications of different O_3 regime schemes are compared with each other. Improved three regime scheme (3R) has better performance in tracking O_3 contributions from its precursors. Then, the Community Multi-scale Air Quality (CMAQ) model is applied to predict O_3 concentrations in NCP with meteorological conditions generated by the Weather Research and Forecasting (WRF) model. Model performance from using anthropogenic emissions from the updated Emissions Database for Global Atmospheric Research (EDGAR+) and the Multi-resolution Emission Inventory for China (MEIC) are validated. The statistical analysis reveals a better performance from EDGAR+. The source-oriented simulation with 3R technique indicates that NO_x emissions dominate in most regions while contributions from VOCs are higher in megacities than in other regions in NCP. Industry, on-road and energy emissions are major sources, which account for ~75% of total emission-related O_3 formation. Emissions from local and surrounding regions are the main O_3 contributors and emissions from central China and YRD have strong impacts in peak episodes. O_3 simulation and source apportionment in SUS reveal that NO_x emissions from on-road, energy dominate the emission-related O_3 while VOCs emissions have less contribution except those from biogenic sectors. Health risk analysis indicates that more

than 0.11 million premature mortalities are associated with O_3 level in NCP due to respiratory (0.04-0.05 million) and cardiovascular (0.07-0.06 million) diseases. A total of 0.03 all-cause premature mortality is estimated for SUS with ~4.6 and ~7.9 thousand from respiratory and cardiovascular diseases, respectively.

CHAPTER 1. INTRODUCTION

Tropospheric ozone (O_3), as one of the six common air pollutants identified in the Clean Air Act (CAA), is associated with adverse impacts on air quality, public health and ecosystem. It is mostly referred to severe air pollution, mortality and life year lost from respiratory and cardiovascular diseases, changes of vegetation and crop yield, and impacts on climate and land surface changes [1-8]. In 2015, the U.S. Environmental Protection Agency (EPA) revised the O_3 standard to 70 parts per billion (ppb), and they declared that area meeting with the standard is classified as "attainment" area [9]. Increasing number of days with harmful observations (concentration is higher than threshold of 70 ppb) is reported for both China and the U.S. [10-12]. O_3 in the air that people breath in can cause muscle constriction in airways and lead to breathing difficulties when the concentration reaches an unhealthy level. Old people, children and people with asthma are at high risk of suffering O_3-related diseases. O_3 also attacks sensitive vegetation, causes reduction of photosynthesis and slows plant growth. As a result, vegetation functions are decreased, and the ecological diversity is lost. Both China and U.S. are facing severe O_3-related issues. Around 4,700 O_3-related mortalities and 36,000 life years lost were reported to be associated with O_3 concentrations in U.S. in 2015 [13]. In the same year, around 55,341 to 80,280 mortalities were estimated due to chronic obstructive pulmonary disease (COPD) in China, and the cumulative population exposed to high maximum eight-hour average O_3 (8h-O_3) concentrations (>100 $\mu g/m^3$) was estimated to be 816.04 million [14]. O_3 level in 2000 induced 6.4%-14.9% yield loss of food crop, and estimated O_3 concentration in 2020 would cause 47.4 million metric tons losses of four grain crop production in China [15].

With increasing attention paid on this specific pollutant, O_3 is intensively monitored in different countries and observational data have shown its temporal and spatial variations. An averaged increase rate of 1.13 ± 0.01 ppb/year of 8h-O_3 was observed in north of eastern China from 2003 to 2015, and total O_3 variations were due to short-term (36.4%), seasonal (57.6%) and long-term (2.2%) changes[16]. Significant increases that averaged 1.7 ppb/year in June and 2.1 ppb/year in July to August during 2003-2015[17] were also observed in Mt. Tai (China). O_3 concentration were also reported exceeding the ambient air quality standard by 100%-200% in major urban centers over China [12]. On the other hand, the U.S. has ineligible O_3 issue as well. Though significant decreases of O_3 were observed in 83% (summer) and 43 % (spring) of monitoring sites in eastern U.S., increases of springtime O_3 were observed in 50% sites in western U.S. Increases of springtime O_3 were also observed in western U.S. rural sites by 0.2-0.5 ppb/year while decreases of 8h-O_3 were revealed in summertime [18, 19]. Generally, China is experiencing increasing O_3 episodes, while the U.S. is experiencing complex seasonally and temporally O_3 variations. Observation data offers information to understand historical trend of local O_3 variations, but that information is limited within certain geographical range.

Chemical transport models (CTMs) are essential tools for O_3 simulation and predict O_3 production and destruction involving the chemical and physical dynamic processes in the atmosphere with commonly used chemical mechanisms, such as Carbon Bond and SAPRC [20, 21]. CTMs are widely applied in investigating O_3 variations and their responses to changes of climate conditions and emissions. For example, Li, et al. [22] analyzed the chemical productions and transport impacts on diurnal O_3 behavior in Mt. Tai (China) in June 2006 by applying the Nested Air Quality Prediction Modeling System (NAQPMS) that indicated that around 60 ppb and 25 ppb afternoon-maximum concentrations were due to regional transport and chemistry production,

respectively. Yang, et al. [23] applied a global 3D Goddard Earth Observing System chemical transport model (GEOS-Chem) by investigating O_3 variations under changes of sulfate and nitrate. It was observed that O_3 increased in most eastern China in winter, spring and fall when it was dominated by impacts of sulfate while it decreased in summer since nitrate formation played a leading role. Hu, et al. [24] applied the Regional Atmospheric Modeling System-Community Multiple Air Quality (RAMS-CMAQ) model to simulate tropospheric O_3 in the North China Plain (NCP) for summer 2015 and found emissions from Shandong and Hebei attributed largest to not only the highest local O_3 concentration but also to Beijing and Tianjin. The Community Multi-scale Air Quality model (CMAQ) was also used to estimate O_3 response to reduction of anthropogenic emissions in Eastern U.S.. Around 10 to 15 less exceeding days are estimated in Washington, DC as the result of emission reductions since 2002 [25]. A regional model (CAMs) nested in GEOS-Chem was applied in estimating background O_3 variations in North America and the U.S., and the results indicated an increasing trend of background O_3 in western and southwestern U.S which is associated with rising emissions in Asia and Mexico from past 5 decades[26].

O_3 is a secondary pollutant formed by photochemical reactions of nitrogen oxides (NO_x) and volatile organic compounds (VOCs). The photolysis of NO_2 provides atomic oxygen in forming O_3, while VOCs oxidation provides peroxy radicals which helps to convert NO to NO_2. Thus, the relative abundances of NO_x and VOCs would greatly affect O_3 formation. Based on the sensitivity of O_3 to NO_x and VOCs changes, O_3 formation would be classified as NO_x- or VOCs-limited and switch from each other spatiotemporally [27, 28]. For example, O_3 formation in boundary layer in Beijing was proved to be limited by VOCs in haze day while both NO_x and VOCs limited O_3 photochemical productions in clean days [29]. An analysis indicated that Boston, Pittsburgh,

Philadelphia and Washington, D.C were under NO_x-limited condition while New York city was in VOCs-limited regime [30]. When it is decided as NO_x- or VOCs- limited, O_3 formation is regarded only sensitive to single precursor, however, limiting condition is changing all the time.

Source apportionment of O_3 is very important for designing control strategies, but it is very challenging since O_3 formation is highly sensitive to its precursors. To better understand O_3 source apportionment, multiple methods were applied to the air quality model to simulate O_3 contribution from its sources. O_3 contributions from neither NO_x or VOCs have been studied separately by applying High-order Decoupled Direct Method (HDDM), which calculates the sensitivities to perturbations in emissions [31]. Brute force method (BFM) is another approach to investigate O_3 contribution from specific source by zeroing emissions from a single source [32]. Besides, O_3 Source Apportionment Technology (OSAT) uses non-reactive tagged tracers in transport and reaction processes to track O_3 sources by splitting the concentration changes based on emission ratios [33]. Source-oriented methods use reactive-tracers in all chemical and transport processes, it serve as an advanced technique in O_3 source apportionment analysis [34-36]. O_3 formation is strongly sensitive to concentrations of precursors, and its source contributions are varied spatiotemporally, thus improved source apportionment technique is necessary for more accurate results. **The first objective of this study is to** overview source apportionment/sensitivity methods including source-oriented methods, OSAT, HDDM and BFM. An overview of current research related to O_3 source apportionment in China will also be conducted to provide a clearer understanding of current O_3 levels and its sources in China. This objective also includes solid evidence to support further studies for better O_3 simulation and source apportionment in China.

CTMs were very useful for understanding O_3, but the accuracy was highly dependent on emission inventories. Several emission inventories covering China and surrounding regions are

available for different simulation purposes[37, 38]. Inventories from regional to continental scales, for different pollutant species and emission sectors [39-43 32] were created and were successfully applied in O_3 simulation. Widely used inventories such as Emission Database for Global Atmospheric Research (EDGAR), Multi-resolution Emission Inventory for China (MEIC), MIX, Regional Emission inventory in ASia (REAS) help to analyze air quality in China[44-49]. However, to a large extent, these inventories are not entirely bottom-up, and they have been created for multiple purposes for simulation, which leads to large uncertainties in simulation results [50]. EDGAR and MEIC are two most widely used inventories in O_3 simulation in China, while their performances in O_3 simulation vary in years and regions [41, 51]. **The second objective of this study is to** validate model performance based on EDGAR and MEIC. Evaluating and improving their performance in O_3 prediction would provide convincing results for a deeper understanding of O_3 formation, health risks, and design of controlling strategies. This objective also supports the next objective in O_3 source apportionment.

Source apportionment of O_3 is very important to quantify source contributions and to design control strategies, but complex nonlinear reactions of O_3 precursors make it a challenge for model simulation. To determine O_3 contribution from NO_x and VOCs, ratios of photochemical chain reaction production rates, which are widely known as regime indicators, are introduced to classify O_3 contribution. Traditional two regime (2R) approach was implemented in the CMAQ model [52] by applying indicator production ratio of H_2O_2/HNO_3 with correlation coefficients ranging from 0.58 to 0.99. An improved method that applied production ratio indicator of $(H_2O_2+ROOH)/HNO_3$ in three regime scheme (3R) was introduced into CMAQ [53] and compared with traditional 2R method; results indicated higher contributions from NO_x in high O_3 concentration regions in China by 5 to 15 ppb. Results also varied when using different source

apportionment methods. **The third objective of this study is to** use improved source-oriented version of CMAQ for O_3 source apportionment in NCP. O_3 precursors from different emission sources will be tagged as tracers to quantify source contributions during study period. Regional source apportionment will also be conducted in this study to provide evidence for regional transport and their contributions.

O_3 variations are very complicated in the U.S. It was observed that surface O_3 decreased by 6-10 ppb/decade in rural sites based on hourly O_3 mixing ratios from 1989-2007 in eastern U.S.[54]. Though O_3 concentration decreased in eastern U.S. in past decades, an increasing number of days that 8h-O_3 level that were higher than the threshold was also observed in part of the U.S.[55]. O_3 concentration increased by 0.26 ppb/year in western U.S. based on observation data from 1987 to 2004, and springtime O_3 concentrations were increasing since late 1970s. O_3 mixing ratios during 1995-2008 were analyzed and observed to increase; it was reported that the increases of mixing ratios were heavily influenced by direct transport from Asia [56]. O_3 impacts from emission sources, transport and forming processes and climate conditions were also briefly studied by applying CTMs such as Regional Chemical Transport Model (REAM), GEOS-Chem and CMAQ [57-63]. Although there are many studies on the U.S., there is no study that comprehensively explain O_3 contribution from each source in SUS. **The fourth objective of this study is to** apply similar models mentioned in previous objectives to simulate O_3 level and its source apportionment in SUS. O_3 simulation and source apportionment results in SUS will help to understand O_3 spatiotemporal variation patterns, sources of O_3 formation and impact factors under complex climate conditions in this region. Comparison between regions from developed country (SUS) and developing country (NCP) will provides information for differences between these regions.

Human health impacts under certain O_3 level are highly concerned. Short-term exposure to daily 1-hour maximum O_3, 8h-O_3, daily and daytime averaged O_3 were all shown to correspond to increase of non-accidental mortality [64]. Around 70800 premature mortalities were reported through 339 cities in China based on hourly O_3 for the year 2015 [65]. Urbanization also induced increases of O_3, which resulted in 1,100 O_3-associated premature mortality in the Pearl River Delta (PRD) [66]. It was estimated that ~200,000 premature respiratory mortalities in China were associated with long-term exposure while only ~34,000 were estimated in the U.S. [67]. It was shown that mortality of COPD, congestive heart failure and lung cancer increased by 1.03 (± 0.02) due to long-term exposure to O_3 in U.S. based on data recorded from 2000-2008 [68]. However, less studies focused on this topic in NCP and SUS. Thus, more studies are needed for a comprehensive understanding of the health effects and related sources in these regions [69]. **The last objective of this study is to** estimate health risk under simulated O_3 level in NCP and SUS. Premature mortality due to respiratory and cardiovascular diseases will be estimated. Attributions from each emission sources will be also estimated.

With objectives listed above, this study aims to provide a comprehensive understanding of formation, source attribution and health effects of O_3 in NCP and SUS, which would offer information for designing efficient O_3 controlling strategies.

CHAPTER 2. OVERVIEW OF OZONE SOURCE APPORTIONMENT TECHNIQUES

2.1 Introduction

To evaluate and quantify the impacts of emission sources, source apportionment provides spatial and temporal assessments especially in the field of atmospheric science. There is no existing technique that can directly distinguish O_3 contribution from its sources by using observation data. It is a challenge for scientists to figure out a reliable method to analyze and quantify the sources of O_3. Rapid development of computational resources supports the calculations in full-scale CTMs by combining physical and chemical processes in the atmosphere. It also helps to extend the air quality models (AQM) to further simulate the impacts from sources. This advanced technique is widely used in air quality analysis and applied to estimate O_3 contributions from its precursor sources.

Source analysis technique has been applied to estimate air pollution and in support for improving assessments for air pollutions and controlling strategies since 1960s [70, 71]. To track air pollutants contribution from specific source, the principal component analysis and the factor analysis methods were initially applied in early studies for aromatic hydrocarbon content and particle compositions[72, 73]. Following efforts focused on improving the atmospheric mass-balance model introduced by Miller, et al. [74] and Winchester and Nifong [75]. Though there were some limitations initially, termed effective variance least squares helped to solve problems[76]. Consequently, many source analysis methods were developed in the following years. Sensitive equations and decoupled direct method (DDM) were recruited as the sensitivity analysis technique in air quality models since 1976 [77] and 1981[78]. O_3 source apportionment technology (OSAT) is an

advanced technique which quantitatively apportions the O_3 pollution concentration at a user specific location and time to emission sources by adding non-reactive tracers. This technique was also compiled into AQMs to measure source contributions [79]. The simplest technique called brute force method (BFM) measures source contributions by conducting simulations with and without given source emissions. An advanced approach, called source-oriented approach, tracks tagged species in emission sources in air quality models, that allows sources contribution to be easily calculated. The above approaches are the most commonly used current techniques in O_3 source apportionment; however, these usually investigate O_3 and its contribution from precursors in high O_3 pollution region.

Source apportionment methods are widely used in distinguishing and quantifying source contributions to O_3. But their abilities and performances are varied since they estimate the contribution in different ways. A comparison of OSAT and DDM indicated that they had a similar agreement of major contributor of O_3 productions in Lake Michigan but OSAT predicted greater relative importance to anthropogenic emissions and boundary concentrations than DDM did[80]. Comparison between OSAT and BFM also declared the similarity of these methods with correlation coefficients ranging from 0.58 to 0.99, but results also indicated that OSAT had a high sensitivity to secondary reactions than BFM[81]. OSAT and DDM agreed well on the top 10 contributors to O_3 formation in eastern U.S. but OSAT indicated more contributions from anthropogenic emissions but results from DDM shown a higher contribution from biogenic emissions. And OSAT predicted more NO_x-limited regions which were classified as VOCs-limited in DDM [82]. It is also pointed out that OSAT has a better performance in studying source contributions while BFM prefers to reveal the response of changes of emission[83]. These methods are commonly used in O_3 simulations in China since increasing attention were paid to its severe

O_3 pollution. To fully understand source apportionment to O_3 formation, this work examines four main source apportionment methods including DDM, BFM, OSAT and source-oriented methods and their applications in China.

2.2 DDM

DDM, a direct investigation method, is applied in air quality models to calculate the sensitivity coefficient to emission sources. DDM was initially developed in order to solve time-dependent and non-stiff air pollution issues though chemical and meteorological models since 1980s [84]. Finite-difference approximations were employed in DDM to estimating two or more sensitivity coefficients simultaneously in linear, nonlinear and 3D-CTMs within simulations [85]. Hakami, et al. [86] applied DDM to estimate second- and third-order sensitivity coefficients, which is called higher-order decoupled direct method (HDDM). DDM and HDDM calculate sensitivity coefficients following same functions. The outputs in target space and time period indicate the relationship between pollutant concentrations and perturbations from user specific interests. Following equations give a clear understanding to how HDDM works in air quality models. Advantages of HDDM includes conceptually simpler, higher accurate in calculating first-order sensitivities, and less array storage and lower program computing resources compared to other direct methods.

Equation 1:

$$C_j(x,t) = C_0(x,t) + \Delta\varepsilon_j s_j(1)(x,t) + 0.5\left(\Delta\varepsilon_j(2)s_j(2)(x,t)\right) + H$$

Equation 2 :

$$S_j(x,t) = \delta C_j(x,t)/\delta\varepsilon_j(x,t)$$

Equation 1 and Equation 2 show the basic processes to estimate sensitivity coefficient (S). The C_j in Equation 1: represents concentration of pollutant under perturbation of j in space x and time step of t. C_0 represent the base concentration (unperturbed) in same space and time. S_j represents the sensitivity coefficient of pollutant j in space of x and time of t. $\Delta\varepsilon_j$ is the fractional perturbation of parameter j. $s_j(1)$, $\varepsilon_j(2)$ and $s_j(2)$ represent first and second order sensitivity coefficients, which can be calculated by Equation 2. H in Equation 1: represents higher order terms.

Due to its ability in sensitivity analysis, DDM is employed in air quality models to estimated O_3 and its impact factors. For example, DDM-3D was coupled with CIT (California/Carnegie Institute of Technology) airshed model and indicated that uncertainty of reaction rate constants have significant impacts on O_3 levels in Los Angeles; the results also suggested that uncertainty of O_3 prediction depends highly on uncertainty of HNO_3 formation rate constants. Jeon, et al. [87] applied CMAQ model with DDM-3D technique and found that high O_3 concentration in rural area of Chungcheong in the air mass from Seoul was very sensitive to NO_x mainly due to the contribution from VOCs emissions from biogenic sector. Following table summarizes O_3 source apportionment simulations in recent decades applying DDM.

Table 1. Summarization of studies using DDM in O_3 source apportionment.

Model/methods	Study field	Study period	Studied sources	References
CMAQ/DDM	Chungcheong, Korea	Summer in 2009 and 2011	Emissions of NO_x and BVOCs	87
CIT/DDM	California, U.S.	Aug. 1987	Gas phase reaction rates	88
CMAQ/DDM	Texas, U.S.	Aug. and Sep. in 2005	Emissions of NO_x and VOCs	89
CAMx/DDM	Houston, Texas, U.S.	Jun. 2005	Emissions of NO_x and VOCs	90
CIT/DDM	Mexico–U.S. border	July 1993	Emissions of NO_x and VOCs	91

(Table cont'd)

Model/methods	Study field	Study period	Studied sources	References
CMAQ/DDM	The U.S.	Jan. and Jul. in 2011	O_3 and HCHO precursors	[92]
CMAQ/DDM	Central California, U.S.	July in 2007	OH productions	[93]
CMAQ/DDM	Southeastern U.S.	Aug. 2000	Emissions of NO_x and VOCs	[94]
CAMx/DDM	The U.S.	2006	Anthropogenic emissions of NO_x and VOCs	[95]
CMAQ/DDM	Eastern U.S.	2001–2002 and 2011–2012,	Mobile and EGU emission sources of NO_x and VOCs	[96]
CMAQ/DDM	Atlanta, U.S.	2001	Mobile and EGU emission sources of NO_x and VOCs	[97]
CMAQ/DDM	Texas, U.S.	August to September 2006	Emissions of NO_x	[98]
CAMx/DDM	Continental U.S. and eastern U.S.	July 2030	Emissions of NO_2	[99]
CMAQ/HDDM	East Asia	2007	Emissions of NO_x and VOC	[100]
MAQSIP/DDM	Central California, U.S.	August 1990	31 organic compounds and CO	[101]
CAMx/HDDM	Texas, U.S.	June 2005	Emissions of NO_x and VOCs	[90]
CMAQ/DDM	PRD, China	October 2004	Emissions of NO_x and VOCs	[102]

From Table 1, DDM is widely recruited in source apportionment studies especially applied in CMAQ. The goals of most studies are to assess the relationship between O_3 formation and emissions of NO_x and VOCs. However, DDM has its limitations in analyzing sensitivities to secondary air pollutions such as O_3; even HDDM has limitations in investigating source contributions through nonlinear reactions. Its ability in simulating O_3 source apportionment was studied in 2002 [79] and indicated that DDM can only explain 70% of O_3 concentration through first-order reactions; however, great uncertainties remained for the O_3 contributions from higher order reactions. In addition, DDM also takes more simulation resources compared to OSAT if it considers higher order reactions. It is concluded that DDM, as a first order prefer technique, is commonly regarded as source sensitive technique, and may not provide accurate results in O_3 source analysis study.

2.3 BFM

CMAQ model and the Comprehensive Air Quality Model with Extensions (CAMx) employed brute force method (BFM) to estimated single source contribution to air pollution [32, 103]. BFM is processed by comparing base simulation with control case. Emissions are remained unchanged in base case while the target emission is removed in control case. The differences between cases indicate the impacts from target sources. BFM is conceptually accurate for linear chemistry and small emission changes. It also directly relates to impacts from emissions controlling measures and also investigates indirect effects such as oxidant-limiting effects[104]. Besides, BFM has strong ability in investigating the development of emission reduction scenarios, thus it is used in air dispersion modeling [105]. Though BFM is widely applied in air quality models, most of these studies aim to analyze pollutants such as particulate matter instead of secondary air pollutants. There are limited studies applying BFM as O_3 source apportionment method since it will miss information from secondary reactions after interested emissions are removed. A brief summary of studies applied BFM in O_3 source apportionment is listed in Table 2.

Table 2. Summarization of studies using BFM in O_3 source apportionment

Models	Study field	Study period	Studied sources	Reference
NAQPMS	Beijing, China	August 2006	NO_x and NMVOC	106
CAMx	BTH region, China	Summer 2007	NO_x and VOCs	107
CAMx	Mexico City Metropolitan Area (MCMA)	1991 to 2006	CO, NO_x and VOCS	108
CMAQ	California, U.S.	Summer 2007	NO_x and VOCs	32
CAMx	The U.S.	May-September 2011	BVOC	109
CMAQ	The U.S.	June and April 2011	Emissions from wildfires and prescribed fire	110

(Table cont'd)

Models	Study field	Study period	Studied sources	Reference
CMAQ	Western U.S.	April–October 2007	Background O_3	111
STEM-2K1/ MM5	Guangdong province, China	March 2001	Emissions from power plant, transport and industry	112
CMAQ	Southern California, U.S.	July 2005	Seven emission sources	113

BFM is not a truly source apportionment technique, it is widely called as source sensitive method. BFM is not a priority choice in O_3 source apportionment study since its limitations result in unrealistic and undesired changes to source contributions. This method is mainly used in predicting results from changes of O_3 sources, especially in evaluating impacts from emission controlling strategies and climate change[110]. Most studies listed in Table 2 compared the results from BFM and other source apportionment methods to provides overall source contributions. Besides, this method requires large amount of computational resources to process analysis for multiple contributors.

2.4 OSAT

An additional function is needed in photochemical grid models in simulating O_3 formation and presenting source contribution without changing the predictions of total O_3 formation, thus the OSAT was designed in 1995 and first released in CAMx in 1996 to fulfill this purpose [114]. OSAT generates tracer species in O_3 precursors (NO_x and VOCs), which allow CAMx to predicts their contributions to O_3 formation simultaneously with O_3 predictions. Four tracers are introduced to represents the proportion of precursors contributions to O_3 formation. Emission tracers from NO_x and VOCs are grouped as the tracer families which are represented as N_i and V_i for source group i for each grid cell in model as shown in equation 1 and 2. Movement of traces would be tracked thus to apportion NO_x and VOCs emissions. O_3 productions are predicted at given time step and

locations in models, tracer families (O_3N_i and O_3V_i in Equation 3 and Equation 4) are generated simultaneously to estimate the proportion of O_3 formation to emissions of NO_x and VOCs under certain O_3 regime scheme.

Equation 3 :

$$\sum_{i=1}^{I} N_i = NO_i + NO_{2_i}, \text{ i=1, 2, 3…, I}$$

Equation 4 :

$$\sum_{i=1}^{I} V_i = VOCs_i, \text{ i=1, 2, 3…, I}$$

Equation 5 :

$$\sum_{i=1}^{I} O_3N_i + O_3V_i = O_{3_i}, \text{ i=1, 2, 3…, I}$$

OSAT is improved to advanced version to increase accuracy in calculating O_3 contributions from its sources by considering the feedbacks of reactions in O_3 production and destruction. Tagged atomic oxygen in predicted net O_3 production are traced in deforming process, and O_3 destruction rate due to reactions with species such as HO_x (OH and HO_2) helps to quantify the potential O_3 reformation. Such improvements were released in 2005 known as OSAT2 with updated version of CAMx [115]. A subsequent improvement (OSAT3) was released in 2015 along with CAMx version of 6.3. The odd oxygen in chemical reactions of O_3 reforming processes is tagged with associated source groups, thus regenerated O_3, NO and NO_2 are evaluated. As results, predicted O_3N and O_3V contain information of O_3 reforming, and the accuracy of O_3 source apportionment is improved. This technique is commonly used in recent O_3 source analysis, summary of recent studies applying OSAT is listed in Table 3.

Table 3. Summarization of studies using OSAT in O_3 source apportionment.

Model	Study field	Study period	Studied sources	Reference
MM5	PRD, China	Jul. and Nov. 2006	Local emissions	116
CAMx	Beijing, China	Jul. 2000	Regional emissions	117
CAMx	The U.S.	May. to Sep. 2011	BVOCs emissions	118
CAMx/CMAQ	The U.S.	2018/2030	Emissions and background O_3	83
MM5	Hong Kong and PRD, China	2006	Regional emission sources	119
CAMx	The U.S.	2011	Tropospheric and stratospheric O_3 contributions	120
CAMx	YRD, China	2013	Regional emissions and long-range transport	121
CAMx	Continental North America	2008	Tropospheric and stratospheric O_3 contributions	122
GEOS-Chem/CAMx	The U.S.	2006	Background O_3 contribution	123
CAMx	PRD, China	October 2004	VOCs emissions	124
CAMx	Europe	2010	Anthropogenic emissions	125
CAMx	YRD, China	summer 2013	VOCs emissions	126
CAMx	YRD, China	summer 2013	Anthropogenic emission sources	127
CAMx	YRD, China	2013-2017	Transportation and industry emissions	127
CAMx	The U.S.	2025	On road emissions	128
CAMx	The U.S.	1970-2020	NO_x emissions	129
CMAQ	The U.S.	2030	On-road mobile emissions	130

OSAT is an advance technique that tracks transport traces of O_3 precursors, thus O_3 productions associated with NO_x and VOCs can be calculated for grouped sources. This technique is successfully applied in CTMs and provides reliable evidences for estimate source contributions to O_3 pollution. However, this method is highly depended on user specific grouping processes. For example, emission inventories such as EDGAR, MEIC and NEI provide sectoral emissions from different categories, thus, grouped sources are not consisted by varying inventories.

2.5 Source-oriented methods

NO_x and VOCs are regarded as main precursors of O_3 formation, NO_2 is formed through the oxidation of NO by O_3 while organic peroxy radicals (RO_2) and hydroperoxy radicals (HO_2), which play important roles in forming O_3 formation, are formed through reactions of VOCs[131]. O_3-oriented technique provides the detailed surface O_3 source apportionment for multiple targets (sources, regions and species) in single simulation in air quality models[132, 133]. This advanced technique is developed to track O_3 formation by tagging O_3 precursors in their source emissions while air quality model is conducting. As main precursor of O_3, NO_x emissions are always tagged in this approach. Detail tagging method is briefly introduced in Zhang and Ying [134]. Generally, following reactions of Equation 6 and Equation 7, O_3 formation from different sources can be identified.

Equation 6:

$$NO_{2n}+hv\text{---}NO_n+O(3P)_n,\ n=1,2,3\ldots,N$$

Equation 7:

$$O(3P)_n+O_2\text{---}O_{3n},\ n=1,2,3\ldots,\ N$$

In equation above, superscript n represents NO_x emissions from source n, these functions are added in air quality simulation so that O_3 formation in simulation outputs show their source tagged emissions.

As another main precursor, VOCs contributions to O_3 formation is hard to evaluate since their variety of components and intermediate reactions. As recorded in Ying and Krishnan [135], reactions of a general reactive hydrocarbon (RH) from emission source n are tagged to tracking VOCs contributions by following equation:

Equation 8:

$$RH_n+HO—RO_{2n}+H_2O, n=1,2,3…, N$$

Equation 9:

$$RO_{2n}+NO—NO_2+RO_n, n=1,2,3…, N$$

In these reaction processes, contribution of HO_2 from emission sources can be directly calculated and conversion rate (R) from NO to NO_2 can be determined as F in following equations, thus O_3 apportionment can be estimated.

Equation 10:

$$F_n=R(NO_{2n})/R(NO_{2tot}), n=1,2,3…, N$$

Equation 11:

$$O_{3n}=F_n*O_{3tot}, n=1,2,3…, N$$

$R(NO_{2n})$ in Equation 10 represents conversion rate from source n, NO_{2tot} represents overall NO to NO_2 concentration rate in all VOCs sources. O_{3tot} is the predicted overall net O_3 formation rate. O_3 contributions from VOCs emission sources can be calculated by applying above functions in AQMs.

Based on source-oriented technique, O_3 contribution from NO_x and VOCs emissions can be processed in single simulation, however uncertainties due to nonlinear photochemical reaction rate which greatly varied from different NO_x and VOCs concentration, multiple classification schemes, such as NO_x-sensitive, VOCs-sensitive, two-regime (2R) and three-regime (3R), are applied in source oriented simulations to investigate O_3 contribution from NO_x and VOCs. In following sections, these regime schemes will be brief reviewed.

2.6 O_3 regime schemes

Four regime schemes are discussed in this section. These schemes are mostly used independently in O_3 simulation in which NO_x or VOCs are determined as dominant precursor. In case where NO_x is determined as dominant precursor, O_3 formation is attributed to NO_x emission only; similarly, the same idea for VOCs dominant regions. For example, Zhang and Ying [134] studied NO_x contributions to O_3 in Houston-Galveston-Brazoria (HGB) and Beaumont-Port Arthur (BPA) in the U.S. were determined as NO_x sensitive regions. However, it is hard to determine whether O_3 production generated in specific periods or regions is relative to NO_x-sensitive or VOCs-sensitive. 2R scheme is introduced to determine O_3 attribution to NO_x and VOCs. O_3 production is attributed to either NO_x or VOCs emissions based on O_3 chemical formation regime. Regime is classified by different indicator ratios. Kwok, et al.[52] applied the ratio of production of hydrogen peroxide to nitric acid, to determine if O_3 product occurs in either NO_x- or VOCs-sensitive chemical regime. Besides, indicator ratio was set to 0.35 based on previous studies [136, 137]. Some other indicators are also applied to identify O_3 sensitivity to NO_x and VOCs. Ratio of $H_2O_2/(O_3+NO_2)$, $HCHO/NO_y$ and $HCHO/NO_z$ were applied to determine VOCs-limited O_3 formation with transit value of 0.02, 0.28 and 1, respectively[138-141]. Within these indicators, production rate of H_2O_2/HNO_3 is most widely recruited to identify O_3 sensitivity to NO_x and VOCs as 2R in recent studies. A summary of recent studies that applied 2R in O_3 source apportionment analysis are listed in Table 4.

Table 4. Summary of studies using 2R scheme in O_3 source apportionment

Model	Study field	Study period	Study sources	Reference
CAMx	PRD, China	Jun. 26–Jul. 2, 2000	NO_x and VOCs emissions	[142]

(Table cont'd)

Model	Study field	Study period	Study sources	Reference
WRF-Chem	Eastern China	Summer 2011	Diurnal pattern and regional sources	[143]
CCM/CHASER	Japan	1980–2005	Regions of emission sources	[144]
CMAQ	California, U.S.	Jun. to Jul. 2007	Emissions of NO_x and VOCs	[52]
CAMx	YRD, China	2015	Emissions of NO_x and VOCs	[145]
CAMx	YRD, China	Summer 2013	Emissions of NO_x and VOCs	[146]
CAMX	PRD, China	2006	Emissions of NO_x and VOCs	[147]

Though 2R approach is mainly used as current O_3 source analysis method, uncertainties remain. A single threshold (ratio indicator) might not be sufficient since both NO_x and VOCs control O_3 formation simultaneously. Thus, the transition regime is introduced to improve measurement that O_3 attribute to both NO_x and VOCs. Thus, 3R scheme is improved to estimate O_3 contributions from transition regime. Based on analysis of O_3 production efficiency and formation kinetics[136], production ratio of $(H_2O_2+ROOH)/HNO_3$, as a widely used indicator, was reevaluated based on 2R scheme in SAPRC photochemical mechanism in a model based estimation [53]. The transition regime is defined when ratio is between 0.047~5.142. 3R regime is updated and validated in 2018, its ability in providing understanding of O_3 attribution to NO_x and VOCs carried out a higher accurate result O_3 contributions from its sources[148].

2.7 O_3 source apportionment in China

Severe O_3 pollution is reported in previous studies in eastern China with high 8h-O_3 concentration exceeding the Chinese National Ambient Air Quality Standard (CNAAQS) of 82 ppb (160μg/m^3) especially in warm and dry summertime[51]. Many studies analyzed sources of O_3 in China. Generally, a shifting trend from NO_x-limited to VOCs-limited was observed in rural area as the latitude increases, and NO_x emissions were estimated as the dominant precursors in southern China while rural regions in north China were classified as VOCs-sensitive area[149]. Surface O_3 concentration in eastern China was more sensitive to photochemistry while the transport processes

dominate the O_3 in western regions where the climate conditions such as cloud convections play an important role in forming O_3[150]. Biogenic emissions were listed as one of the major sources that enhance O_3 formation in southeast and east China, and it also shift the dominant precursor from NO_x to VOCs in these regions[151, 152].

High O_3 episodes were frequently observed in many Chinese areas such BTH region, YRD, Sichuan Basin and PRD[153, 154]. Increasing O_3 concentrations were proved to associated with growth of NO_x and VOCs emissions as the result from urbanization and economic development in recent years. It is also revealed that high concentrations in summertime were due to on-road vehicles emission of NO_x and VOCs[155]. Research has focused on O_3 and its source apportionment in high risk areas to assess the dominant sources. Results are provided as solid evidence for making a strategic policy to reduce O_3 pollution in China.

It was reported that 8h-O_3 concentration in YRD increased from 144 μg/m^3 to 168 μg/m^3 since 2013 to 2017. Emissions from industry and vehicle sectors were found to be as the major sources[127]. Surface O_3 in Shanghai was briefly analyzed since it was one of the biggest cities in China located in YRD and suffered high summer O_3 concentration by more than 300μg/m^3 [156]. A regional source apportionment study revealed that Shanghai was greatly affected by local emission which account for ~28.9% of total O_3. Contributions from emissions of surrounding regions also caused significant increases of O_3. Emissions from north Zhejiang provinces were estimated to associate with ~19.9% of total O_3 concentration in Shanghai [156, 157]. Sectoral source apportionment results revealed high contributions from industry (~39.2%), mobile source (~21.3%), biogenic (~13.0%) and power plants (~7.1%) in Shanghai[121]. As one of major sources, biogenic emissions of VOCs were estimated to contribute maximum of 36 μg/m^3 O_3 in YRD especially in rural area, it also enhanced daytime O_3 by maximum of ~15 μg/m^3 [158, 159].

PRD is another high-risk area where O_3 is listed as the major air pollutant. High concentration episodes were always observed in autumn at urban regions with maximum of > 100 ppb[160, 161]. Local emissions were evaluated cause more than 50% (maximum of ~70%) of total O_3 formation, and mobile emission was the major source for high concentration episodes [116]. Emissions from central and west PRD were transported to south regions and induced high concentration episodes with concentrations higher than 100 ppb under a low air pressure system and slow south wind[160]. VOCs emissions were evaluated as dominant precursors in PRD, species such as p-xylene, 1,2,4-trimethylbenzene, 2-methyl-2-butene, 1-butene and α-pinene were listed as the dominant species. Besides, VOCs emissions were reported associate with ~64.1% of total O_3 formation potentials[162, 163]. Mobile source (40%) was also estimated as the major source of O_3 followed by biogenic emissions (29%)[164]. An analysis in Guangzhou indicated a similar result of contribution from mobile emission while the second source was industrial emission rather than biogenic due to high urbanization and industrialization in this megacity[165].

As one of most polluted regions, NCP is facing severe O_3 pollution due to increasing emissions of NO_x and VOCs. Emissions from Hebei and Shandong provinces enhanced the O_3 formation in summertime, which is always referred as the high concentration episode[166]. High O_3 concentrations recorded in Beijing ranged from 80 to 159 ppb in urban area during summertime, and the major source was estimated to NO_x emissions especially those from urban area[167, 168]. O_3 pollution in urban Beijing was also estimated due to emissions from Tianjin and the south Hebei province[169]. Shandong was also reported to enhance O_3 concentration in high concentration episodes [170]. Though O_3 pollution in NCP is getting worse, there is insufficient data to fully analyze O_3 source apportionment in this region. Without solid evidence to quantify the effects from emission sources, no effective controlling strategies could be implemented to reduce O_3 pollution

in NCP; however increasing concern for this issue demands an improvement in air quality in capital regions. Thus, greater effort should be put to analyze O_3 and its source apportionment in NCP.

2.8 Conclusions

Four main methods for O_3 source analysis are reviewed in this chapter, and each approach has their own limitations and advantages. As the source sensitive methods, DDM and BFM provide limited information for source contribution from emissions. They miss information from complex nonlinear chemical reactions and potential contributions from removed sources[102]. OSAT offers a much more reliable and simpler way to estimate source contributions to O_3. Tagged tracers help to identify the source contributions. However, non-reactive tracers in this method limit its ability to track source contribution during chemical reactions. An alternative method, the source-oriented approach, clearly quantifies O_3 contribution from its precursors. This method has a strong ability in tracking O_3 formation from non-linear chemical processes, O_3 formation from NO_x and VOCs are involved. Thus, the tagged sources can be identified in simulation outputs. This method overcomes limitations in methods mentioned above and has been widely accepted in recent O_3 source apportionment studies. Though source-oriented approach has advantages in tracking sources of precursors, limitations also existed. In most case, the study domain is not dominated by single precursor, and is affected by seasons and regions. NO_x- or VOCs-sensitive simulation might not be able to provide accurate source apportionment. 2R scheme is introduced to fix this issue, which solve most problem, but results would be varied due to application of different indicators. O_3 formations in "transition" regime also lead to uncertainties in 2R scheme. 3R is developed to overcome this issue as it which offers higher accuracy results of contributions from NO_x and VOCs emissions.

Many studies analyzed O_3 source apportionment in China and pointed out that emissions from mobile vehicles, industry and biogenic cause high O_3 concentration. O_3 sensitivity to NO_x and VOCs were also analyzed. BVOCs was revealed to enhance O_3 concentration significantly. However, insufficient studies have been conducted to analyze O_3 source apportionment in NCP which is one of the most polluted regions in China. More attention should be put on this area. As one of air pollutants, O_3 leads to serious risk in human health and ecological lost. Efforts are needed to improve accuracy in measuring O_3 from complex non-linear photochemical processes, such as evaluating a better regime indicator in 3R scheme for different locations. Choosing a reasonable source apportionment method also makes sense in different simulation purposes. Although these methods have their own limitations, they also provide realistic results in each study, which contributes to a better understanding of O_3 in the world.

CHAPTER 3. IMPROVING OZONE SIMULATION IN THE NCP

3.1 Introduction

Numerous studies have shown adverse environmental and public health impacts associated with tropospheric O_3 pollution [5, 171, 172]. O_3 exposure is associated with respiratory-related hospital admissions, cardiovascular diseases, school day loss, asthma-related emergency department visits, premature mortality, etc. [3-6]. Fann, et al.[13] revealed that 4700 deaths and 36,000 life-year losses were due to long-term O_3 exposure based on O_3 concentration in 2005 across the continental United States. In China, around 55 to 80 thousand mortalities in 2015 were attributed to chronic obstructive pulmonary disease (COPD), and a total 816.04 million cumulative population was estimated exposed to 8h-O_3 concentrations (>100 $\mu g/m^3$)[14, 154]. O_3 level in 2000 also induced 6.4%-14.9% yield loss of food crop, and estimated O_3 concentration in 2020 would cause 47.4 million metric tons loss of four grain crops produced in China [15].

Increasing O_3 concentration were reported in many studies. Country scale statistical analysis in 74 cities indicated that 8h- O_3 increased from ~69 ppb in 2013 to 75 ppb in 2015, and a 15% increase of non-compliant cities were also revealed with increasing O_3 level in China [69]. An average increase rate of 1.13 ± 0.01 ppb/year of 8h- O_3 was observed in north of eastern China from 2003 to 2015, and total O_3 variations were due to short-term (36.4%), seasonal (57.6%) and long-term (2.2%) changes [16]. About 50% of the days with O_3 concentration exceeding 80 ppb in Beijing-Tianjin region (maximum of 170 ppb) were reported during 1983-1986 [173]. Significant increases were also observed in Mt. Tai with an average increase by 1.7 ppb/year in June and by 2.1 ppb/year in July to August during 2003-2015[17]. Recent studies reveal that China is

experiencing severe O_3 pollution, but O_3 variations and its impact factors are not well studied. Lacking comprehensive analysis leads to a challenge in lowering O_3 pollution.

Chemical transport models (CTMs) are commonly used tools to understand the formation and transport of O_3. Li, et al.[12] analyzed the impacts of chemical production and transport on diurnal O_3 behaviors in Mt. Tai and revealed that regional transport and chemistry production contribute ~60 and ~25 ppb, respectively, in afternoon-maximum concentration in June 2006 based on results obtained from the Nested Air Quality Prediction Modeling System (NAQPMS). Yang, et al.[23] applied global three-dimensional Goddard Earth Observing System chemical transport model (GEOS-Chem) to analyze impacts of sulfate and nitrate on surface-layer O_3 concentration in China and indicated that sulfate dominates in O_3 increases while nitrate dominates in O_3 reductions. Hu, et al.[24] simulated tropospheric O_3 in the North China Plain (NCP) for 2015 summer by applying the Community Multiscale Air Quality (CMAQ) model and found that emissions from Shandong and Hebei make the largest contribution not only to the highest local O_3 concentration but also to Beijing and Tianjin. They also pointed out that most urban O_3 pollutions are mainly dominated by conditions sensitive to volatile organic components (VOCs), and figured out that emission control strategies in industry, residential and power plant sectors would make significant effects on reducing O_3 concentration. Though O_3 is receiving increasing attention, limited understanding of its variation and impacts require comprehensive analysis in China specially in the NCP [16, 17, 174, 175].

CTMs are very useful for understanding O_3, but the accuracy is highly dependent on emission inventories. Several emission inventories covering China and surrounding regions are available for different simulation purposes[37, 38]. Inventories from regional to continental scales, for different pollutant species and emission sectors [39-43] [32] were created and were successfully applied

in O_3 simulation in China, including Emission Database for Global Atmospheric Research (EDGAR), Multi-resolution Emission Inventory for China (MEIC) and Regional Emission inventory in ASia (REAS) [44-48]. However, to a large extent, these inventories are not entirely from bottom-up, leading to large uncertainties in simulation results [50]. EDGAR and MEIC are two most widely used inventories in China, while their performances in O_3 simulation vary in years and regions [41, 51]. Evaluating and improving their performance in O_3 prediction would provide convincing results for deeper understanding of O_3 formation, health risks, and design of controlling strategies.

This study applies the CMAQ model to estimate the pollution level and health risks of O_3 in the NCP during summer 2017 with the anthropogenic emission inventories of MEIC and EDGAR+ (improved version of EDGAR). O_3 variations and the impacts from meteorological conditions and precursors emissions are discussed in detail.

3.2 Methods

3.2.1 Model description

O_3 concentrations are simulated using the CMAQ model v5.0.1 [176, 177] in 12km×12km horizontal resolution domain (Figure 1) that covers NCP including Beijing, Tianjin, Hebei, Shandong, part of Henan, Jiangsu, Anhui and Inner Mongolia (note that the map is generated by using NCAR Command Language (NCL) [178]). Initial and boundary conditions are both generated by simulation on coarse domain (36 km ×36 km) which covers mainland China and part of surrounding countries. Photochemical mechanism SAPRC-11[177] and aerosol chemistry mechanism AERO6 [179] are used. The Weather Research and Forecasting (WRF) v 3.7.1[177, 180, 181] model is applied to generate meteorological inputs with initial and boundary conditions from National Centers for Environmental Prediction (NCEP) FNL (Final) Operational Global Analysis

data (http://dss.ucar.edu/datasets/ds083.2/)[181, 182]. Meteorology-Chemistry Interface Processor (MCIP) v4.2 is applied to convert WRF outputs into CMAQ ready meteorological inputs. Different anthropogenic emission inventories are re-gridded to designed domain by using the Spatial Allocator [183]. The Model for emissions of Gases and Aerosols from Nature (MEGAN) [184] is used for biogenic emissions and the Fire Inventory from NCAR (FINN) [185] provides biomass burning emissions.

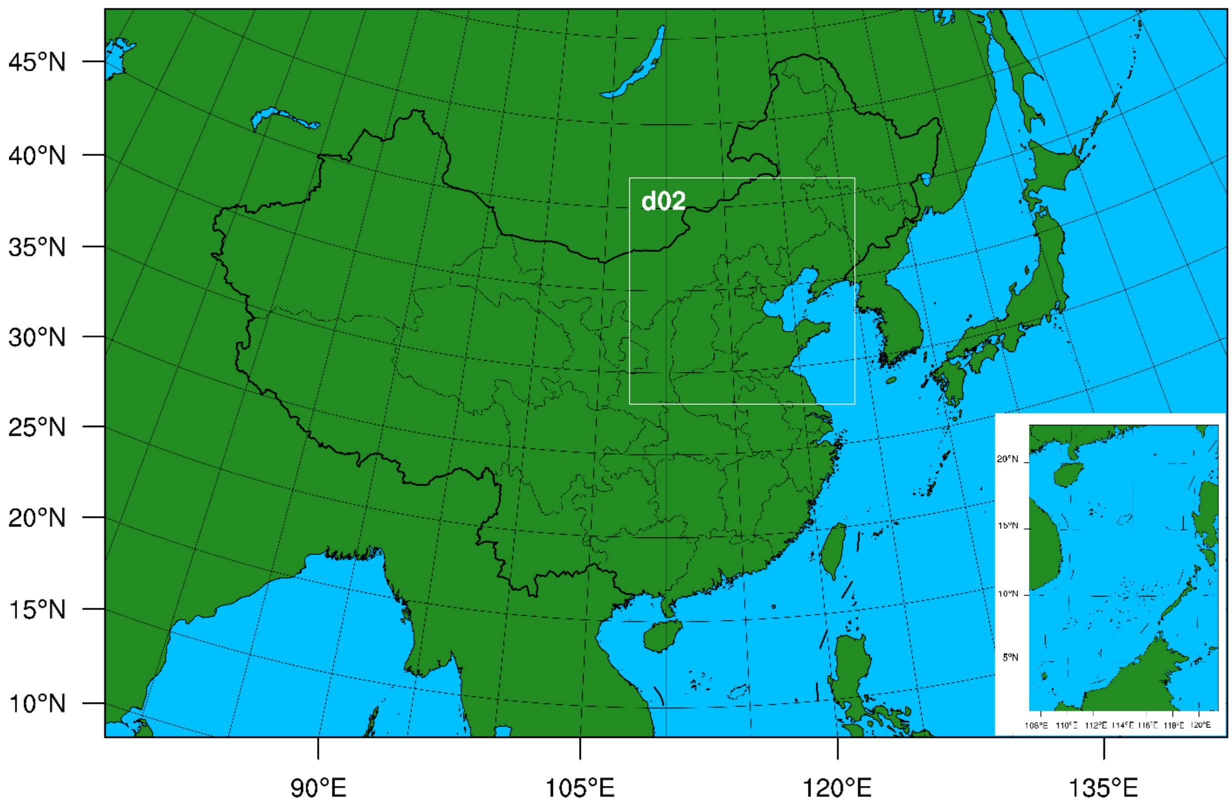

Figure 1. Simulation domains. Coarse domain (36km by 36km) covers mainland China and part of surrounding countries. NCP (d02) is included as the finer domain (12km by 12km).

3.2.2 Case description

3.2.2.1 EDGAR+ inventory

As precursors of O_3 production NO_x and VOCs play important roles in O_3 simulation. Two anthropogenic emission inventories with modified NO_x and VOCs are applied in this study for

comparison. In first scenario, which is referred as "EDGAR+" hereinafter, anthropogenic emissions of VOCs and NO_x from EDGAR [186] for China are scaled to 2012 (off-road), 2015 (industry, residential, on-road and energy), and 2016 (industry, residential, on-road and energy for Beijing) to represent as in 2017. Scaling factors for VOCs and NO_x are shown as in Table 5 and

Table 6. On-road emissions are scaled down to the national total given for 2017 in China Vehicle Environmental Management Annual Report (http://dqhj.mee.gov.cn/jdchjgl/zhgldt/201806/P020180604354753261746.pdf). Emissions from energy, residential and industry sectors are scaled down from KNMI (Royal Netherlands Meteorological Institute) DECSO (Daily Emission estimates Constrained by Satellite Observation) based on Ozone Monitoring Instrument (OMI) data [187, 188] to match year-on-year reduction rate given for 2016 (4%) and 2017 (4.9%) in Government Working report. NO_x emissions in off-road and agriculture remain as in 2012 since there is not enough evidence to determine scaling factors for them.

Table 5. Scaling factors for VOCs emissions in NCP

	Agriculture	Residential	Industry	Energy	On-road	Off-road
Beijing	3.64	0.08	1.13	1.19	1.59	1.39
Tianjin	21.87	0.04	4.31	2.90	0.67	7.44
Hebei	44.78	0.46	1.25	2.92	2.88	4.41
Shandong	22.39	0.40	1.58	4.16	2.39	3.58
Shanxi	37.78	0.42	0.24	2.62	2.17	3.57
Henan	13.75	0.46	1.07	2.24	3.09	2.01
Jilin	175.52	0.59	2.31	3.23	2.67	0.59
Liaoning	36.32	0.36	0.80	4.17	2.62	7.32
Heilongjiang	116.51	1.12	1.07	2.23	2.74	0.36

Table 6. Scaling factor for NO_x emissions in NCP

	Agriculture	Residential	Industry	Energy	On-road	Off-road
Beijing	1.00	0.96	0.10	0.08	0.63	1.00
Tianjin	1.00	1.05	1.42	0.22	0.50	1.00
Hebei	1.00	1.26	1.13	0.42	2.16	1.00
Shandong	1.00	0.88	0.66	0.45	1.92	1.00
Shanxi	1.00	1.59	0.82	0.42	2.24	1.00
Henan	1.00	0.61	0.73	0.34	2.32	1.00
Jilin	1.00	0.59	1.02	0.61	2.28	1.00
Liaoning	1.00	0.83	0.30	0.60	1.48	1.00
Heilongjiang	1.00	2.03	0.68	0.73	2.22	1.00

3.2.2.2 MEIC inventory

In another scenario, MEIC[189] (http://www.meicmodel.org), developed by Tsinghua University, provides monthly NO_x and VOCs emissions from transportation, residential, power, industry and agriculture in China[190, 191]. Latest version for 2016 is applied to represent emissions in 2017 for this work. MEIC allows for gridding to user specific domain based on its flexible spatiotemporal and sectoral resolution [192]. Emission for all sectors are estimated at provincial or county level and allocated to user-specific grids except for power sector which are calculated with unit-based method for individual plants[15, 193]. In this study, MEIC is applied in CMAQ simulation with same meteorological inputs and model settings as in the EDGAR+ case. Total emissions of NO_x and VOCs for both scenarios and their differences are shown in Figure 2, while total emission rates from each source are listed in Table 7 and Table 8.

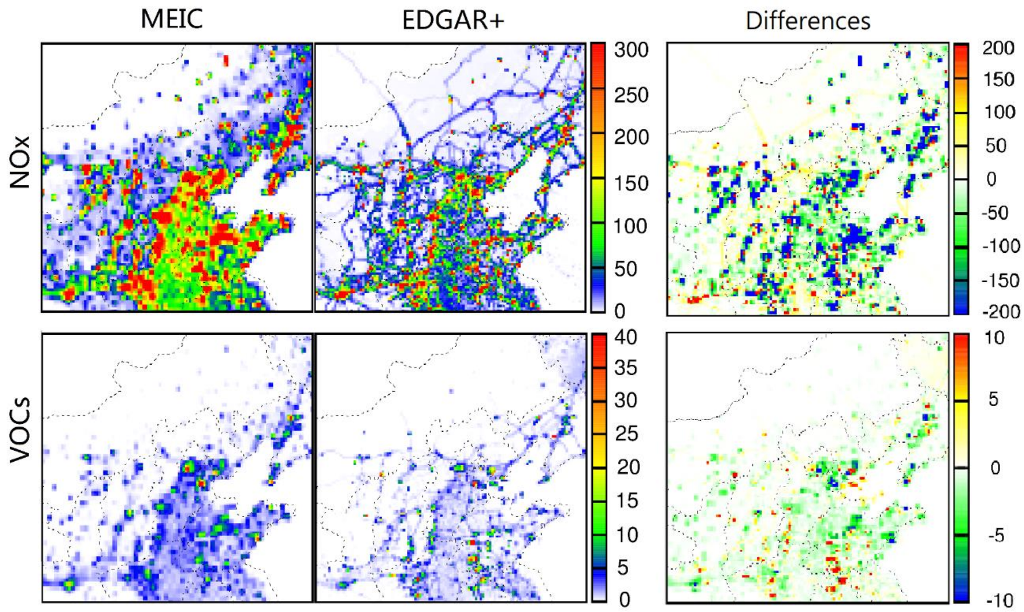

Figure 2. Averaged NO_x and VOCs emission rates from MEIC and EDGAR+ and their differences (subtracting EDGAR+ by MEIC) in summer 2017. Units are tons/month.

Table 7. NO_x emission from each source for different inventory in NCP 2017 summer.

	MEIC (10^4 ktons/month)		EDGAR+ (10^4 tons/month)
Agriculture	NA	Agriculture	6.19
Residential	4.18	Residential	3.57
Power	60.73	Energy	38.58
Industry	106.34	Industry	53.41
Transportation	83.05	On-road	38.10
NA	NA	Off-road	12.32
Total	254.30	Total	152.16

Table 8. VOCs emission from each source for different inventory in 2017 summer.

	MEIC (10^3 ktons/month)		EDGAR+ (10^3 ktons/month)
Agriculture	NA	Agriculture	1.90
Residential	4.21	Residential	3.15
Power	0.11	Energy	0.35

(Table cont'd)

	MEIC (10^3 ktons/month)		EDGAR+ (10^3 ktons/month)
Industry	24.77	Industry	16.15
Transportation	6.50	On-road	5.66
NA	NA	Off-road	0.29
Total	35.58	Total	27.50

3.4 Results and discussions

3.4.1 Overall performance

Predicted meteorological conditions (temperature (T), wind speed (WS), wind direction (WD) and relative humidity (RH)) from WRF for the simulation period are validated using observed data from National Climate Data Center (NCDC, https://www.ncdc.noaa.gov/). A total of 108 stations are involved. The mean bias (MB), gross error (GE) and root mean squared error (RMSE), as well as mean observation (OBS) and prediction (PRE) of meteorological parameters are shown in Table 9. Statistical results are compared with benchmarks from **Emery, et al.** [194]. Generally, WRF slightly over-predicts temperature and wind speed but underestimates RH in summer. Uncertainties of these biases are believed to result from the model itself including domain resolution, model configuration and parameterization[195]. Though biases exist, predictions from WRF are normally accepted in previous work over China with similar statistical results [196, 197].

Table 9. Summertime model performances of meteorological conditions in NCP for temperature (T), wind speed (WS), wind direction (WD) and relative humidity (RH).

	T (°C)	WS (m/s)	WD (º)	RH (%)
OBS	24.32	3.27	168.99	63.41
PRE	25.35	3.82	169.89	58.40
MB	1.03	0.56	1.71	-5.01
RMSE	2.72	1.85	58.51	15.3
GE	2.04	1.42	41.89	11.79

1. Benchmark of MB for T, WS and WD is ±0.5, ±0.5 and ±10, respectively.
2. Benchmark of GE for T, WS and WD is 2, 2 and 30, respectively.
3. Benchmark of RMSE for WS and WD is 2 and 30, respectively.

8h-O_3 observations from CNEMC are used to validate model performance on O_3. Table 10 shows the comparison of model and predicted concentrations in 11 major cities in the NCP from June to August 2017, together with statistics including averaged observations (OBS), averaged predictions (PRE), the mean fractional bias (MFB), the mean fractional error (MFE), the normalized mean error (NME) and the normalized mean bias (NMB). For cities with multiple monitoring stations, averaged concentrations are applied. Different cutoffs for O_3 (from 40 to 60 ppb) are used to analyze the performance of the model as suggested by the US EPA[198]. In this study, 8h-O_3 concentrations higher than 30 ppb are included in analysis based on a previous study [199].

Table 10. Model performances in 11 major cities in NCP for 8h-O_3 simulation using EDGAR+ (E) and MEIC (M). Units are ppb for OBS and PRE. Bold represents the statistical result exceeds criteria.

City	Baoding	Beijing	Datong	Hohhot	Jinan	Shijiazhuang	Taiyuan	Tangshan	Tianjin	Xuzhou	Zhengzhou
OBS	83.13	71.98	63.14	67.53	71.26	72.21	72.38	73.24	70.60	70.71	78.84
PRE (M)	78.17	80.62	65.17	63.76	71.77	79.10	67.99	51.47	68.19	65.08	74.3
PRE (E)	73.98	75.35	62.06	61.55	68.51	79.45	69.68	65.83	62.55	62.73	73.75
MFB (M)	-0.05	0.11	0.05	-0.05	0.03	0.09	-0.05	-0.4	-0.15	-0.07	-0.06
MFB (E)	-0.09	0.09	-0.03	-0.11	-0.01	0.06	-0.09	**-0.17**	**-0.21**	-0.06	-0.05
MFE (M)	0.20	0.25	0.14	0.16	0.17	0.23	0.19	**0.49**	**0.40**	0.21	0.16
MFE (E)	0.15	0.29	0.14	0.15	0.18	0.16	0.14	0.29	0.3	0.22	0.13
NME (M)	0.20	**0.32**	0.17	0.15	0.19	**0.26**	0.20	**0.39**	**0.39**	0.21	0.15
NME (E)	0.14	**0.34**	0.15	0.14	0.19	0.17	0.13	**0.26**	**0.26**	0.22	0.12
NMB (M)	-0.02	**0.20**	0.09	-0.03	0.06	0.15	-0.02	**-0.27**	-0.01	-0.03	-0.04
NMB (E)	-0.07	**0.17**	-0.01	-0.09	0.02	0.09	-0.08	-0.12	-0.15	-0.03	-0.04

Figure 3 and Table 10 indicates that simulations for each inventory generally agree well with observed O_3 concentrations in NCP. MEIC always predicts higher O_3 concentration than EDGAR+ except in Tangshan and Taiyuan. Over-predictions occur in Beijing, Datong, Jinan and Shijiazhuang for MEIC. It is noted that significant exceedances are observed in Beijing and Shijiazhuang for MEIC. On the other hand, EDGAR+ usually under-predict O_3 in this period. The NMB in most cities match the US EPA criteria [200] of ±0.15 except in Tangshan for MEIC. Similar outcomes are observed in the NME. The NME for both scenarios generally agree well with US EPA suggested criteria of 0.25 [200] , but there are 3 and 1 exceedances for MEIC and EDGAR+, respectively. It is noted that the only exceedance in EDGAR+ is 0.29 (Tangshan), but 3 exceedances are observed in MEIC with one extreme case (Tangshan, 0.32). The MFB and MFE in EDGAR+ match suggested criteria of ±0.15 and 0.35 [200] with only one slight exceedances in Tangshan (MFB of -0.16). The MFB and MFE for MEIC also indicates that model results meet performance goals in most cases except in Tangshan where both indices are not within suggested criteria. Based on statistical results, EDGAR+ has better performance in major cities in NCP. These major cities generally represent the air quality in the NCP, thus, both inventories result in satisfactory model performances and are reliable for further analysis in this study. Though uncertainties of O_3 simulation are associated with meteorological field, emissions, model treatment, and configurations [199], statistical results indicate the CMAQ model is capable of estimating short/long term O_3 concentrations variations and effects in NCP.

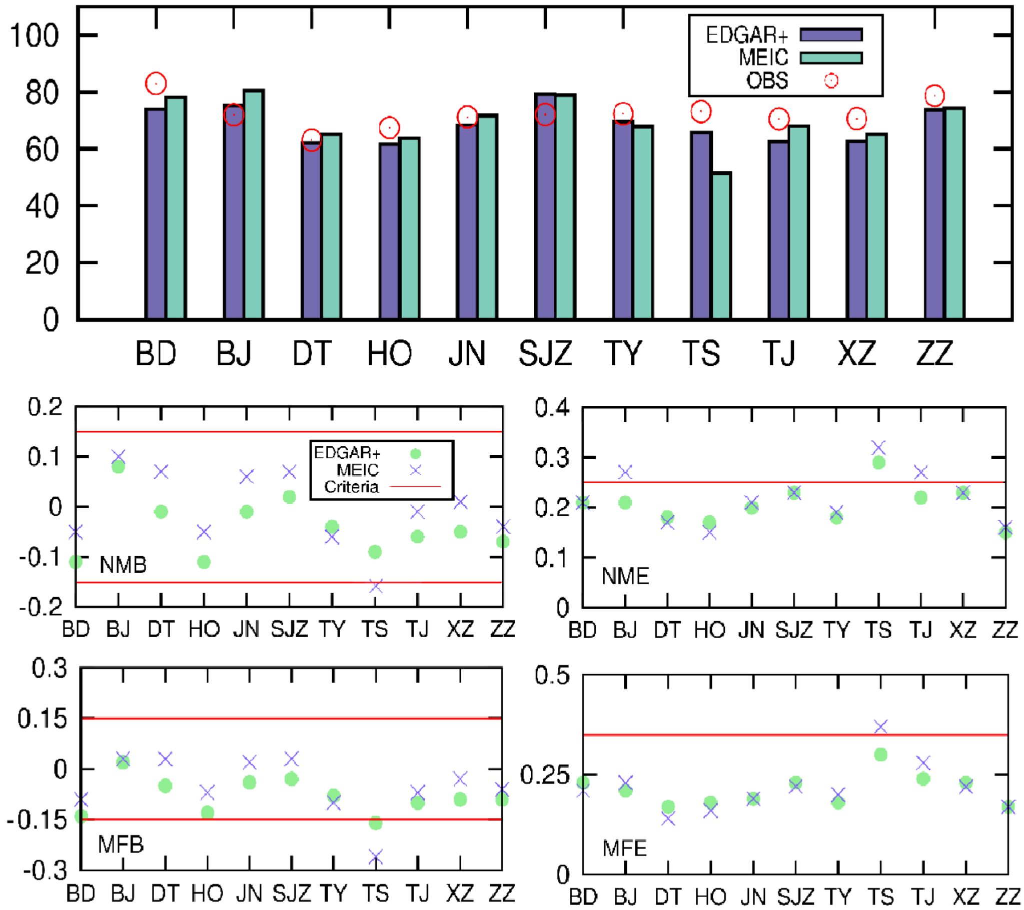

Figure 3. Model performance statistics on average daily 8h-O_3 concentration. Summertime average concentration (top), MFB, MFE, NME and NMB for 11 major cities are shown. Red lines represent suggested criteria by US EPA for each index.

3.4.2 Temporal and spatial variations

Figure 4 illustrates the comparison of averaged daily 8h-O_3 concentration from prediction and observation in 8 major cities in NCP from June to August in 2017. Generally, predicted concentration from EDGAR+ and MEIC agree well with observation. Results from both inventories successfully match the absolute level and temporal variations in major cities, even though biases occur in specific period. It is noted that predictions in late June and early July are mostly lower than observations for most cities (except Shijiazhuang and Zhengzhou) especially

when O_3 concentration is higher than 100 ppb. Unexpected biases exist for many reasons such as uncertainties in meteorological conditions, inventories and model treatment and configuration [177]. In Beijing, under-predictions (~30 ppb) also occur in the beginning of August when O_3 concentrations are ~120 ppb. Over-predictions are observed in late July and early August and part of late August exceeding > 40 ppb. This uncertainty may due to uncertainties in precursor's emission (such as NO, NO_2 and VOCs) inventories [201]. Simulation in Tianjin indicates that EDGAR+ has higher accuracy in June and July but fail in matching variations in early August. MEIC yields similar predictions before mid-July but result in under-predictions in late July, and it shows a better performance in August than EDGAR+. There are clear differences between EDGAR+ and MEIC in Shijiazhuang before end of July, with MEIC predicting significantly higher concentration (10~30 ppb) than EDGAR+. Both inventories over-predict by ~50 ppb on around July 22nd. Over-predictions are also observed in Jinan during the same period. Another significant over-prediction is observed in Xuzhou at the end of July and beginning of August where the observation is lower than 60 ppb. Simulations in Hohhot generally agree well with observation except two significant under-prediction periods (late June to early July and early August). Zhengzhou also has great agreement with observation except that specific extreme bias occurs in middle June and early August. Generally, EDGAR+ and MEIC predict similar O_3 concentration, and MEIC predicts slightly higher concentration than EDGAR+ in most cities. Comparison between observations and model predictions help to point out that EDGAR+ has better predictions in summertime at most cities.

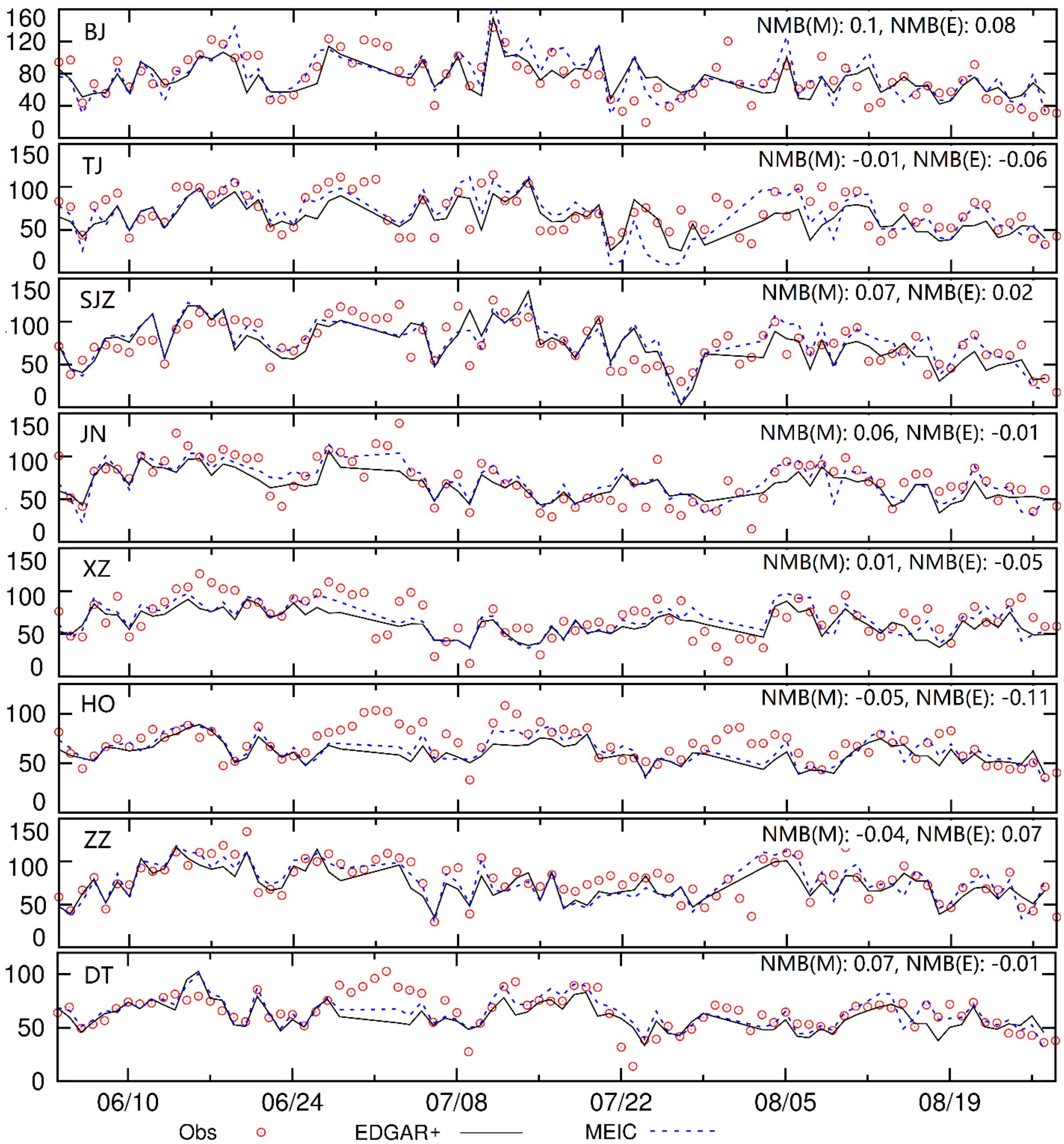

Figure 4. Average daily 8h-O_3 concentration in major cities. Results from EDGAR+ (E) and MEIC (M), observation (Obs) and statistical results (NMB) are shown in each row. Units for O_3 concentrations are ppb.

Average diurnal variation of 8h-O_3 concentration and corresponding meteorological conditions are shown in Figure 5. In Beijing, MEIC predicts significant higher concentration (~10 to 20 ppb) before noon time (12:00 pm) and lower after 15:00 pm till the sunrise in the next day

compared with observation data while over-predictions in EDGAR+ are lower (~5 to 10 ppb) than MEIC during the day time compared with MEIC. Both EDGAR+ and MEIC over-predicts the peak value before noon time. In Beijing, EDGAR+ shows a higher sensitivity to temperature since peak concentrations are predicted when the temperature is also high while MEIC always predicts peak concentration ~2 hours ahead of EDGAR+. MEIC and EDGAR+ have similar performance in predicting concentration in Hohhot, and MEIC always predicts ~5 to 10 ppb higher concentration during the nighttime than EDGAR+. In Hohhot, MEIC and EDGAR+ always predict peak values at a similar time around noon time to afternoon (12:00pm – 18:00 pm) and agree well with the observations. MEIC predicts higher concentration during morning to noon time in Jinan, and a significant bias can be observed between MEIC and observation data. In contrast, EDGAR+ has a better accuracy in matching the daily peak value as well as daily variations in Jinan. EDGAR+ predicts lower concentration by ~5 to ~10 ppb in Shijiazhuang then MEIC while both inventories always over-predict peak concentration by ~10 ppb compared to observation data during noon time. Significant under-predictions of ~10 to 20 ppb are observed using both inventories at nighttime. Predictions in Tianjin indicate that both inventories perform well in matching the peak concentration around noon time (12:00 pm) while significant under-predictions are observed at nighttime with a maximum by more than 30 ppb before sunrise (~4:00 am). Predictions in Zhengzhou indicate that MEIC and EDGAR+ yield slightly over-estimates (5 ppb and 10 ppb for EDGAR+ and MEIC, respectively) O_3 concentration in daytime while significantly under-predicting (~10 ppb lower) at night. MEIC predicts ~5 ppb higher O_3 concentration in daytime when EDGAR+ match well with observation data in Xuzhou. However, EDGAR+ has a lower accuracy in predicting concentration before 6:00am, in which MEIC matches well with observed concentration.

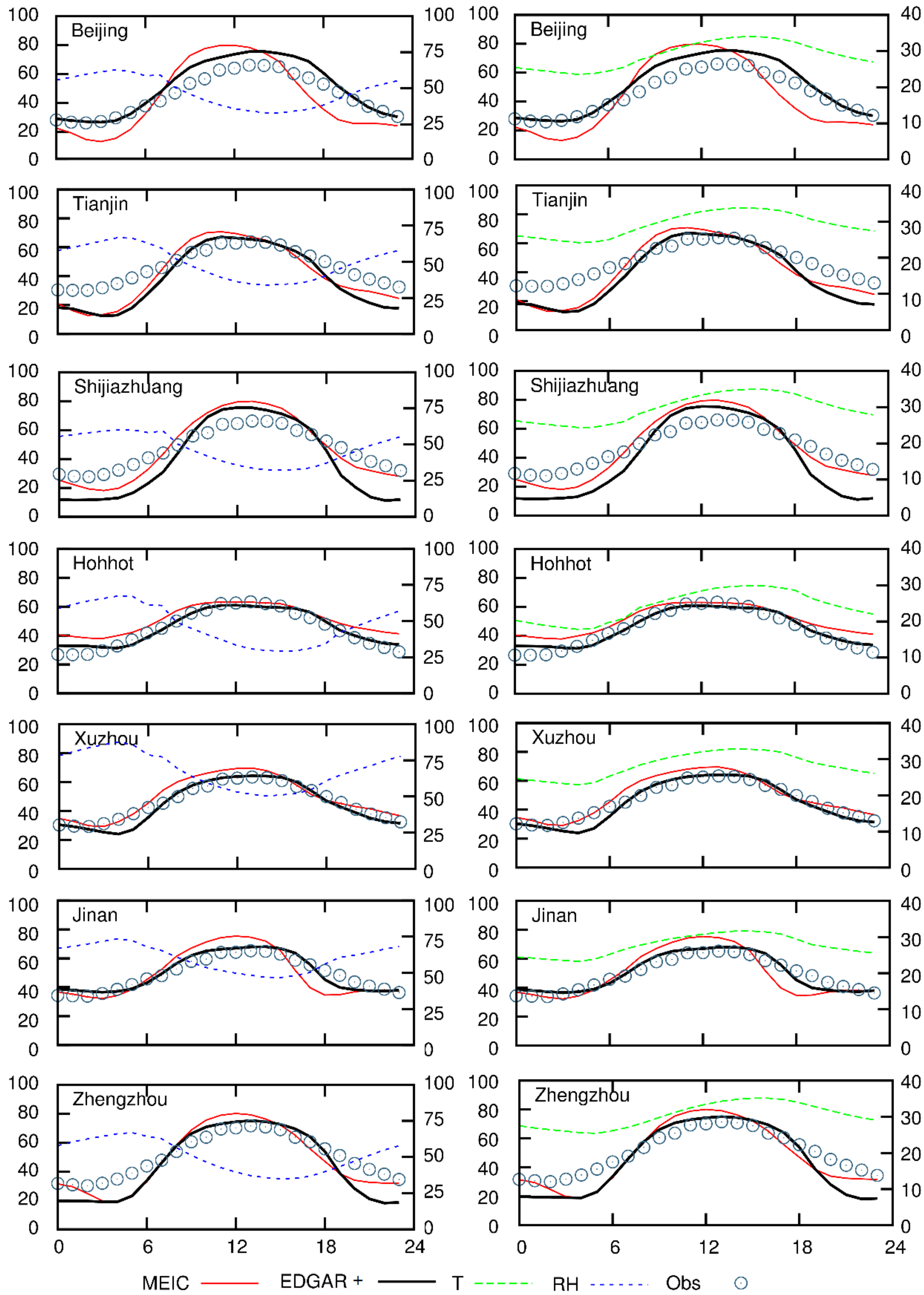

Figure 5. Diurnal variations of 8h-O_3 from EDGAR+, MEIC and observation (Obs), temperature (T) and relative humidity (RH) in major cities, Units for O_3 concentration are ppb, for T are ˚C, for RH are %.

Generally, MEIC predicts a slightly higher (~5 ppb) concentration than EDGAR+ before noon time (12:00 pm) but not higher or even lower when the temperature is high, and RH is at a low value in the afternoon. It is noted that both inventories predict O_3 peak value well or only slightly higher (< 5 ppb) in diurnal variations. In nighttime, the model predicts lower concentration especially the time before 6 am. In other words, model has better performance in daytime. Variations in all cities indicate that O_3 concentrations are greatly affected by RH and temperature. Diurnal variation also reveals that high O_3 concentration is correlated to high temperature and low RH. In the meantime, it also provides valid evidence that EDGAR+ has a higher accuracy in predicting O_3 concentration in NCP.

Figure 6 shows the spatial distribution of averaged 8h-O_3 concentrations in the summer for MEIC and EDGAR+ and their differences. Overall, O_3 concentration increases from inner land to coastal area, from rural to urban area and around major cities in each province. For both inventories, high O_3 concentrations occur at Beijing, Tianjin, Hebei, coastal Shandong and Jiangsu and junction regions between Hebei, Shanxi and Henan with >100 ppb. It is noted that O_3 concentrations are also very high on surface of Bohai Sea with ~90 ppb. Concentrations in the rest of area range from ~60 to 80 ppb. Compared to MEIC, EDGAR+ predicts higher concentrations in eastern Tianjin, western Hebei, Qingdao and Yantai by ~10 ppb but lower concentration in the rest region, especially in Beijing, northern Shandong and southern Jiangsu by >10 ppb. Generally, MEIC predicts slightly higher O_3 concentrations in most of NCP and ocean surface above the Bohai Sea while EDGAR+ results in higher predictions in part of major cities. The differences between two scenarios are mainly due to emissions as shown in Fig 1. Higher emissions in MEIC induce higher O_3 concentrations in NCP, but since the O_3 formation is not a linear reaction from NO_x and VOCs,

higher O_3 concentration in EDGAR+ is also due to lower emissions in specific regions such as in western Hebei province. Detailed analysis will be discussed in following sections.

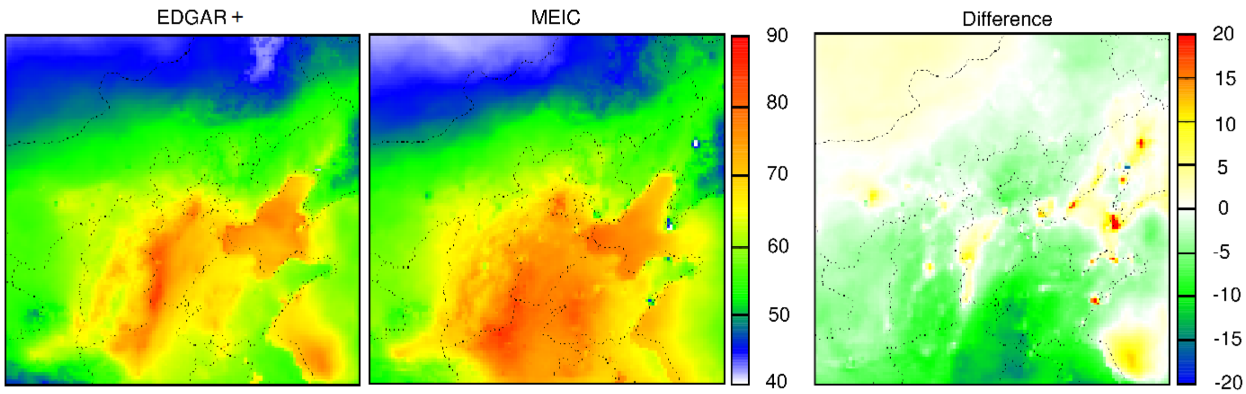

Figure 6. 8h-O_3 concentrations in NCP for 2017 summer predicted by EDGAR+ and MEIC, and their differences (subtracting EDGAR+ by MEIC). Units are ppb.

3.4.3 Peak episodes

There are 3 peak episodes observed during the simulation period including June 14th to 21st, June 22th to 29th and July 8th to 15th (Figure 7). O_3 variations in 8 major cities for these episodes are analyzed. Hourly 8h-O_3 in Figure 7 indicate the variation during peak episodes, in which peak daily 8h-O_3 concentrations are >100 ppb. In Beijing, peak values for each episode are ~120 ppb. Simulation results in June are mostly slightly lower than observation data while over-predictions on June 19th and July 11th with ~30 and 50 ppb higher than peak value, respectively, are shown in S4 and S6 for MEIC. On the other hand, predictions from EDGAR+ match better in these episodes with bias less than ±20 ppb. The model has higher accuracy in predicting high concentrations in Tianjin compared with in Beijing. Most peak values match well with observation as shown in S4 and S5 except on June 14th to 16th when under-prediction occurs in both scenarios. It is noted that over-prediction also existed on June 23rd and July 9th though part of observation data is missing for these days. Peak concentrations are also caught in Shijiazhuang except on June 27th. EDGAR+

and MEIC match high concentration during peak episode, but they also over-predict on some days such as June 15th, June 18th, June 26th and July 14th. The peak value on June 15th in Jinan is under-predicted. From July 8th to 15th, simulations mostly agree well with observed concentration with maximum bias on July 10th with around 15-20 ppb. Simulations in Hohhot indicate that predictions from MEIC correspond much more closely to the peak concentration in the study. Similar situation also occurs in Zhengzhou that peak concentrations are matched well on June 25th and July 10th but not on June 20th when prediction are ~20 ppb lower. Peak concentrations are under-predicted in Datong on June 15th, 28th and July 13th while predictions during the other peak episodes match well and slightly higher than observations except on June 16th where the simulation results are extremely higher. Spatial plots of 8h-O_3 concentrations in 3 episodes (Fig. 6) indicates that EDGAR+ predicts higher 8h-O_3 than MEIC in most regions especially in west Hebei and the Bohai Sea (~10 to 30 ppb) but lower in some major cities such as Beijing, Tianjin, Shijiazhuang and Jinan by 10 ppb.

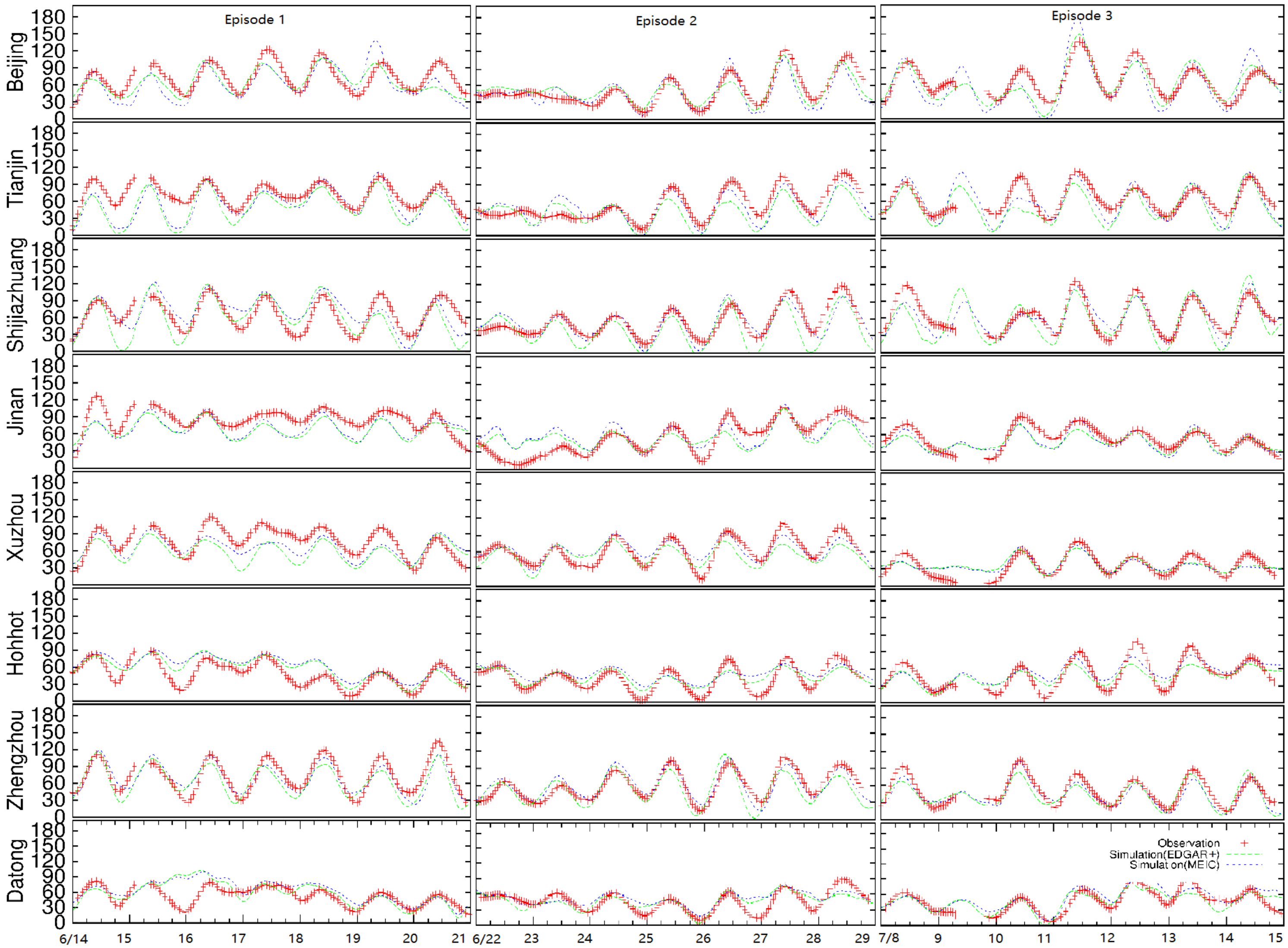

Figure 7. Hourly 8h-O_3 concentration at major cities for peak episodes. Units are ppb.

Compared with averaged summertime differences in

Figure 8, EDGAR+ predicts a higher concentration during peak episodes although its emissions of O_3 precursors are lower than those in MEIC. High concentrations occurring during these episodes might be due to specific climate conditions and emissions. Figure 9 shows climate conditions (average temperature (T), relative humidity (RH), wind speeds (WS) and wind directions (WD)) in 3 episodes. Spatial variation of meteorological conditions indicates that high O_3 concentrations always occur in locations where the temperature is higher than in the surrounding region such as in south Hebei and north Henan. Low relative humidity and slow wind speed are also observed in these regions to be associated with high O_3 concentration. It is obvious that high temperature, low RH and steady low air flow conditions are associated with high O_3 production in NCP. However, the opposite situation occurs in Bohai sea where temperature is lower than surrounding area with higher RH and WS. After comparison, it is noted that wind direction has less influence on O_3 production then other variables.

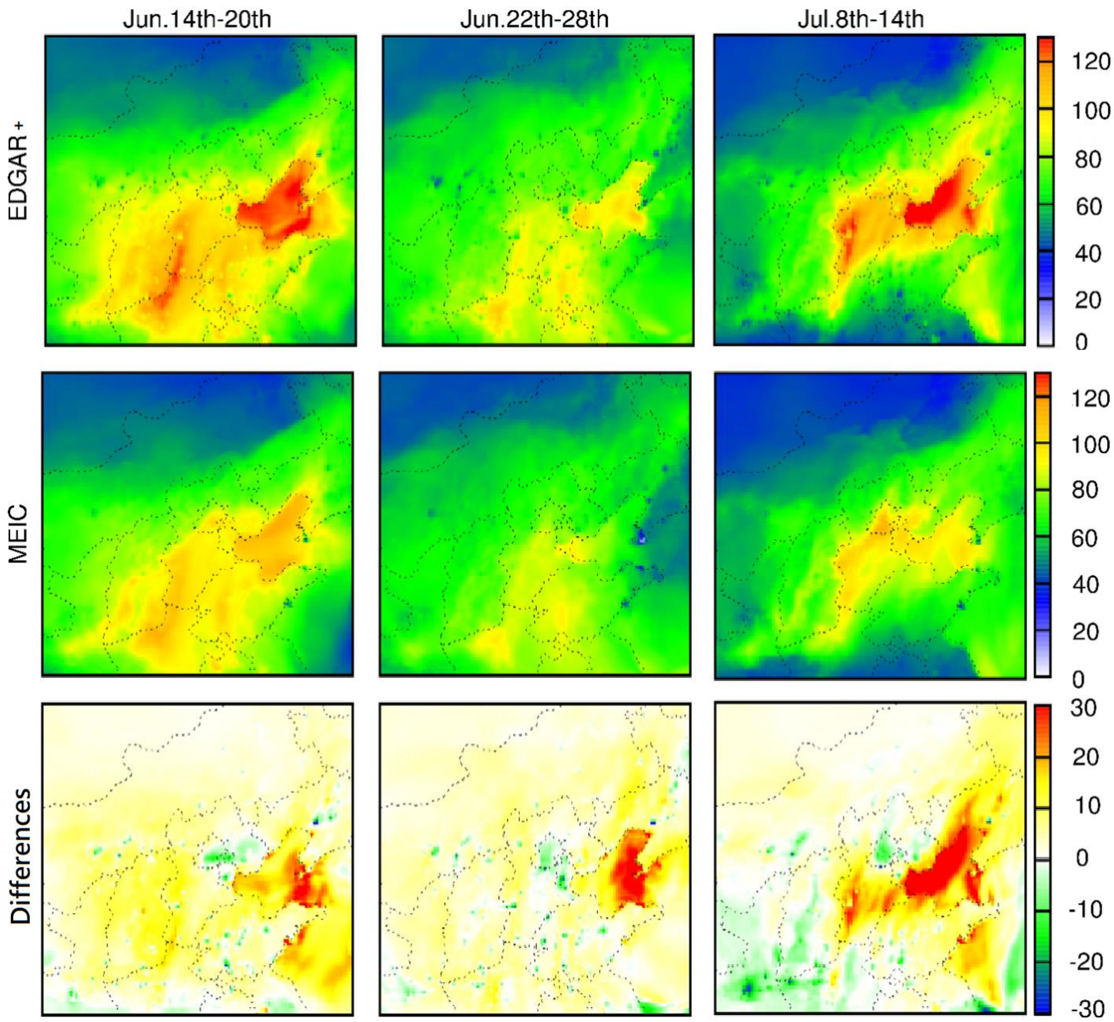

Figure 8. Spatial distribution of 8h-O_3 concentrations in 3 peak concentration episodes predicted by EDGAR+ and MEIC, and their differences (subtracting EDGAR+ by MEIC). Units are ppb.

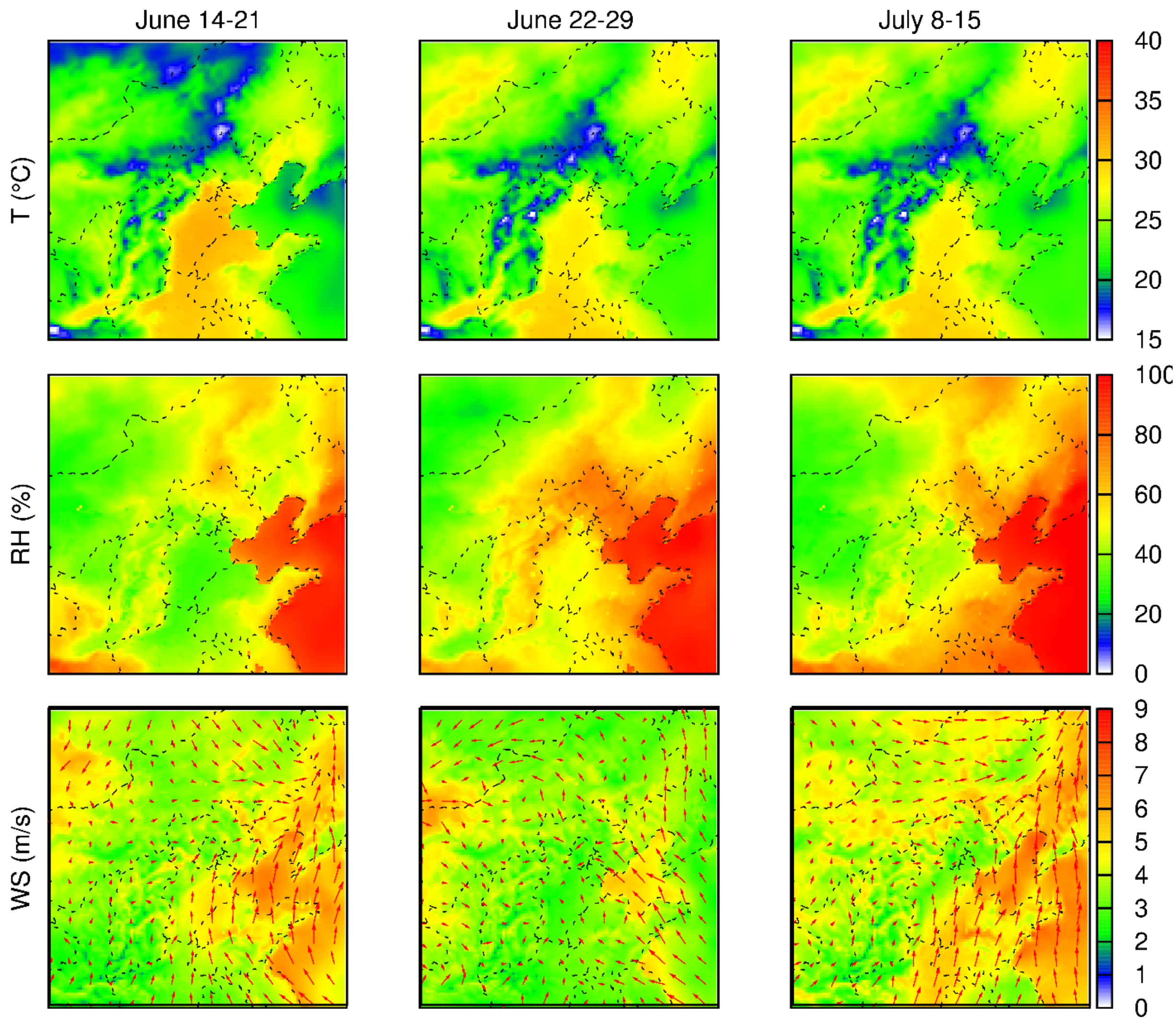

Figure 9. Meteorological conditions in NCP during 3 peak episodes. T represents temperature, RH represents relative humidity, WS represents wind speed, red arrows in the third row represent wind direction, arrow length represents wind speed.

Besides meteorological conditions, emission of O_3 precursors also help to explain high concentration occurrences in NCP. Figure 2 (right panel) shows the differences in NO_x and VOCs emissions between EDGAR+ and MEIC which are associated with differences in O_3 concentrations in these periods. As emissions are generated using weekly data so the emissions in three peak episodes are same (for five workdays and two weekend days). Significantly lower NO_x emission is noticed in south Hebei, north Henan and northwest and west Shandong in EDGAR+

while VOCs emission in these regions are not significant lower or ever higher than MEIC. High O_3 concentration in central NCP could mainly be due to NO_x emissions. lower NO_x leads to high O_3 concentration when VOCs emission is not too low. However, in Beijing and Tianjin, both NO_x and VOCs emissions in EDGAR+ are lower than in MEIC. As a result, EDGAR+ predicts lower O_3 in these regions. In south Shandong province, lower NO_x emission with higher VOCs emission barely change O_3 formation in these regions. Overall, since O_3 concentration is greatly dependent on emission of precursors, changes of NO_x and VOCs would influence O_3 concentration in different direction. Compared to MEIC, significantly lower (>200 tons/month) of NO_x and similar (difference within 5 tons/month) VOCs emissions in EDGAR+ induce more O_3 formation; less O_3 is predicted when both NO_x and VOCs emissions are significantly lower (>200 tons/month and >10 tons/month, respectively); O_3 concentrations are barely changed (within ±10 ppb) when NO_x emissions are significantly lower (>200 tons/month) and VOCs emissions are significantly higher (>10 tons/month) in EDGAR+. Due to nonlinear reactions of O_3 formation, NO_x and VOCs play different roles in forming O_3 under different conditions. It is concluded that a higher concentration is always associated with slight lower emission under high temperature, low RH and steady wind field. Though there might be some other reasons that could explain O_3 concentration variations such as solar radiation, cloud accumulation and concentration of particular matters (PM), analyzing impacts from changes of emissions and meteorological conditions helps to figure out the relationship between O_3 and its impact factors, which will provide deeper understanding of their impacts on forming and transporting O_3. It is also offered as evidence for designing strategies and policies to reduce O_3 pollution.

3.5 Conclusions

The WRF/CMAQ modeling system is applied to simulate O_3 concentrations in the NCP during summer 2017 and the results using EDGAR+ and MEIC are compared. Generally, both emission inventories perform well in predicting O_3 concentrations in major cities. Statistical metrices indicate that EDGAR+ performs better with fewer and smaller exceedances of suggested performance criteria compared to MEIC. EDGAR+ is slightly better in representing overall concentrations in NCP while MEIC shows better ability in predicting peak daily 8h-O_3 concentrations. EDGAR+ also shows higher accuracy in matching O_3 concentration in daytime. NO_x and VOCs emissions play different roles in forming O_3 under different conditions, and high concentrations are always associated with slightly lower emissions under high temperature, low RH and steady wind field.

CHAPTER 4. OZONE SOURCE APPORTIONMENT IN THE NCP

4.1 Introduction

With its adverse impacts on human health, ground-level O_3 is receiving increasing attention in recent years in China[14, 15, 69]. As one of the most polluted regions in China, the NCP is facing severe O_3 issues. A report pointed out that more than 50% of the days O_3 concentrations were higher than 80 ppb during 1983-1986 in central NCP (Beijing-Tianjin-Hebei region) with peak value of 170 pp[173]. Many studies also provided evidence that O_3 concentration increased from 1980 to 2003, with peak mixing ratio to be up to 286 ppb in Beijing in 2005[174, 175, 202]. A long-term station recorded O_3 concentration in the NCP also indicated an increase of 1.13 ppb/yr during 2003-2015[203]. Both long- and short-term analysis in the NCP show the increasing trend of O_3 concentration but not enough studies have analyzed O_3 and its sources. Thus, comprehensive analysis is necessary to better understand the impact factors and source of O_3 formation in this area.

Chemical transport models (CTMs) are widely used to simulate O_3 and understand its sources and impact factors. Source apportionment of O_3 is very important to quantify source contributions, which helps to design control strategies. But complex nonlinear reactions of O_3 precursors, nitrogen oxides (NO_x) and volatile organic compounds (VOCs), make it a challenge for model simulation. To determine O_3 contributions from NO_x and VOCs, ratios of photochemical chain reaction production rates, widely known as regime indicators, are introduced to classify O_3 contribution. Traditional two regime (2R) approach was implemented in the Community Multi-scale Air Quality (CMAQ) model [52] by applying indicator ratio of H_2O_2/HNO_3 with correlation coefficients ranging from 0.58 to 0.99. An improved method applied production ratio of

$(H_2O_2$+ROOH)/HNO_3 as the indicator in three regime scheme (3R) was introduced into CMAQ [53] and compared with traditional 2R method, and results indicated higher contributions from NO_x in high O_3 concentration regions in China by 5 to 15 ppb. 3R scheme was shown to provide more accurate O_3 contribution from its precursors[53]. Traditional O_3 Source Apportionment Method (OSAT) uses non-reactive tagged tracers in transport and reaction processes to track O_3 sources by splitting the concentration changes based on emission ratios[33]. An improved source-oriented method that applied in CMAQ using reactive-tracers in all processes are also used in O_3 source apportionment[34-36]. O_3 formation is strongly sensitive to concentrations of precursors, and its source contributions are varied spatiotemporally, thus improved source apportionment technique is necessary for more accurate results. In this study, improved source-oriented version of CMAQ combined with 3R scheme will be applied in simulating O_3 contribution from its precursors.

Due to the ability in irritating respiratory and cardiovascular system, O_3 causes cough, asthma, lung function reduction and other diseases. It was reported that 0.52% and 0.64% increases of daily mortality and cardiovascular/respiratory mortality are associated with 10 ppb increase of weekly O_3 concentration [204]. It was also reported that 10 $\mu g/m^3$ increases of 8h-O_3 were related to 0.42%, 0.44% and 0.50% increases of non-accidental mortality, cardiovascular mortality and respiratory mortality, respectively, in China[205, 206]. However, there are inusfficient studies focusing on O_3 source attribution to these human health risk.

This study will quantify O_3 contribution to sectoral/regional emissions of NO_x and VOCs by using source-oriented version CMAQ model with improved 3R scheme in NCP. Regional and city-scale analysis provide a comprehensive understanding of source impacts in high O_3 concentration season. Results from this chapter would provide O_3 source contribution for further analysis of O_3 impacts on human health, economic benefits and ecosystem.

4.2 Methods

4.2.1 Model description

O_3 concentrations are simulated by applying the CMAQ model (version of 5.0.1) with AERO6 aerosol chemistry mechanism and SAPRC99 photochemical mechanism[179, 207]. The Weather Research and Forecasting (WRF) version of 3.7.1 generates meteorological inputs by using initial condition (ICs) and boundary conditions (BCs) from WRF preprocessing system (WPS), which applies FNL operational global analysis data from National Center for Atmospheric Research (NCAR, http://dss.ucar.edu/datasets/ds083.2/). Meteorological inputs are converted to CMAQ ready format by using Meteorology-Chemistry Interface Processor (MCIP) v4.2. In this study, improved Emission Database of Gas and Atmospheric Research (EDGAR+), which is validated in previous chapter, provides anthropogenic emissions from sources of agriculture, residential, energy, industrial, off-road and on-road. Biogenic emissions are provided by the Model for Emissions of Gases and Aerosols from Nature (MEGAN) [184], and Fire Inventory from NCAR (FINN) [185] is used to generate open-burning (wildfires) emissions. NO_x and VOCs emission from these sectors in NCP are shown in Figure 10 and Figure 11.

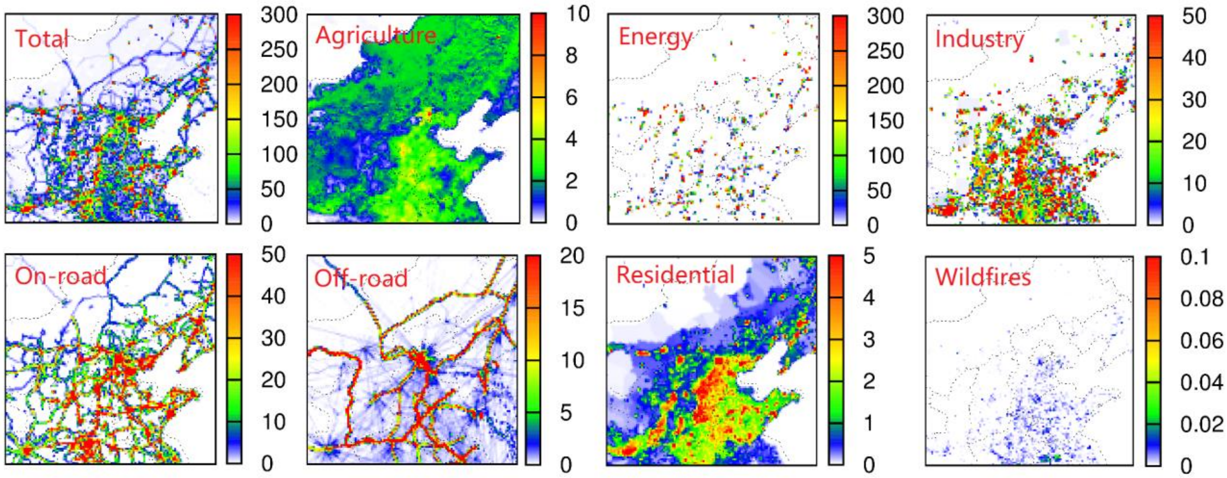

Figure 10. Averaged sources of NO_x emissions in NCP 2017 summer. Units are tons/month.

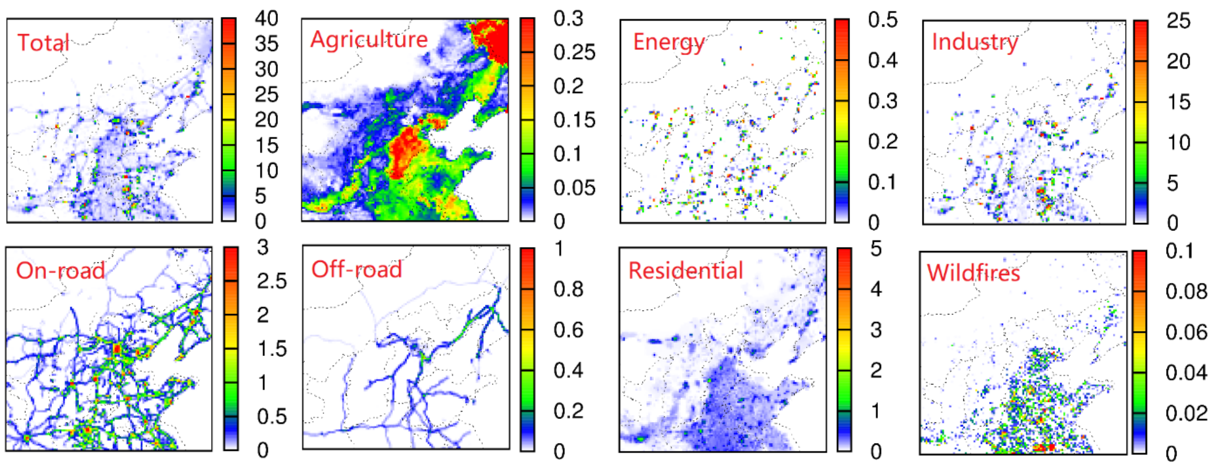

Figure 11. Averaged sources of VOCs emissions in NCP 2017 summer. Units are tons/month.

Tagged tracers are introduced into source-oriented version CMAQ in this work, which have been successfully applied in many previous studies[134, 208, 209]. Generally, atomic oxygen (O(3P)) that created in photochemical reaction between O_3 precursors are tagged for each emission sources following reactions, which are recorded in previous works [135].

Equation 12:

$$NO_{2_n} \xrightarrow{hv} NO_n + O(3P)_n \,, n = 1,2,3 \ldots, N$$

Equation 13:

$$O(3P)_n + O_2 \rightarrow O_{3_n}, n = 1,2,3 \dots, N$$

Equation 14:

$$RH_n + HO \rightarrow RO_{2_n} + H_2O, n = 1,2,3 \dots, N$$

Equation 15:

$$RO_{2_n} + NO \rightarrow NO_{2_n} + RO_n, n = 1,2,3 \dots, N$$

Where n represents the identification number of emission source, N represents total number of emission sources. NO_2 and NO are tagged for tracking NO_x attribution while reactive hydrocarbon (RH) are tagged for VOCs. Contribution rate (R) from NO to NO_2, which is from attribution of RO_2, can be calculated and presented as O_3 contribution from VOCs as shown in Equation 16 and Equation 17. F_n represents contribution from source n, and O_{3tot} in this equation stands for net O_3 formation predicted in model. O_3 contribution from source n can be calculated following Equation 17 by adding these functions in air quality models.

Equation 16:

$$F_n = \frac{R\left(NO_{2_n}\right)}{R\left(NO_{2_{tot}}\right)}, n = 1,2,3 \dots, N$$

Equation 17:

$$O_{3_n} = F_n * O_{3_{tot}}, n = 1,2,3 \dots, N$$

Besides source attribution, O_3 also sensitive to concentration of its precursors. Traditional approaches classified O_3 sensitivity to NO_x and VOCs to NO_x-limited, VOCs-limited and 2 regime scheme (2R) when the indicator ratio of $PH_2O_2/PHNO_3$ is ~0.35[52]. An improved 3 regime (3R) scheme, which is approved provides higher accuracy in predicting O_3 contribution from NO_x and

VOCs in high polluted region in China, will be applied in this work. The indicator in this scheme is defined between 0.047~5.142[53], O_3 production in this regime is classified contributions from both NO_x and VOCs.

4.2.2 Model application

O_3 concentrations are simulated using the CMAQ model v5.0.1 with a coarse domain (36km×36km) covering China (Figure 12) and nested finer domain (12km×12km) covering the NCP, including complete Beijing, Tianjin, Hebei, Shandong and Shanxi and partial of Henan, Jiangsu, Anhui, Inner Mongolia and the three northeast provinces. Both sectoral and regional source apportionment will be conducted in this work. Based on classification in EDGAR+ (improved version of EDGAR as in Chapter 2), biogenic and open-burning sources, emissions are grouped into 8 sources, including agriculture, energy, industrial, residential, on-road, off-road, biogenic and wildfires.

Regional tracers are based on 9 provincial groups as shown in Figure 12, including Beijing, Tianjin, Hebei, Shandong, north (Heilongjiang, Liaoning, Jilin and Inner Mongolia), West (Shaanxi, Shanxi, Xinjiang, Ningxia and Qinghai), YRD (Zhejiang, Jiangsu and Shanghai), central China (Henan, Hubei, Anhui) and others (emissions from other countries and the rest provinces in China). It should be noted that only Beijing, Tianjin, Hebei, Shandong and Shanxi are fully included in the finer domain, thus emission tracers are tagged only on emissions that are involved in this domain.

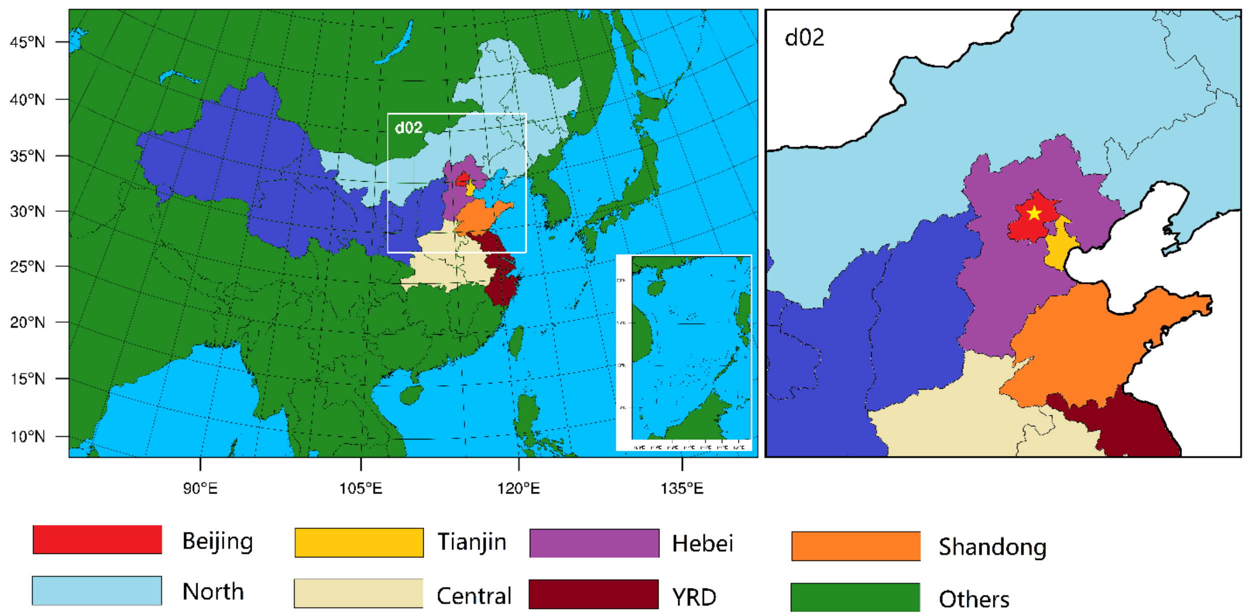

Figure 12. Simulation domains and regional classifications for emissions. Coarse domain (36km by 36km) covers mainland China and part of surrounding countries. NCP (d02) is included as the finer domain (12km by 12km).

To compare results using different O_3 regime schemes, four scenarios are created to evaluate O_3 contributions from sectoral emission sources. O_3 regime schemes of 1) 3R scheme; 2) 2R scheme; 3) NO_x-limited scheme and 4) VOCs-limited scheme are applied in source-oriented simulation with same domain and mechanism settings.

4.3 Results and discussions

4.3.1 Overall O_3 in coarse and finer domains

O_3 concentrations in this chapter are generated from CMAQ using same mechanism and settings as in Chapter 2, O_3 source-oriented technique makes no change to overall O_3 predictions, thus model performances are validated, and the results are reliable for further analysis. In Figure 13, summertime 8h-O_3 concentration and its contribution from background (BG) and emissions (EM) in coarse domain are illustrated. It is obvious that NCP and YRD are in the highest

concentration region with more than 80 ppb in summertime. Concentrations in west and south China are lower than 50 ppb except in the Sichuan Basin (~60 ppb), which is known as another high-risk area [210]. From this simulation, most O_3 formation in low concentration area attributes to BG, while anthropogenic and natural emissions have higher contributions to NCP and YRD by more than 50 % (> 40 ppb) of total 8h-O_3. Emissions play the essential roles in NCP, thus sectoral and regional (provincial) contributions are investigated in following sectors.

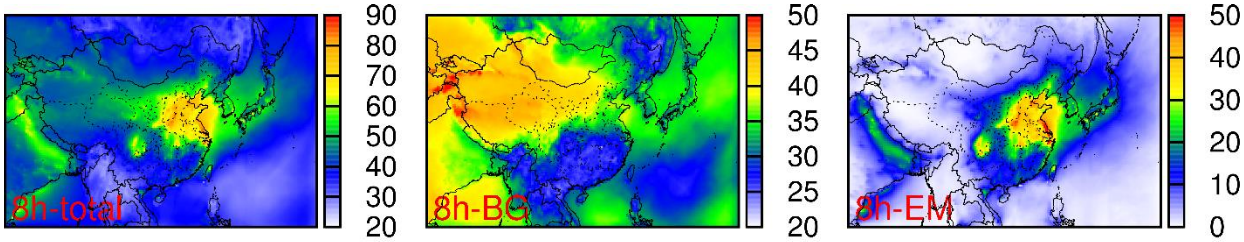

Figure 13. Summertime 8h-O_3 concentration in China and their contribution from background (BG) and emissions (EM). Units are ppb.

From Figure 14, YRD, Shandong and Hebei are major sources to NCP, they contribute around 20 ppb to surrounding regions and attribute maximum of 35 ppb locally. Though Beijing and Tianjin have limited city area, emissions from these cities also cause maximum of 20 ppb to local concentration. Contribution from north, central and other regions barely account for high concentration in NCP. Sectoral contribution (Figure 15) reveals that energy and industry are major sources (15-20 ppb) in NCP, followed by on-road (5 ppb) and biogenic emissions (5ppb). Emissions from other sources provide limited O_3 in NCP. It is concluded that emissions have strong effects in NCP and their contributions to O_3 are complicated, thus comprehensive analysis for finer resolution is needed for more clear understanding.

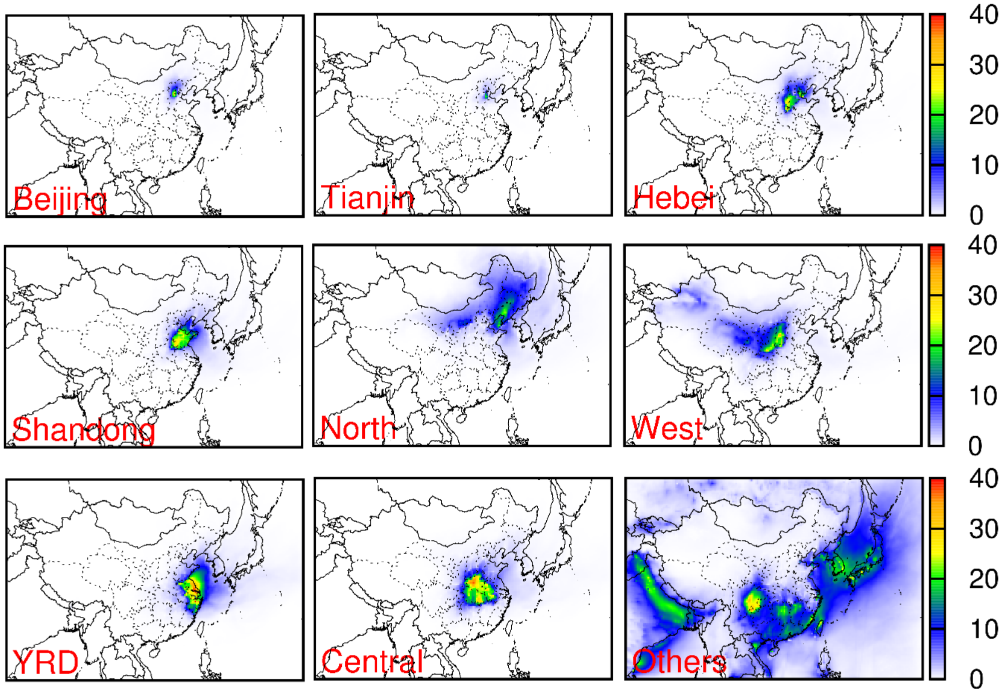

Figure 14. Summer 8h-O_3 contribution from regional emission sources in China. Units are ppb.

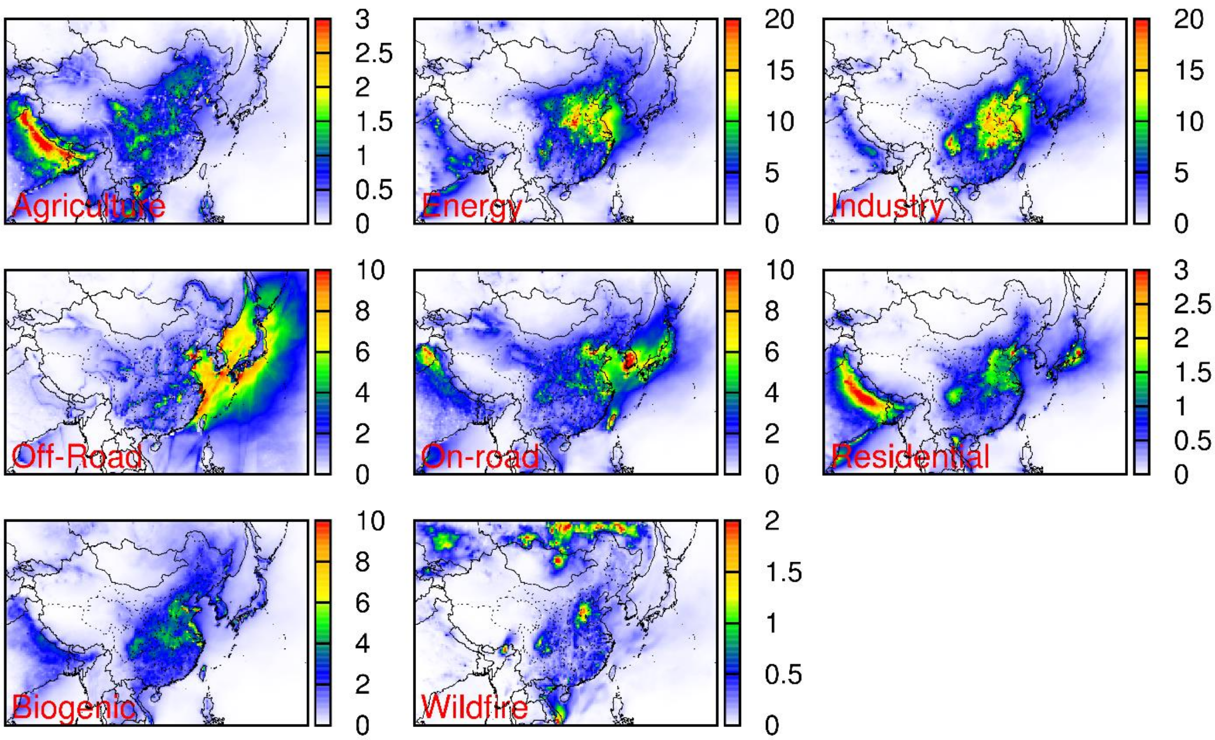

Figure 15. Summer 8h-O_3 contribution from sectoral emission sources in China. Units are ppb.

Figure 16 shows summertime 8h-O_3 concentration in NCP and its contributions from BG and EM. Generally, O_3 is high in central NCP with ~80 ppb (maximum of ~90 ppb at southwest Hebei and north Henan province). High concentration also occurs in Beijing which is the capital city of China. Background O_3 is high in northwestern NCP (~40 ppb) rather than central region (30 ppb). At the meantime, emissions attribute ~40-50 ppb (~ 50% of total O_3) to central NCP, where the concentration is high, but less contributions are illustrated in surrounding regions with lower than 35 ppb (~30%). High contributions from EM are found in Beijing, southwestern Hebei and northwest Henan with maximum contributions are more than 50 ppb (> 50%). It is concluded that high concentrations in central NCP are mainly due to emissions rather than background O_3. Emissions lead high concentration in NCP, thus comprehensive analysis is needed. Regional and sectoral contribution will be analyzed in following sectors.

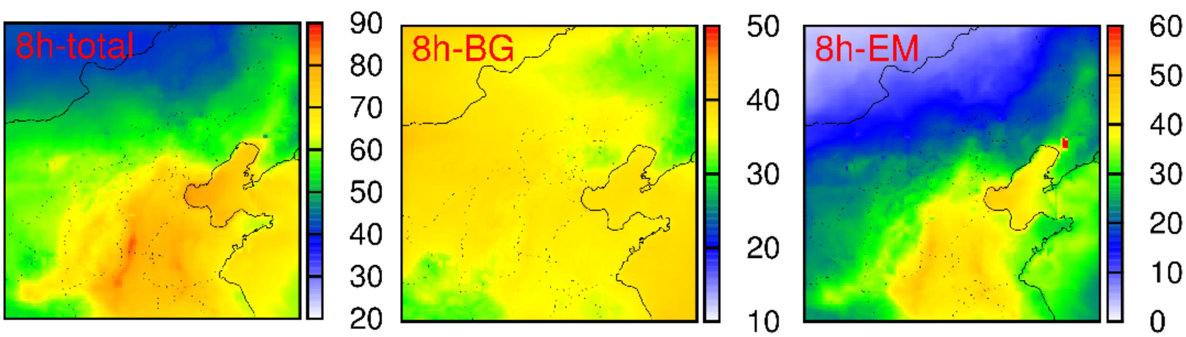

Figure 16. Summertime 8h-O_3 concentration in NCP and their contribution from background (BG) and emissions (EM). Units are ppb.

4.3.2 Sectoral and regional contribution

Figure 17 reveals sectoral contributions to summertime 8h-O_3 concentration. Industry and on-road emissions are major sources in the NCP. Industry contributes to more than 50% (maximum of ~24 ppb) to O_3-EM in central NCP (southern Hebei, Shanxi and western Shandong), which accounts for more than 25% of total 8h-O_3 in these regions. On-road emissions account for ~30%

of O_3-EM in Beijing, Tianjin and central Hebei with maximum of ~50% (~10 ppb). High contributions from energy sector are found at specific cities and regions in southern and southwestern NCP by ~16 ppb, which accounts for maximum of 30% to total O_3. Off-road emissions contribute ~6 ppb to O_3 along inland water channels in NCP and cause more than 10 ppb O_3 above sea surface east to NCP. Residential, agriculture and biogenic emissions cause less than 5 ppb in NCP, respectively. Wildfires also have low contributions except in south western Hebei with maximum of ~5 ppb.

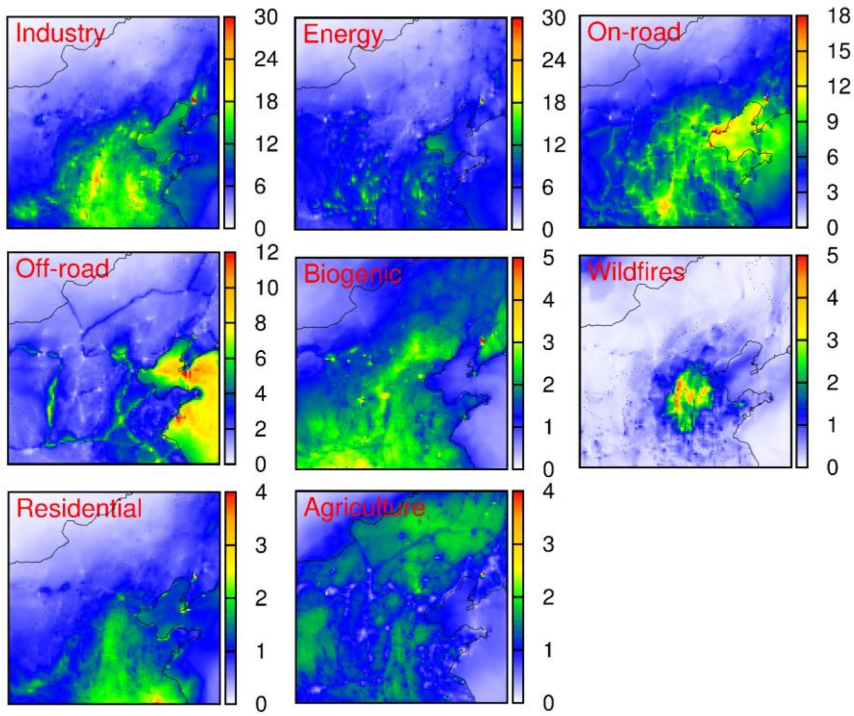

Figure 17. Summertime 8h-O_3 contribution from sectoral emissions in NCP. Units are ppb.

Figure 18 reveals regional contributions to summertime 8h-O_3 concentration. O_3-EM is generally affected by local emissions. For example, high concentrations in south Hebei, west Shandong, Shanxi and north Henan are greatly dependent on local emissions (~70%) except O_3 from background. Local emissions induce ~20 to 30 ppb O_3 in high concentration region (with maximum of ~35 ppb). It is noted that local emissions in Beijing and Tianjin provide maximum

of 20 ppb to local O_3 formation, and they induce limited effects on each other (less than 5 ppb). Due to being surrounded by Hebei, Beijing and Tianjin are affected by emissions from Hebei significantly with 10% of total O_3 from Hebei emissions (~10 ppb). Other provinces in NCP also result in slightly effects on O_3 formation in Beijing and Tianjin (less than 5 ppb). Local emissions always result in 10 ppb O_3 formation in conjunction area between neighbor provinces. At the meantime, effects from long-distance transport are also observed. For instance, emissions in YRD induce ~10 ppb O_3 in whole southwestern Shandong and contribute to ~5 ppb O_3 in southeastern Hebei. Emissions from central China also affect O_3 concentration in NCP by ~5 to 10 ppb. Emissions from other regions (the rest provinces in China and other countries) have limited impacts in NCP, but they affect O_3 formation above ocean surface east to NCP by ~10 ppb.

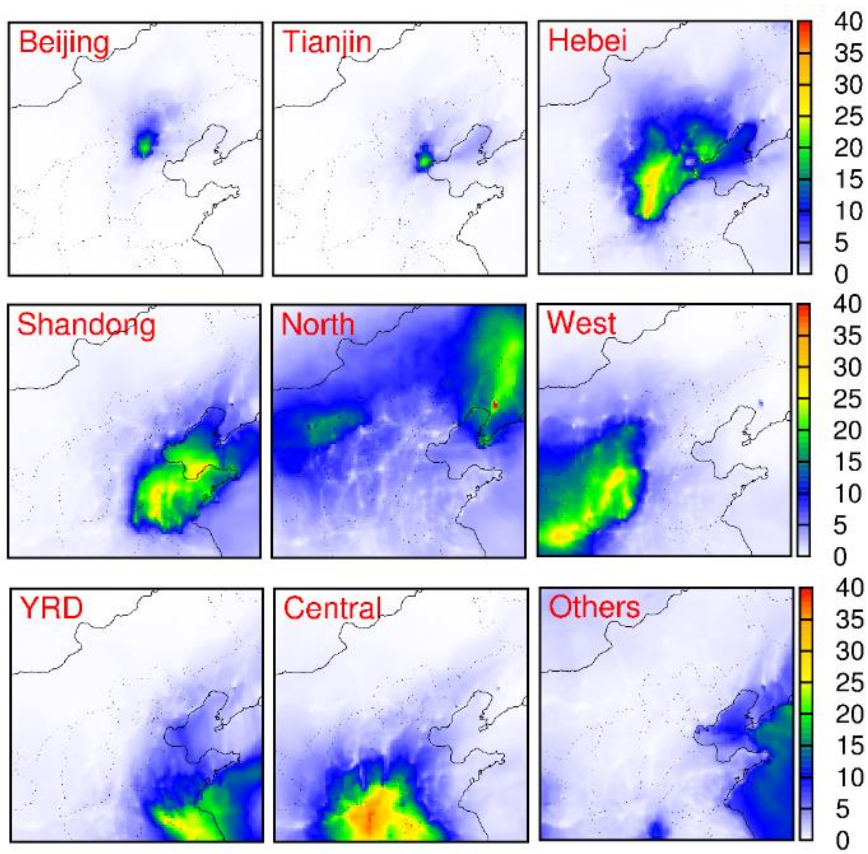

Figure 18. Summertime 8h-O_3 contribution from regional emissions in NCP. Units are ppb.

4.3.3 Source apportionment of O_3 precursors

O_3 contributions from total NO_x and VOCs emissions are shown in Figure 19. Generally, NO_x accounts for more than 50% (maximum of ~80%) O_3-EM in most provinces except Beijing and Tianjin. NO_x contributes to more than 25 ppb O_3 formation in NCP, high contributions occur in central NCP, which refers to south Hebei, north Henan and west Shandong with contributions are evaluated to ~40 ppb. It is concluded that NO_x is the major precursor in most NCP while opposite phenomenon is observed at Shijiazhuang and southwestern Tianjin where VOCs dominates O_3 formation with more than 20 ppb while NO_x induces ~10 ppb only. VOCs emissions also dominate in specific cities such as Tianjin, Shijiazhuang, Baoding and Qingdao. VOCs contributes less than 10 ppb to O_3 in NO_x dominant regions. O_3 contributions from NO_x and VOCs emissions (by sectoral and regional groups) are detailed analysis from following discussions.

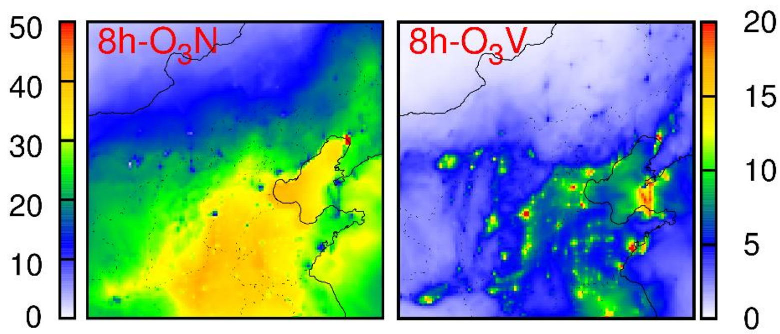

Figure 19. summer 8h-O_3 contribution from NO_x (8h-O_3N) and VOCs (8h-O_3V) in NCP. Units are ppb.

Figure 20 shows regional contribution of summertime O_3 from NO_x and VOCs. Consisted with previous discussion, local emissions (both NO_x and VOCs) dominate local O_3 formation. NO_x contributes more than 20 ppb to local O_3 in high concentration regions such as south Hebei, north Henan and west Shandong, which account for ~70% of total O_3-EM in these regions. It is noted that local NO_x emissions also have significantly impacts to surrounding provinces and regions. For

example, NO_x emissions from YRD induce ~5 to 10 ppb O_3 in Shandong, which accounts for approximately 20% of O_3-EM. NO_x dominant O_3 formation lead high concentration in NCP for most provinces except in Beijing and Tianjin. NO_x accounts maximum of 40% O_3-EM in Beijing while NO_x emission from Hebei accounts for 20%. VOCs emission affects less in most NCP compared with NO_x while VOCs also accounts for more than 30% of total 8h-O_3 in specific regions such as south Tianjin, Shijiazhuang, Tangshan, Taiyuan and Datong. Efforts from VOCs emissions are much more significantly than NO_x, thus VOCs dominates O_3 formation in these regions.

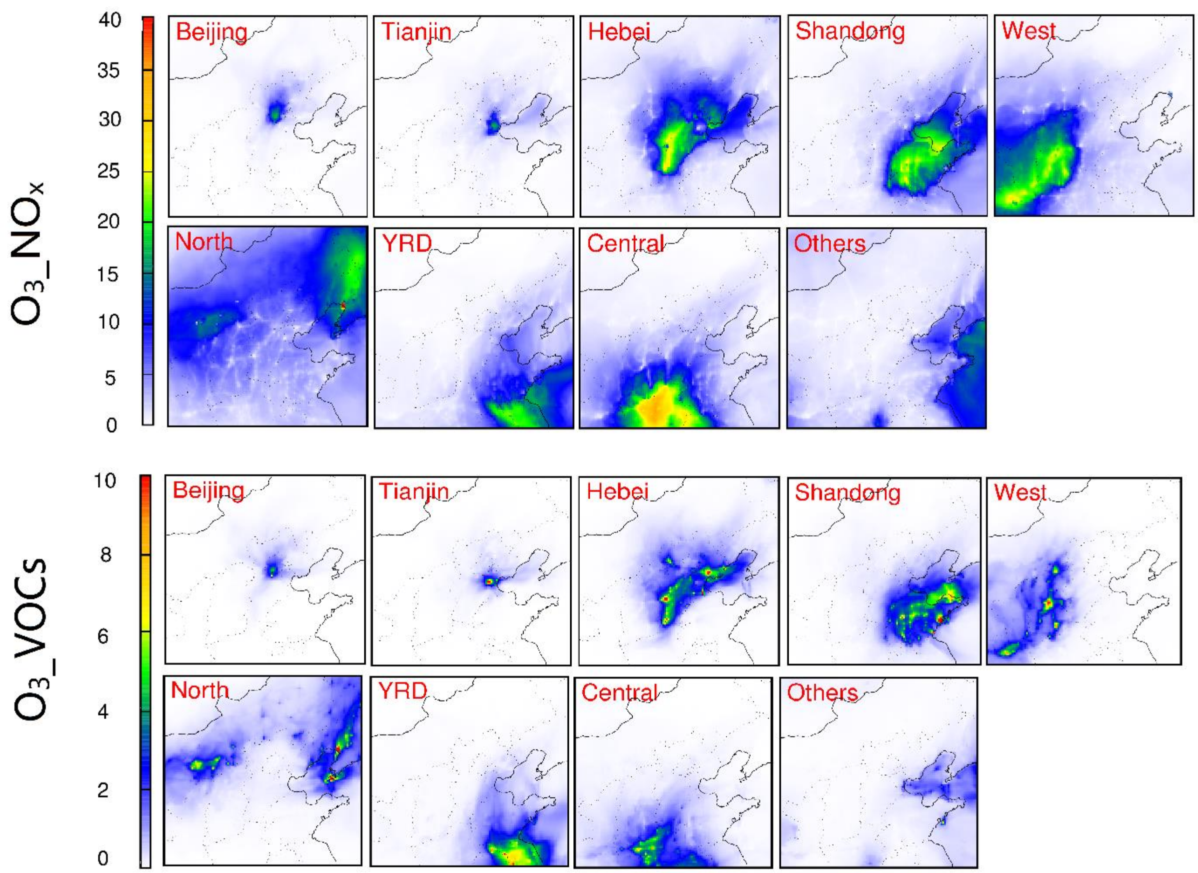

Figure 20. Summertime NO_x and VOCs regional contributions to 8h-O_3 concentration. Units are ppb.

Sectoral source apportionment results (Figure 21) reveal that O_3 is mainly relied on NO_x emissions from all sources except biogenic emissions. Industry emissions induce maximum of ~20

ppb O_3 formation related to NO_x in central NCP. NO_x emissions from energy sector also induce ~15 ppb in cities in south NCP. NO_x emissions from on-road and off-road transportation form ~6 and ~9 ppb O_3 in NCP, respectively. It is noted that they also form more than 10 ppb O_3 above sea surface east to NCP. VOCs emissions barely result in O_3 formation (less than 2 ppb) for most sources except the emission from industry and biogenic. VOCs emissions from industry cause 5 to 10 ppb O_3 in specific cities such as Tianjin and Qingdao. High VOCs emissions from industry and on-road transportation help to explain their contributions to O_3 formation. Overall, NO_x emissions from industry, energy and on-road transportation contribute to greatly in NCP, they provide ~75% of O_3-EM, which account for ~40% of total O_3 in NCP.

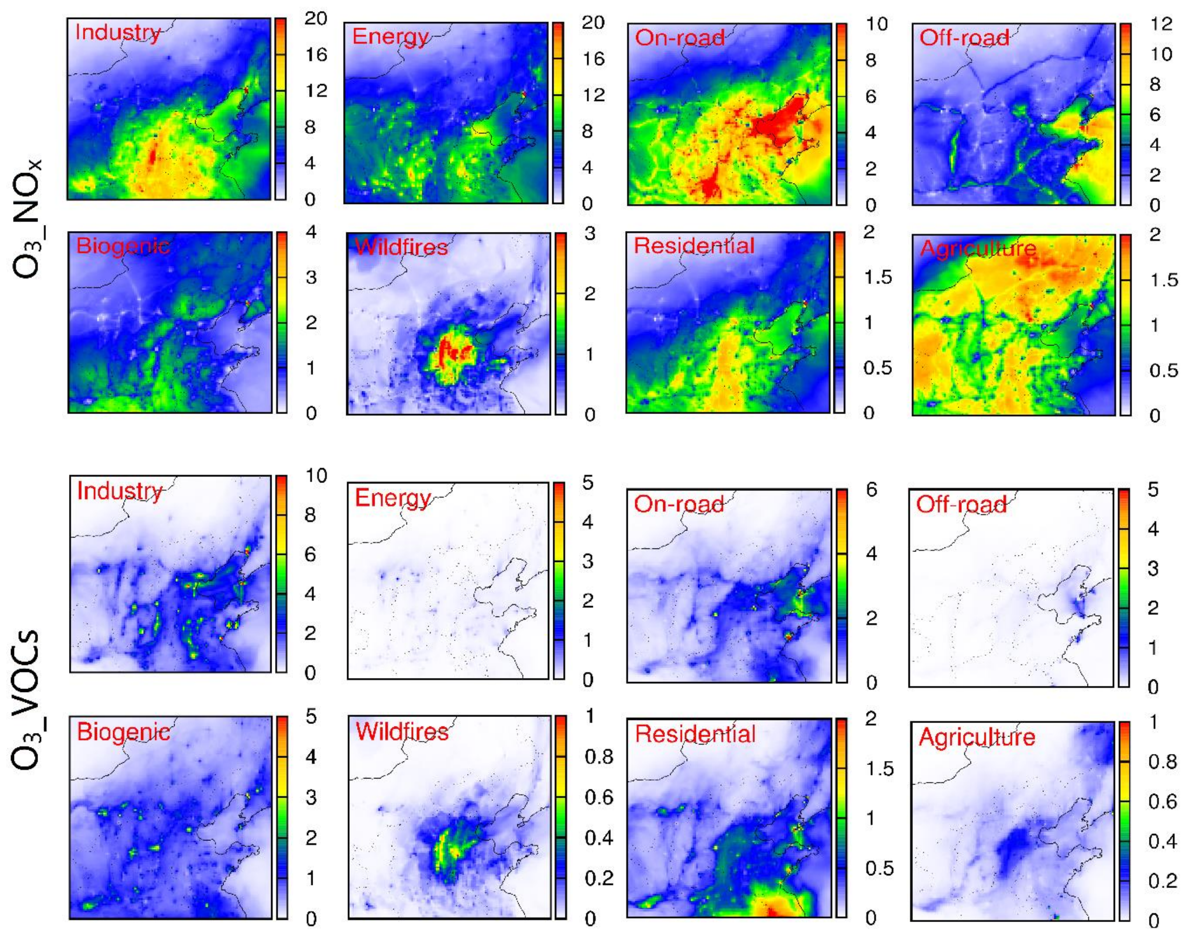

Figure 21. Summertime NO_x and VOCs sectoral contributions to 8h-O_3 concentration. Units are ppb.

4.3.4 Comparison of 3R and other O_3 regime schemes

O_3 contributions from NO_x and VOCs are calculated using different source analysis techniques. In 3R scenario, NO_x and VOCs related O_3 formations in transition regime are classified into O_3N and O_3V already, respectively. The concentrations and differences between each scenario are shown in Figure 22. Basically, four source-oriented approaches predict same total O_3 concentration in NCP, different attributions to NO_x, VOCs and background compared with 3R are shown. In first row, results from 3R indicate that high O_3 concentrations are always occurred in central NCP while north and northwest regions are under low concentration.

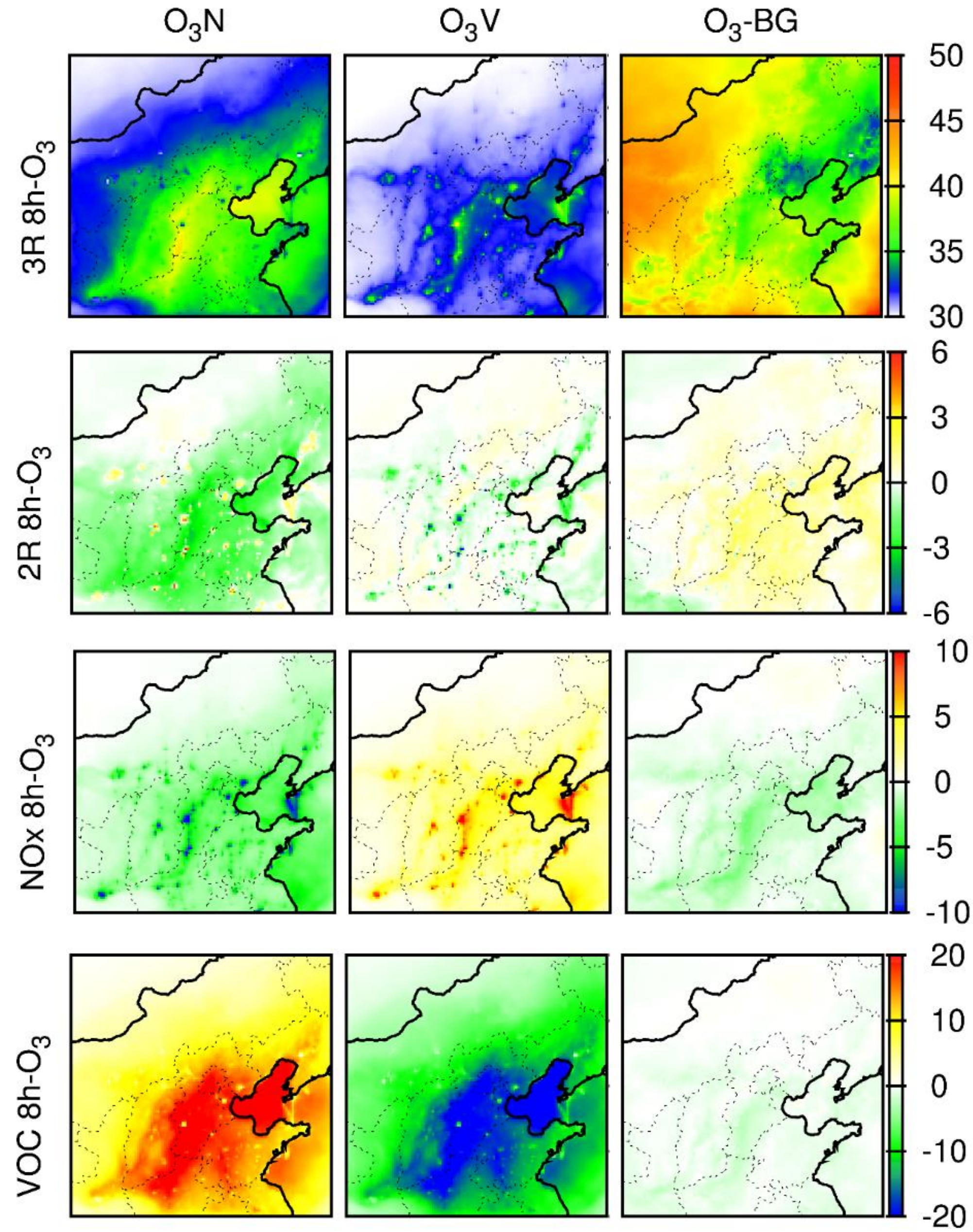

Figure 22. 8h-O_3 contributions from NO_x (O_3N), VOCs (O_3V) and background (O_3-BG) in the 3R scenario (first row) and differences with 2R, NO_x-limited and VOC-limited scenarios (subtracting 3R by the results from each case). Units are ppb.

Due to O_3 formations in NO_x- and VOCs-limited cases only due to NO_x and VOCs, thus the differences with 3R are significant. O_3V in VOCs-limited case is much higher (>20 ppb) than in 3R widely in central NCP as well in surface of Bohai Sea. At the meantime, same situation

happens to NO_x-limited case where O_3 formation is due to NO_x only, thus O_3V is significantly lower than in 3R. It is worthy to note that the differences between 3R and 2R provides interesting findings. Generally, 3R predicts lower O_3 contributions from NO_x emission in NCP except in cities such as Tianjin, Shijiazhuang and Taiyuan where more O_3 formation (~6 ppb) are classified as to from VOCs emissions. As results, 2R predicts more VOCs dominant cities than 3R, O_3 contributions from VOCs are increased in these cities in 2R. Compared to single precursor limited approaches, 3R predicts lower background O_3 by ~ 5 ppb in central NCP. However, 2R has even ~3 ppb lower than 3R in these areas. Due to higher accurate O_3 regime scheme that applied in China, source apportionment results from this work indicate more contributions from NO_x and less from VOCs in major cities in NCP, these results help to better quantify impacts from emission sources and for more accurate further analysis in O_3-related impacts on human health, economic benefits and ecosystem.

4.3.5 City scale analysis

Source apportionment analysis in major cities provide detailed evidences for controlling strategies. Emissions and background contributions to total 8h-O_3 in 8 NCP major cities are shown in Table 11. Long-term urbanization and industrial development cause high contribution from background O_3 in NCP[211], which accounts for ~50% of total O_3 in these major cities. However, as result of increasing emissions of O_3 precursors (NO_x and VOCs) [152, 212], O_3 contributions from emissions are nonnegligible. Emissions induce ~ 45% to 52% of total O_3 in major cities except in Datong where emissions only account for 35% of total O_3. There are three peak episodes observed in study period as discussed in chapter 2. O_3 contributions from background O_3 in these periods are slightly higher while significant contributions from emissions are estimated as shown in Table 12. In all studied cities, high O_3 concentrations are associated with emission sources which cause

more than 50% of total O_3 formation (with maximum ~60% in Jinan and Taiyuan). It is concluded that high pollution episodes are mainly due to emissions rather than background O_3 contributions. Sectoral source apportionment results (Figure 23) indicate industrial emission is the major source of O_3-EM, which results in more than 10 ppb O_3 (more than ~33% of O_3-EM, and maximum of 58% (Tianjin)). On-road and energy emissions also strongly affect O_3 concentration. They account for more than 70% (maximum of ~85%) O_3-EM in major cities together with industrial emission. Industry and on-road emissions account for ~65% of total O_3 in Beijing as the results of high population and emissions from mobile vehicles. It is noted that on-road emission has similar attribution as industrial emissions in Beijing while it accounts significantly less in other major cities. Energy emissions in Jinan has similar attribution as industrial emissions while on-road emission has less impact on total O_3-EM. Wildfires, agriculture, residential and biogenic emissions are always having low impacts. Sectoral contributions in high concentration episodes reveal that high O_3 concentration in these periods are caused greatly from emission sources, which cause large amount of O_3 formation. More than 50 % of total O_3 (more than 50 ppb) are estimated from emission sources (as shown in right panel for each city in Figure 23). High emission contributions are mainly caused from industry and energy emissions. In all major cities except Datong and Baoding, contribution from industry emissions are increased by ~30 to 50% in high concentration period, which refers to maximum of 10 ppb. Contributions from energy emissions are estimated to more than twice in Baoding and Tangshan compared with regular summertime. It is also noted that contribution from wildfire emissions also has obvious increase in Beijing.

Table 11. Summertime 8h-O_3 contribution from background and emissions. Units are ppb.

8h-O_3	Beijing	Tianjin	Shijiazhuang	Baoding	Tangshan	Jinan	Datong	Taiyuan
Total	73.04	71.89	72.80	74.96	68.8	77.63	60.93	72.18
BG	37.54	38.21	38.69	37.52	37.27	36.53	39.27	38.87
EM	35.5	33.68	34.11	37.44	31.53	40.90	21.66	33.31

- EM: O_3 contribution from emissions; BG: contribution from background

Table 12. 8h-O_3 concentration and its contribution from background and emissions in peak episodes. Units are ppb.

8h-O_3	Beijing	Tianjin	Shijiazhuang	Baoding	Tangshan	Jinan	Datong	Taiyuan
Total	96.55	94.24	93.59	94.01	95.57	91.92	66.3	98.05
BG	41.54	42.48	41.72	41.56	40.22	37.19	39.8	40.24
EM	55.01	51.76	51.87	52.45	55.35	54.73	26.5	57.81

- EM: O_3 contribution from emissions; BG: contribution from background

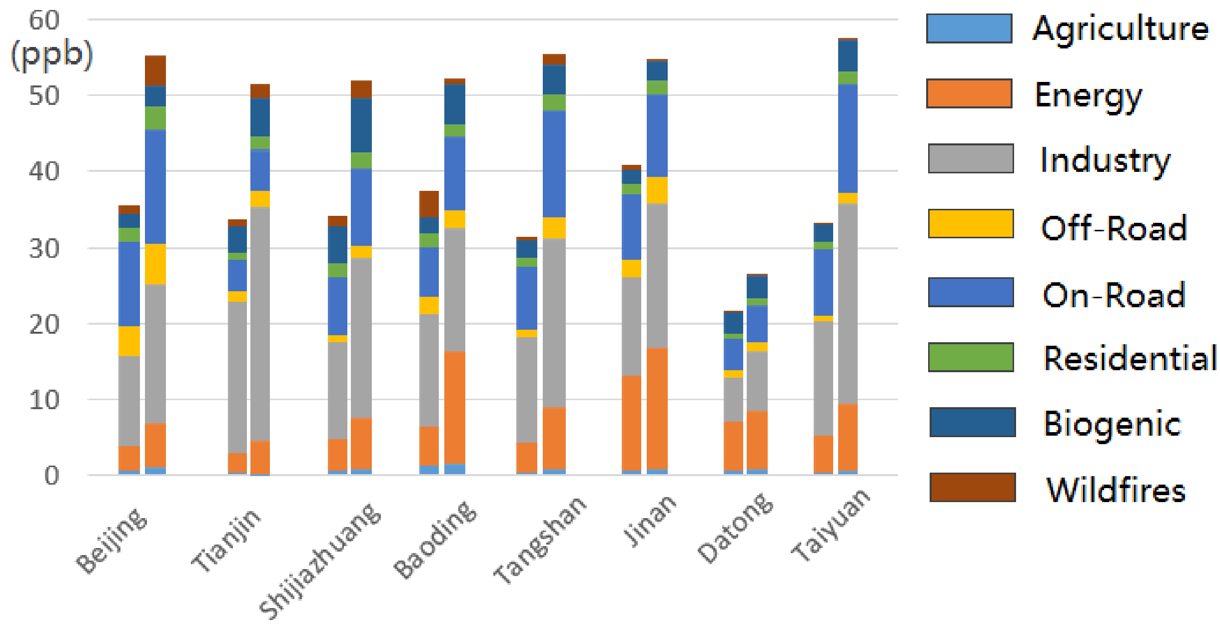

Figure 23. 8h-O_3 contributions from sectoral emissions in major city in summertime (left column) and peak episodes (right column). Units are ppb.

Regional source apportionment (Figure 24) reveals the similar results as other studies that local emission would be the major source of O_3-EM. However, impacts from surrounding regions are also nonnegligible. For example, local emission in Beijing accounts for 50% of O_3-EM while emissions from Hebei also induce ~20% of them. Being Surrounded by Hebei makes Beijing very sensitive to emissions from Hebei. However, Tianjin has different situation even if it is also surrounded by Beijing and Hebei. O_3-EM in Tianjin are mainly due to local emissions but less to emissions from surrounding regions. It might be because the geophysical characters in Tianjin that emissions from Hebei and Beijing will be limited locally or spread to ocean surface southeast to Tianjin. Further analysis in needed in future for this. Emissions from north and central China also has slight impacts on O_3-EM in NCP with ~2-6 ppb. Analysis of regional source apportionment indicates an interesting finding. Though contributions from local emission increased, emissions from central China have strong impacts on increasing O_3 concentration in central, south and

southwestern NCP such as in Beijing, Shijiazhuang and Baoding. Contributions from central China are increased to ~10 ppb in these cities. However, emissions from YRD has significant impacts in eastern NCP which refers to Tianjin, Tangshan and major cities in Shandong such as Jinan. Contributions from YRD emissions and local emissions cause high O_3 concentration in these episodes. It is also concluded that emissions from Beijing and Tianjin have less impacts on each other in high concentration events but only induce local increases of O_3 concentration.

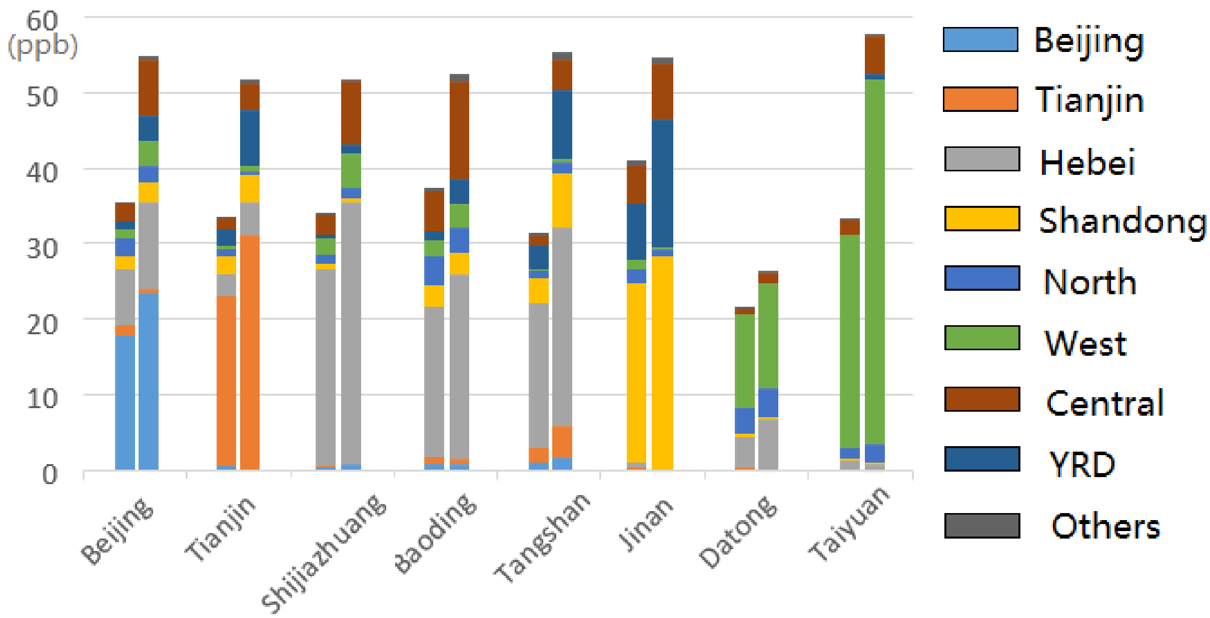

Figure 24. 8h-O_3 contributions from regional emissions in major city in summertime (left column) and peak episodes (right column). Units are ppb.

4.4 Conclusions

This work applies source apportionment method in simulating O_3 concentration and its contributions from natural and anthropogenic emission in NCP for 2017 summer by using source-oriented version of WRF/CMAQ modeling system. Comparison of results from different source apportionment methods indicates the advanced source-oriented method with improve 3R regime scheme increase the accuracy of source apportionment results. Sectoral and regional source

apportionment analysis indicate that industry, energy and on-road emissions are the major sources. Contributions from on-road and industry are significantly increased in peak episodes. Local emissions and emissions from surrounding regions are main sources of O_3 formation. Emissions from central China have significant impacts in Beijing, central, south and southwestern NCP while Tianjin, eastern NCP are more associated with emissions from local and YRD. This work provides information for estimating regional and sectoral contributions to O_3 pollution, which helps to deeper understand the sources of high O_3 concentration. It also offers solid evidences for further estimation of health risk. An effective emission controlling strategies can be designed based on results of this work to reduce O_3 concentration in future.

CHAPTER 5. OZONE SOURCE APPORTIONMENT IN SOUTHEAST U.S.

5.1 Introduction

O_3 is a secondary pollutant which is associated with a long-standing air quality problem in the U.S. for decades. Though O_3 concentration has significantly decreased through efforts from reducing anthropogenic emissions, many nonattainment events are observed over the U.S., and the O_3 concentration has remained higher than NAAQS requested threshold of 70 ppb in some regions [213] [26, 55, 214]. Many studies analyzed O_3 variation trends and impact factors in high concentration area over the U.S. A springtime increases of O_3 concentration were reported in western U.S. rural area by 0.2-0.5 ppb, while the increases were recorded in wintertime over eastern U.S.[215]. Dry deposition was revealed as the primary sink for O_3 and it was estimated to be increased in southeastern U.S.[216]. The increased air stagnation also induced significantly positive effect to raise O_3 concentration associated with dry tropical weather in midwestern U.S.[217]. Global warming trend was proved to induce high O_3 concentration events in mid-Atlantic region of the U.S. under a 30-years historical analysis[218].

Increasing concern of O_3 pollution requires researcher to analyze sources of O_3 formation. Background O_3 concentration was estimated to shift maximum O_3 event to early summer, and its contribution from global anthropogenic emission was estimated to be increased over the past decades especially in western U.S.[26, 219]. Decreases of emission of NO_x and VOCs cause a reduction of averaged ambient O_3 concentration by ~22% since 1998 [220]. BVOC emission was reported as the major source of VOCs emission in the U.S., which accounted for 75% to 80% of total VOCs emissions. BVOC was classified as a significant contributor to regional O_3

concentration in SUS[118, 221]. In peak episodes, reductions of NO_x emissions from mobile vehicles and point source were estimated to cause the largest reductions O_3 concentration in Texas, U.S.[222].

O_3 formation is very sensitive to emissions of precursors, thus many approaches were applied to quantify the O_3 source contributions from NO_x and VOCs. BVOC was estimated as the major precursor of O_3 formation for extreme O_3 events in SUS[223]. But contributions from other sources are not well studied. This work aims to quantify O_3 sensitivity to precursors and contribution from all emission sources, which will provide information to estimate health impacts, economic benefits and further emission controlling strategies to reduce O_3 concentration so that to match NAAQS requested threshold.

5.2 Methods

5.2.1 Model description

O_3 concentration and its contributions from emission sources are simulated by applying the CMAQ model (version of 5.0.1) with SAPRC99 photochemical mechanism and AERO6 aerosol chemistry[179, 207]. Meteorological conditions are generated by the Weather Research and Forecasting (WRF) version of 3.7.1 with initial condition (ICs) and boundary conditions (BCs) from WRF preprocessing system (WPS), which is obtained from FNL operational global analysis data from National Center for Atmospheric Research (NCAR, http://dss.ucar.edu/datasets/ds083.2/). Emission Database of Gas and Atmospheric Research (EDGAR) provides anthropogenic emission of 2012 and they are scaled to 2016 based on EPA National Emission Inventory (NEI) Technical Support Document (TSD) (https://www.epa.gov/air-emissions-inventories/2014-national-emissions-inventory-nei-technical-support-document-tsd) which includes variation trends of NO_x and VOCs emissions for each sector from 2012 by state scale. Scale factors for NO_x and VOCs emissions in SUS are list in

Figure 14 and Figure 15. Biogenic emissions for 2016 are provided by the Model for emissions of Gases and Aerosols from Nature (MEGAN) [184], and Fire Inventory from NCAR (FINN) [185] is used to generate open-burning (wildfires) emissions for simulation period. O_3 source-oriented method is applied in tracking O_3 contribution from emission sources by tagging reactive NO_x and VOCs tracers as descripted in chapter 3[134, 208, 209]. Benefits Mapping and Analysis Program (BenMAP) model helps to analyzes health impacts associated with O_3 by applying functions recruited from the published epidemiology literature. These functions calculate health impacts by used value of pollutant concentrations, population, incidence baseline rates and coefficients for different health endpoints, which are from simulation results (pollutant concentration) and BenMAP database, respectively, in every grid in study domain.

Table 13. Scaling factor for NO_x emissions for major states in SUS.

	LA	AR	MI	TN	AL	GA	FL	NC	SC
Energy	0.77	0.83	0.45	0.70	0.45	0.46	0.71	0.73	0.42
Industry	0.74	1.23	1.02	0.91	1.11	0.98	0.81	0.89	0.85
Residential	0.83	1.79	1.07	1.13	0.68	1.09	1.14	1.11	1.15
Agriculture	0.91	1.03	0.86	1.25	1.19	1.04	1.23	1.11	1.14
On-road	0.83	0.74	0.54	0.69	0.73	0.72	0.72	0.67	0.70
Off-road	0.43	0.84	1.19	0.78	0.98	0.77	0.94	0.82	0.97

Table 14. Scaling factor for VOCs emissions for major states in SUS

	LA	AR	MI	TN	AL	GA	FL	NC	SC
Energy	0.86	0.97	0.92	0.98	1.17	0.96	0.96	0.94	0.80
Industry	0.98	1.22	0.89	0.81	0.82	1.21	0.94	1.11	0.89
Residential	1.38	1.03	0.48	1.29	1.60	1.74	0.98	1.48	1.46
Agriculture	1.07	1.12	1.20	1.20	1.09	1.06	0.91	1.15	1.06
On-road	0.68	0.79	0.62	0.72	0.75	0.73	0.68	0.64	0.79
Off-road	0.74	0.81	0.85	0.79	0.82	0.78	0.75	0.78	0.78

.

5.2.2 Model application

O_3 and its source apportionment are simulated in a coarse domain with resolution of 36km covering the U.S. except Alaska and Hawaii. Part of surrounding countries such Canada and Mexico are also included. Nested finer domain covers SUS with resolution of 12km. Finer domain includes Alabama (AL), Arkansas (AR), Florida (FL), Georgia (GA), Louisiana (LA), Mississippi (MI), North Carolina (NC), South Carolina (SC) and Tennessee (TN) and part of neighbor states. Domain settings are shown in Figure 25. Emissions from agriculture, energy, industry, on-road, off-road, residential, biogenic and wildfires are tracked by tagging NO_x and VOCs species in emissions inputs. Meteorological and emission inputs for June are generated used to predict summertime O_3 behavior in both domains. Three regime scheme (3R) is applied as O_3 sensitivity chemical scheme to precursors of NO_x and VOCs as described in previous chapter[53].

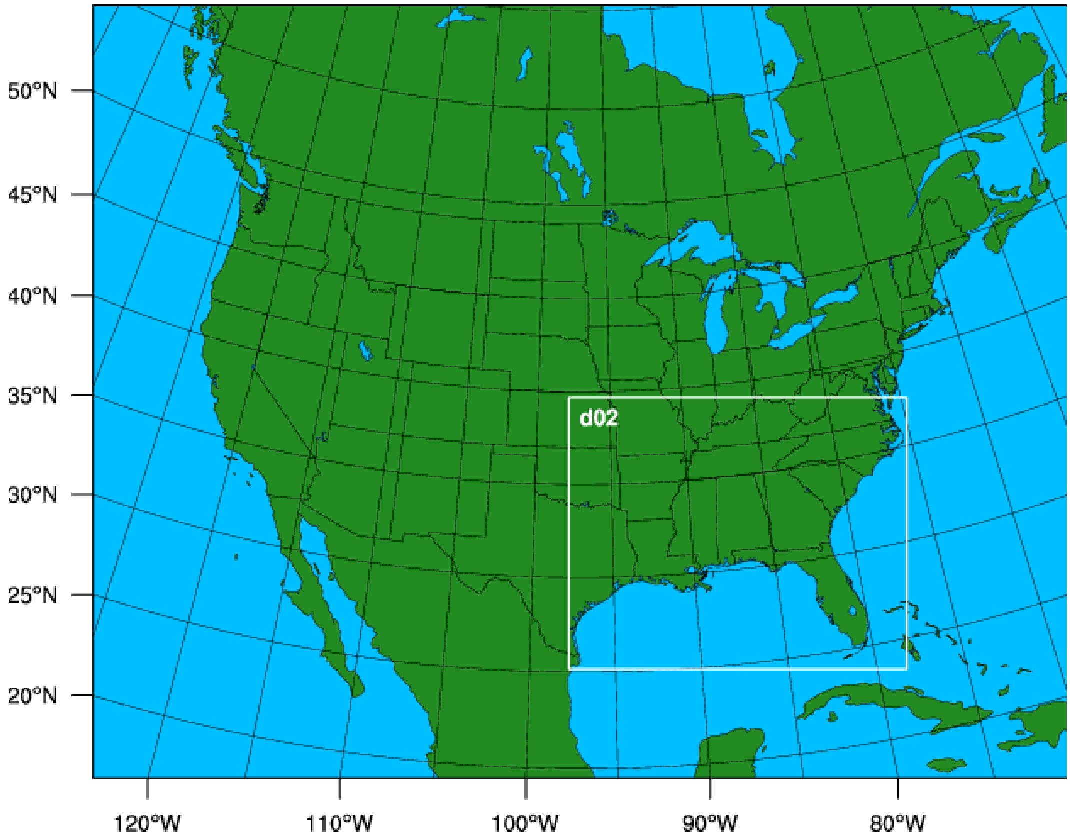

Figure 25. Domain setting of SUS. Outer domain represents parent domain (36km by 36km) covered the United State except Alaska, Hawaii etc. Nested 12km by 12km domain (d02) cover SUS in this study.

5.3 Results and discussions

5.3.1 Overall O_3 simulations

Summertime 8h-O_3 concentrations in U.S. are simulated and shown in

Figure 26, its contributions from background and emission sources are also illustrated. High concentrations occur in western, southwestern and northeastern U.S. with averaged concentration of more than 50 ppb. Highest pollution event is observed in southwest California by concentration of more than 70 ppb. Background O_3 is the major source in western U.S., which provides O_3 formation ranged from 40 to 50 ppb in most west regions. However, contribution from background O_3 is decreased in central and eastern U.S., corresponds to ~30 ppb. Minimum

contribution is observed in SUS with less than 25 ppb. Emissions play essential roles in forming O_3 in coastal California and low background contribution area such as central and eastern regions. Maximum contributions are predicted in southwest California and coastal northeastern U.S. by more than 30 ppb. High contribution also occurs around Lake Michigan and Kentucky by ~20 to 30 ppb.

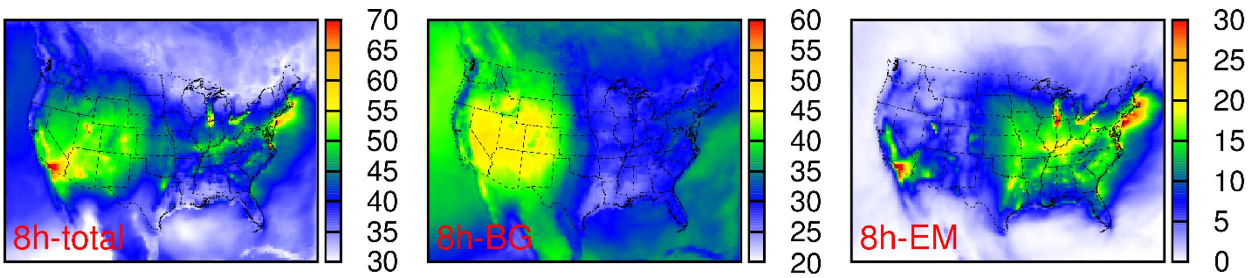

Figure 26. Summertime 8h-O_3 concentration in U.S. and its contribution from background (BG) and emissions (EM). Units are ppb.

Model performance of O_3 predictions in SUS are validated following same suggested statistic criteria [200] introduced in Chapter 2. Predicted O_3 concentrations are compared with observation data recorded from a total of 224 monitoring stations in SUS. The statistic results are shown in Table 15. The MFE in all states match well with suggested benchmark of 0.35, but slightly exceedances of MFB are found in GA, NC, SC and TN. The NMB in these regions also exceed suggested criteria. Biases in these states are mainly due to uncertainties in domain edging area. Model slightly overestimates concentrations in SUS, biases are less than 2 ppb in FL, LA and MI, the best performance is found in LA with bias less than 1 ppb. However, model has a significantly overpredictions in part of central and north SUS such as in NC and TN with exceedances of both MFB and NMB. Biases are mainly due to uncertainties from emissions inventories and model resolutions[224, 225]. Overall, 8h-O_3 predictions in SUS agree well with observation from a total of 244 monitoring stations in SUS. Results from this simulation are reliable for further analysis. Overall, O_3 concentrations in SUS (Figure 27) are less than 50 ppb

except north and west regions. A decrease trend is found from inner land to coastal area. However, contribution from background is high in the northeastern Gulf of Mexico and coastal Florida and Georgia by ~35-40 ppb but low in inland SUS where ~25-30 ppb O_3 formations are estimated due to background O_3. It is noted that emissions strongly affect O_3 formation in central and northwest SUS. Detailed analysis is conducted in following section.

Table 15. Model performances in 9 states in SUS for 8h-O_3 simulation. Units are ppb for OBS and PRE. Bold represents the statistical result exceeds criteria.

	AL	AR	FL	GA	LA	MI	NC	SC	TN	Benchmark
OBS	39.13	41.88	36.45	41.31	39.05	41.00	44.39	41.18	43.58	
PRE	45.31	46.93	37.03	50.20	39.24	42.81	53.20	50.40	53.58	
MFB	0.12	0.10	-0.01	**0.17**	-0.03	0.02	**0.17**	**0.19**	**0.20**	±0.15
MFE	0.25	0.23	0.28	0.29	0.29	0.23	0.25	0.27	0.27	0.35
NMB	**0.18**	0.15	0.04	**0.24**	0.02	0.07	**0.22**	**0.26**	**0.27**	±0.15

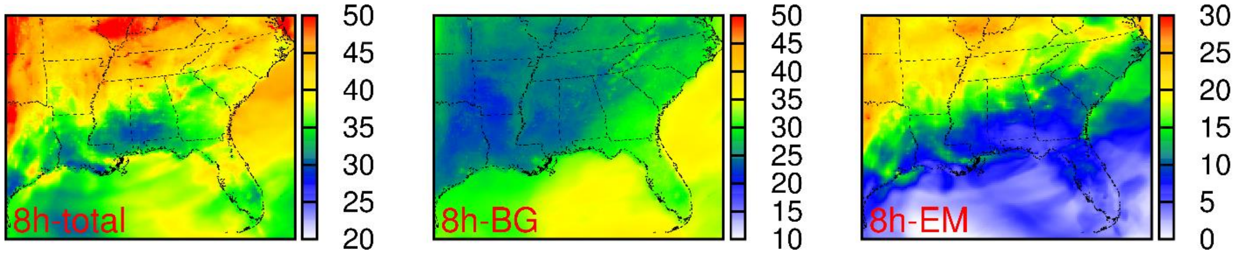

Figure 27. Summertime 8h-O_3 concentration in SUS and its contribution from background (BG) and emissions (EM). Units are ppm.

5.3.2 Source apportionment in SUS

Figure 28 indicates that emissions from NO_x dominate O_3 formation in SUS and barely O_3 contributions are estimated from VOCs. NO_x emissions have strong impacts in northwest SUS, they cause more than 20 ppb O_3 formation in this region. Their impacts are significantly reduced from northwest to southeast regions, and they cause less than 10 ppb O_3 in south SUS

and even less than 5 ppb in south Florida. Impacts from VOCs emissions are generally lower than 2 ppb except in specific cities such as in Houston, Dallas and Nashville where ~5 ppb O_3 are estimated to associate with VOCs emissions.

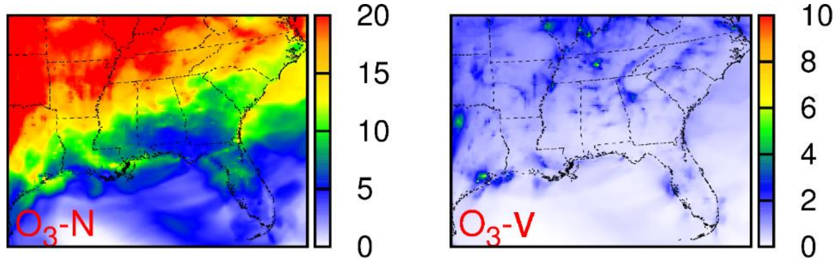

Figure 28. 8h-O_3 contributions from emissions of NO_x and VOCs. Units are ppb.

Sectoral contributions are shown in Figure 29. More than 10 ppb O_3 are from on-road emissions in north SUS, and contributions from on-road emissions are decreased to ~3 ppb in central and south regions. Emissions from energy mainly induce O_3 increasing in north and west SUS by 6 to 8 ppb but cause less impacts on central and southeast regions with less than 2 ppb. Industry has slightly lower contribution than energy emissions, it causes ~4 to 6 ppb O_3 in specific cities in central and west SUS. Besides, significant contributions from biogenic emissions are found in west and northwest SUS, around 4 ppb O_3 are estimated from biogenic sources. It is concluded that on-road emissions are the major sources in SUS followed by emissions from energy, industry and biogenic sector. On-road and biogenic emissions prefer to induce O_3 concentration in north and northwest area while emissions from energy and industry have strong impacts on specific cities in north and west SUS.

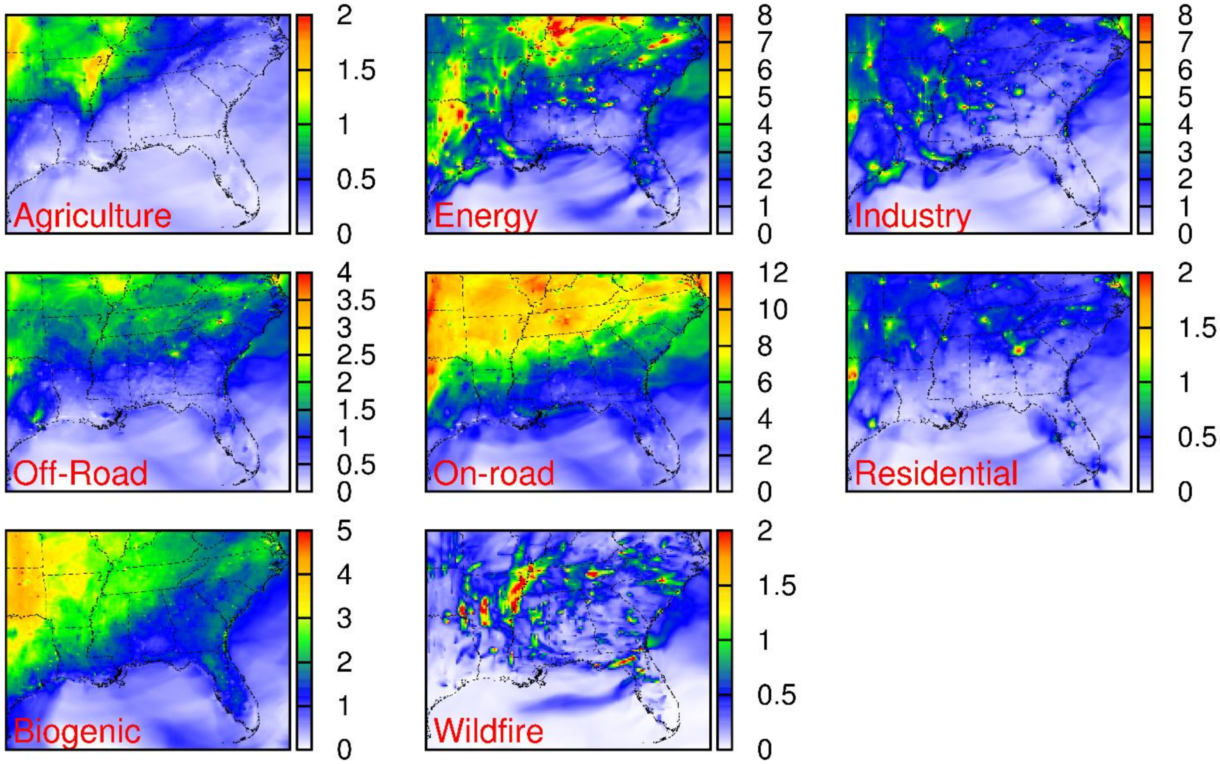

Figure 29. 8h-O_3 contributions from emission sectors. Units are ppb.

Since O_3-EM in SUS is mainly dominated by NO_x, a deeper analysis of its source apportionment would carry out a comprehensive understanding. 8h-O_3 contribution from emission sources for NO_x and VOCs are illustrated in Figure 30. It is noted that VOCs emissions has barely impacts on O_3 formation except the emissions from biogenic and industry. Biogenic emissions are the major sources of VOCs-related O_3, which cause significant impacts in northwestern regions. VOCs industry emissions cause ~ 1 ppb O_3 formation in Houston, Dallas and Atlanta, their impacts on other SUS regions are less than 0.5 ppb. Contributions from NO_x emission has similar spatial pattern as total source contributions, which means a leading position of on-road emissions followed by energy emissions.

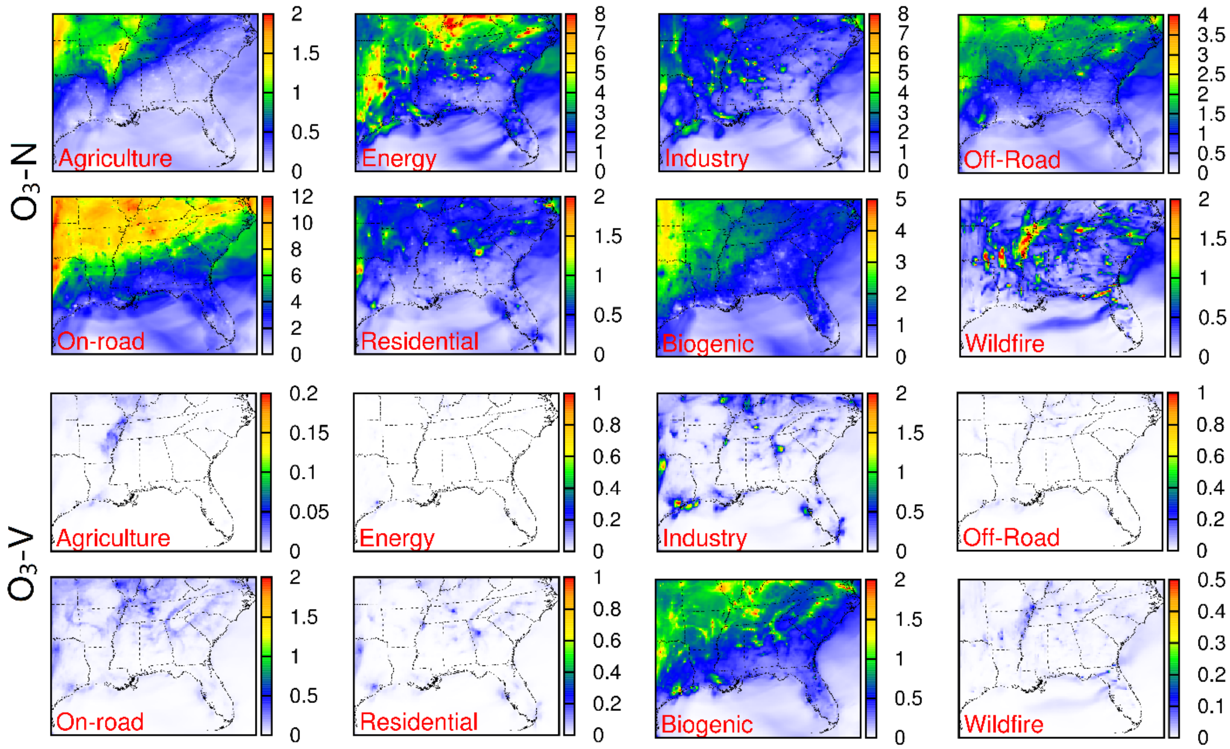

Figure 30. Summertime NO_x and VOCs contributions to 8h-O_3 by sectors. Units are ppb.

5.3.3 Comparison with China

From the results of previous chapters, anthropogenic emissions induce higher contributions in NCP, which lead average of ~30 ppb O_3 in summertime and maximum of more than 50 ppb in peak episodes. However, both anthropogenic emissions of NO_x and VOCs are significantly lower in SUS than in NCP. As shown in

Figure 31, summertime monthly average total NO_x emissions are ~10-20 tons in SUS with maximum of more than 200 tons in megacities such as Houston, Dallas and Atlanta. NO_x emissions are generally higher than 100 tons in central NCP with maximum of more than 300 in specific city such as Beijing, Tianjin and Shijiazhuang. VOCs emissions in NCP also significantly higher than SUS.

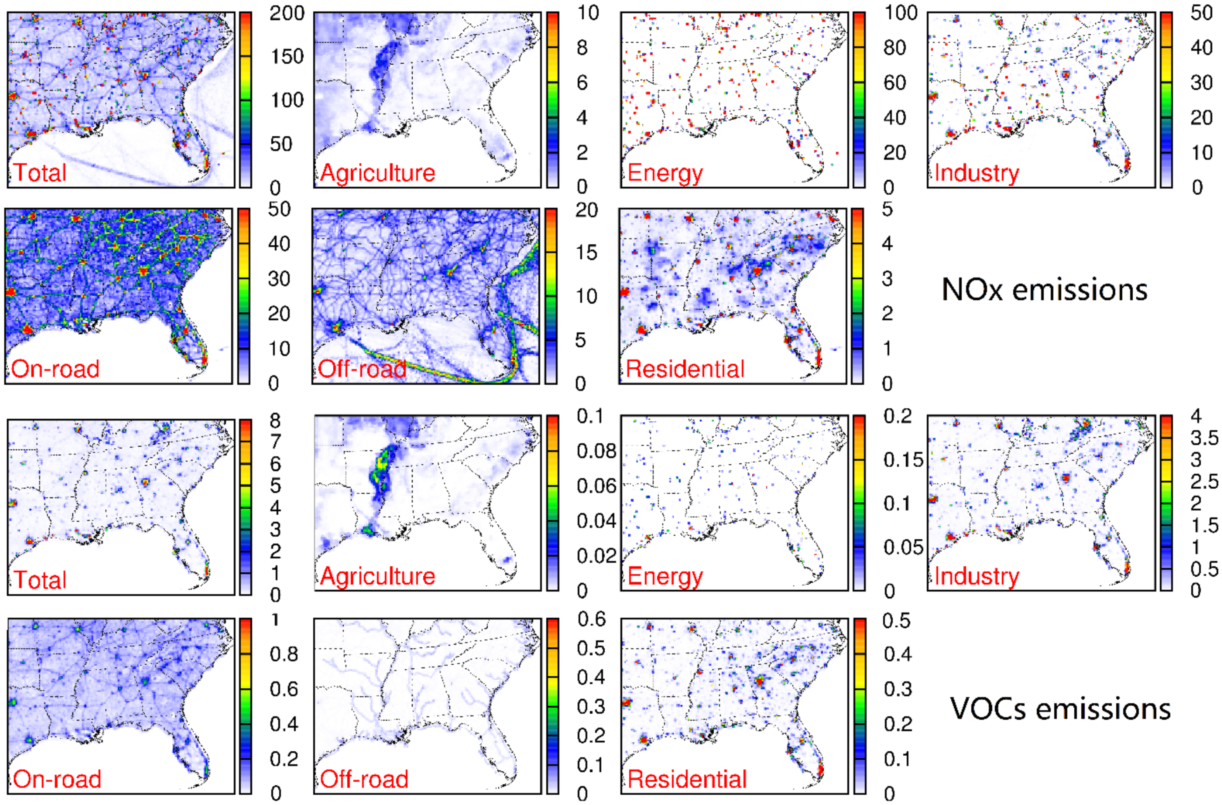

Figure 31. Summertime average monthly emissions of NO_x and VOCs and contribution from anthropogenic sources in SUS. Units are tons/month.

Both NCP and SUS has high energy NO_x emissions but emissions from other sectors are extremely lower in SUS especially for on-road, off-road and energy emissions which are major sources in NCP. High emissions only occur in specific cities in SUS such as Houston, Dallas and Atlanta while emissions in NCP are generally high in most central regions. It is noted that overall NO_x emissions are at the low level (by ~10-20 tons/month) in SUS while a decrease trend is found in NCP from south to north (from 50 tons/month to less than 10 tons/month). VOCs emissions from anthropogenic sources are all significantly lower in SUS with a maximum of ~8 tons/month while the high VOCs emissions in NCP are more than 10 tons/month. As the major VOCs contributors in SUS, emissions from on-road and industry are lower than half of them in NCP. Generally, NO_x and VOCs emissions in SUS are at low levels with only specific high emissions in major cities in each state, and even the high emissions in these cities are much lower than in

most regions in NCP. Emissions in NCP are generally higher in south and central regions. O_3 is estimated to sensitive to emissions in both NCP and SUS, differences in emissions cause greatly impacts on O_3 formation, thus O_3 source apportionment analysis in these regions helps to understand different source contributions under various emission conditions.

Major anthropogenic emission sources are industry, energy and on-road which occupied more than 70% of total O_3-EM in NCP while on-road emissions are the only major anthropogenic source in SUS, less contributions from industry and energy sectors are estimated. Compared to anthropogenic emissions, biogenic emissions contribute less in NCP by causing less than 3 ppb O_3 while it becomes one of the major sources in SUS followed by on-road and energy emission. The maximum contribution from biogenic emissions of more than 5 ppb is occurred in western SUS. Contributions from emission sources show different patterns in NCP and SUS, which request an emergent requirement of reducing emissions from industry and energy so that the O3 pollution could be reduced to matching its level in SUS.

5.4 Conclusions

This work simulates summertime O_3 concentration in SUS and its contributions from anthropogenic and natural emission sources. Model performances are validated. Though overestimations are remained in northern SUS, simulation results are generally match agree well with observation data and reliable for further analysis. High concentrations are found in north and west regions with the concentration of 8h-O_3 higher than 40 ppb. A decrease trend is found from northwest to southeastern coastal regions. Background O_3 contributes ~25 to 30 ppb in SUS while emission sources have strong impacts in high concentration regions by inducing ~30 ppb O_3 formation. O_3 formation in SUS is mainly dominated by NO_x while VOCs emissions cause maximum of 5 ppb in Houston, Dallas and Nashville. Major contributors of NO_x-related O_3

formation are on-road emissions followed by energy, industry and biogenic emissions while biogenic emissions are major sources of O_3V. Comparison between SUS and NCP carries out that anthropogenic emissions cause the high O_3 pollution in NCP. Major sources in NCP are industry, energy and on-road emissions while on-road emission is the only major source in SUS. Results of this work provide information for further estimation of health risk analysis and offer solid evidence for designing the controlling strategies to reduce O_3 concentration in NCP.

CHAPTER 6. OZONE ASSOCIATED HEALTH RISK ANALYSIS

6.1 Introduction

Ground-level O_3, which was listed as one of six major air pollutants as set in NAAQS by EPA, is a highly toxic gas that have harmful effects on human health[213, 226, 227]. Inhaling O_3 causes irritation, inflammation and constriction to human respiratory system and results in health impacts such as decreases of breathing functions, asthma attacks, hearth attacks and premature mortality [228, 229]. Around 142 thousand premature mortalities were estimated with O_3-related COPD caused by long-term O_3 exposure globally[229]. A total of 9-23 million annul asthma emergency room visits were also reported correspond to O_3 pollution around the world. At the meantime, China is shown as one of the most polluted countries that largest impacts from O_3-related health issues were estimated [230].

China is experiencing O_3 increases issue, a total of 318 cities were revealed to exceed WHO recommended O_3 concentration, and 69 of them failed to meet the NAAQS target of China[231]. Many studies tried to quantify O_3 impacts on human health in China. A total of 816.04 million cumulative population was estimated exposed to a circumstance that 8h-O_3 concentration is higher than 100 μg/m^3 in China, which results in around 55 to 80 thousand premature mortality caused by COPD in 2015. At the meanwhile, Beijing, Shandong, YRD, PRD and Sichuan basin were listed as high risk region[14]. A growth rate of mortality increased from 0.42% to 1.11% around China as the result of O_3-related health issue were estimated, which corresponded to 28 to 74 thousand premature mortality[232]. O_3-related health risk is also detailed analyzed in high O_3 risk area. A 39.5% (1100 deaths) increased of premature mortality was estimated as result of O_3

pollution in PRD[233]. An increase of 10 μg/m^3 of 8h-O_3 were associated with 0.55% increases of total mortality in Jiangsu Province. Increases of mortality due to hypertension, coronary diseases and stroke were revealed to associate with 10 μg/m^3 increases of 8h-O_3 country wide by 0.60%, 0.24% and 0.29%, respectively[234]. It was reported that more than 3 million respiratory symptoms and 1 million cases of school-loss days would be avoided if O_3 concentration could be controlled to lower than 75 ppb in the U.S.[235]. Around 0.11% to 0.27% increases of O_3-related daily mortality were revealed on average across 50 cities in U.S., which were associated with increases of daily 1h-O_3 by average of 4.8 ppb (maximum of 9.6 ppb) [236].

O_3 exposure leads a series of adverse health effects including premature mortalities of respiratory and cardiovascular diseases[237, 238]. The concentration response function (CRF) is widely used in WHO and previous studies to quantify O_3-related health impacts[239, 240]. The change rates of 0.42%, 0.44% and 0.50% of mortality due to non-accidental causes, cardiovascular diseases and respiratory diseases were estimated as the result of an increased 8h-O_3 concentration of 10 μg/m^3, respectively[241]. Increase of 10 μg/m^3 of daily averaged O_3 concentration was also estimated to cause increase of 0.6% nonaccidental mortality in China[231]. However, there is no study detailed provides O_3-related health impacts in NCP and their contribution from emission sources. Studies in U.S. is also limited in analyzing health impacts from emission sources. This study will recruit results from previous chapters and apply the reliable health analysis methods to estimate O_3-related health risk in NCP and SUS as well as source contribution in these regions. Results of this study provides information to assess health risk caused by human activities and quantify the contributions from emissions sources. Health analysis results would be further used to estimation on economic benefits.

6.2 Methods

China-specific concentration-response functions (CRF) [242, 243] are adapted in this study to estimate the health impacts due to exposure of O_3. Cardiovascular and respiratory mortalities are calculated in this study. Relative risk (RR) of Cardiovascular and respiratory disease mortalities with a 95% confidence interval with corresponding 8h-O_3 concentrations are calculated using following equation:

Equation 18:

$$RR_i = \exp\left[\gamma(C_i - C_0)\right]$$

Where i refers to the index of the domain grid. γ is fitted by meta-regression based on the previous epidemiological studies for China [242]. C_i and C_0 are the pollution concentration in the target grid and the threshold value, below which will induce no additional risk, respectively. Threshold concentration of 8h-O_3 is 35 ppb (equivalent to 70 $\mu g/m^3$) in this work[172]. Extra health impacts are resulted from concentration higher than the threshold value. The health endpoints (E) for CRF is calculated based on following equation:

Equation 19:

$$E = \sum_i \frac{RR_i - 1}{RR_i} * P_i * F_i$$

Where P_i and F_i refer to population and baseline incidence rate. It is noted that health endpoints in this study include premature mortality due to respiratory diseases (RDM) and cardiovascular diseases (CDM). Major respiratory and cardiovascular diseases including chronic obstructive pulmonary disease (COPD) , ischemic heart disease (IHD) and strokes (STK, including both ischemic and hemorrhagic strokes) are also calculated in this analysis. The baseline incidence rates are obtained from the online GBD database (http://vizhub.healthdata.org/gbd-compare/). The

United Nations (UN)-adjusted population distribution for year of 2017 from the Center for International Earth Science Information Network (CIESIN) is used to represent the population exposure.

CRF is a long-term concentration related function, thus simulated summertime 8h-O_3 concentrations are scaled to annual concentrations by applying provincial average ratio calculated from observation data recorded in monitoring stations following Equation 20 for each grid.

Equation 20:

$$Annual\ 8h\text{-}O_3(S) = Summer\ 8h\text{-}O_3\ (S) \times \frac{Annual\ 8h\text{-}O_3\ (O)}{Summer\ 8h\text{-}O_3\ (O)}$$

S and O in equation (3) refer to concentration from simulation and observation, respectively. Observation data are provided by China National Environmental Monitoring Center (CNEMC, http: //113.108.142.147:20035/emcpublish/).

Benefits Mapping and Analysis Program (BenMAP) model helps to estimate the O_3-related health risk in SUS. Health endpoints includes mortality (all-cause, respiratory and cardiopulmonary diseases), emergency room (ER) visits (for asthma) and hospital admissions (HA, for all respiratory). Health impacts are calculated by applying recruited function from published epidemiology literature in this model. Health impacts are associated with pollution concentrations, population and incidence baseline rates, which are from results of previous chapters and BenMAP database in U.S.

6.3 Results and discussions

6.3.1 Overall health risk in NCP

Based on discussions in previous chapters, simulation results for O_3 concentrations in NCP are in sufficient agreement with observations to act as basis for health impacts analysis. It is noted that annual 8h-O_3 concentrations are scaled from summertime concentration in this estimation. Health risks are estimated for both MEIC and EDGAR+ simulation results. Health impacts in Beijing, Tianjin, Hebei, Shandong and Shanxi are included in the following discussion while the rest provinces are not included since they are not fully contained in the simulation domain. Results from MEIC and EDGAR+ are listed in Table 16. Due to the higher predicted concentration, MEIC results in a higher risk for all health endpoints. MEIC predicts a total of 0.13 million mortalities for all causes (0.05 million for RDM and 0.08 million for CDM) while EDGAR+ predicts ~0.02 million fewer mortalities than MEIC (total of 0.04 and 0.07 million for RDM and CDM, respectively). COPD is the major disease within RDM, accounting for around 1/3 of total mortality in simulations. Both EDGAR+ and MEIC predict similar relative health impacts in different provinces. Hebei and Shandong have the highest impacts with more than total of 0.04 million mortalities. Shanxi also has high mortality followed by Beijing and Tianjin. With high population, Beijing and Tianjin also have severe health problems under high O_3 concentration. Beijing has ~0.01 million all-cause mortality, which is twice as high as in Tianjin.

Table 16. Provincial health risk analysis results within the NCP. Units for health endpoints are cases.

		Beijing	Tianjin	Hebei	Shandong	Shanxi	Total
Total	EDGAR+	9536	4809	40902	40840	16302	112390
mortality	MEIC	12062	5395	45460	48602	19022	130541

(Table cont'd)

		Beijing	Tianjin	Hebei	Shandong	Shanxi	Total
CDM	EDGAR+	5884	2975	25276	25341	10130	69606
	MEIC	7389	3324	27991	29964	11750	80418
RDM	EDGAR+	3652	1834	15626	15499	6172	42783
	MEIC	4673	2071	17469	18638	7272	50123
COPD	EDGAR+	3582	1798	15325	15200	6054	41959
	MEIC	4583	2031	17132	18279	7132	49157
IHD	EDGAR+	2796	1614	12011	12042	4814	33277
	MEIC	3511	1580	13301	14239	5583	38214
STK	EDGAR+	2745	1388	11792	11822	4726	32473
	MEIC	3447	1551	13058	13978	5481	37515

1. Cardiovascular diseases mortality (CDM); respiratory diseases mortality (RDM); ischemic heart disease (IHD); stroke (STK); chronic obstructive pulmonary disease (COPD).
2. Only Beijing, Tianjin, Hebei, Shandong, Shanxi are completely included in this study, the health result for the rest provinces (Rest) are only refer to the part that included in this study domain.
3. Total mortality includes CDM and RDM only.

Due to higher accuracy of concentration results using EDGAR+, spatial distributions of mortality from each disease in EDGAR+ results are shown in Figure 32. The differences between EDGAR+ and MEIC are also shown in Figure 33. Health endpoints in major cities/provinces are also listed in

Table 17. Due to the higher predicted concentration, MEIC results in a higher risk for all health endpoints. MEIC predicts a total of 0.13 million mortalities for all causes (0.05 million for RDM and 0.08 million for CDM) while EDGAR+ predicts ~0.02 million fewer mortalities than MEIC (total of 0.04 and 0.07 million for RDM and CDM, respectively). COPD is the major disease within RDM, accounting for around 1/3 of total mortality in simulations. The spatial pattern indicates that adverse impacts usually peak at megacities in the central NCP such as Beijing, Tianjin and Shijiazhuang. Although O_3 concentrations are not always extremely high in Beijing, high population density leads to this serious health impacts. Such situations are also observed in capital cities in other provinces such as Zhengzhou, Shijiazhuang as well as some big cities with large population such as Tianjin and Yantai. In north Henan and south Hebei, severe health impacts are also estimated due to the high O_3 concentration instead of high population density. However, opposite to central NCP, adverse health impacts are not very serious in coastal regions where O_3 concentrations are relatively lower compared to central NCP except in specific high population cities. In north, west and northwest NCP, O_3-related health impacts are very low due to both low O_3 concentration and population. Figure 33 reveals that EDGAR+ predicts lower health risk than MEIC except in specific cities such as Tangshan, Shijiazhuang, Qingdao and Taiyuan by 10~20 cases/grid. It is significant that EDGAR+ predicts lower mortality (20 cases/grid) in Beijing, where EDGAR+ has higher accuracy in predicting O_3. It is believed that EDGAR+ also predicts health risk more accurately than MEIC.

Table 17. Provincial health risk analysis results within the NCP. Units for health endpoints are cases.

Province		Beijing	Tianjin	Hebei	Shandong	Shanxi	Total
Total mortality	EDGAR+	9536	4809	40902	40840	16302	112390
	MEIC	12062	5395	45460	48602	19022	130541
CDM	EDGAR+	5884	2975	25276	25341	10130	69606
	MEIC	7389	3324	27991	29964	11750	80418
RDM	EDGAR+	3652	1834	15626	15499	6172	42783
	MEIC	4673	2071	17469	18638	7272	50123
COPD	EDGAR+	3582	1798	15325	15200	6054	41959
	MEIC	4583	2031	17132	18279	7132	49157
IHD	EDGAR+	2796	1614	12011	12042	4814	33277
	MEIC	3511	1580	13301	14239	5583	38214
STK	EDGAR+	2745	1388	11792	11822	4726	32473
	MEIC	3447	1551	13058	13978	5481	37515

1. Cardiovascular diseases mortality (CDM); respiratory diseases mortality (RDM); ischemic heart disease (IHD); stroke (STK); chronic obstructive pulmonary disease (COPD).
2. Only Beijing, Tianjin, Hebei, Shandong, Shanxi are completely included in this study, the health result for the rest provinces (Rest) are only refer to the part that included in this study domain.
3. Total mortality includes CDM and RDM only.

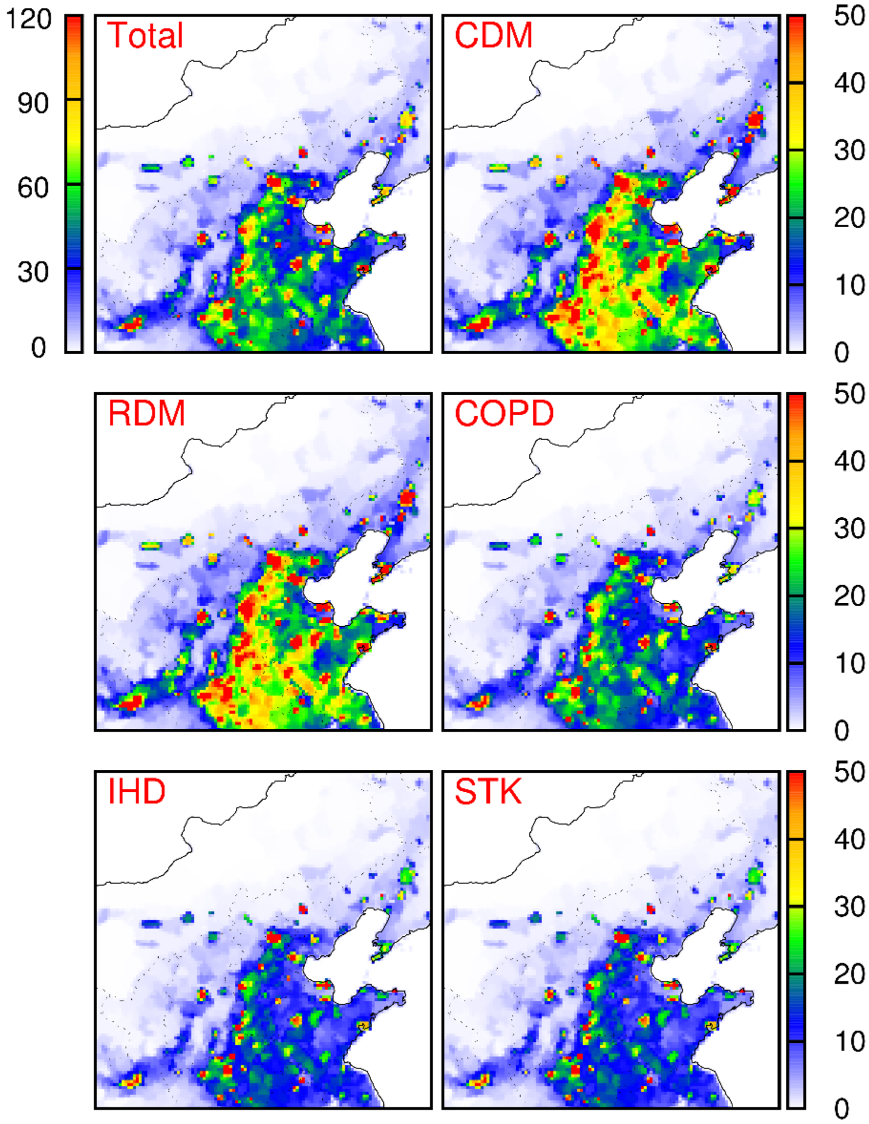

Figure 32. Health end point results of five O_3-associated diseases. Total shows the total mortality due to O_3-related diseases including RDM, CDM COPD, IHD and STK. Units are cases/grid.

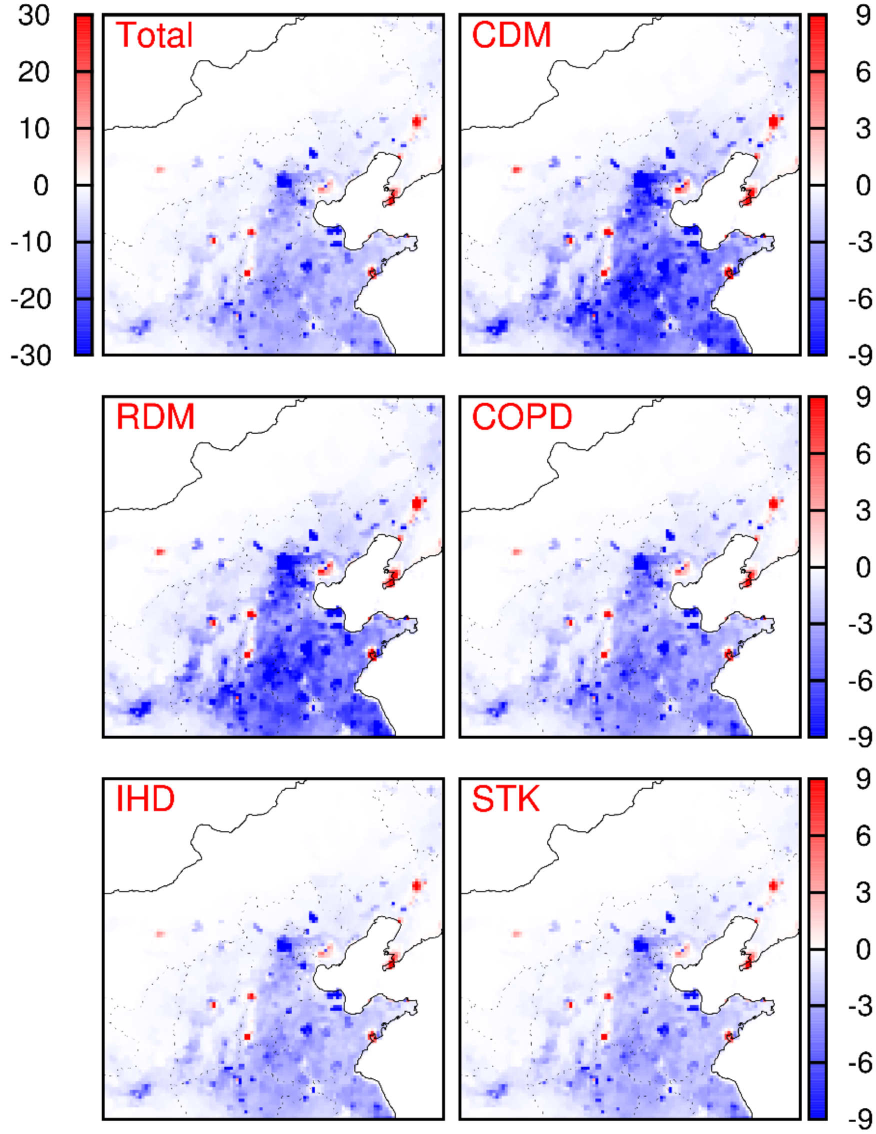

Figure 33. Difference of health endpoints between EDGAR+ and MEIC (subtracting EDGAR+ by MEIC). Units are cases/grid.

Health outcomes from EDGAR+ and MEIC are compared with others' studies for China as shown in Table 18. Most studies used similar function (CRF) to estimate health risk with different corresponding concentrations and thresholds. Mostly, 8h-O_3 is used as the concentration metric in the CRF with a threshold of 75.2 μg/m^3. This study uses a slightly lower threshold (70 μg/m^3) which is validated and successfully used in previous works [172, 235]. Though the national health impacts from other studies are calculated for different years by using varied thresholds, this

comparison also indicates that NCP is a high-risk region in China. EDGAR+ and MEIC predict ~0.04 and ~0.05 million respiratory mortalities, respectively, for five provinces in the NCP, which account for ~50% to 70% of national respiratory mortalities linked to results in Maji, et al. [244]. COPD mortality also amounts for ~61% of national-wide impacts estimated by Liu, et al.[154].

Table 18. Comparison of health outcome with previous studies

Study domain (target year)	Corresponding concentration	Threshold	Health endpoint	Estimated mortality	References
NCP (2017)	8h-O_3	70 $\mu g/m^3$	Respiratory and cardiovascular diseases	112,390	EDGAR+[1]
NCP (2017)	8h-O_3	70 $\mu g/m^3$	Respiratory and cardiovascular diseases	130,541	MEIC [1]
China (2016)	8h-O_3	75.2 $\mu g/m^3$	Respiratory morality	69,536~74,233	[244]
China (2015)	8h-O_3	100 $\mu g/m^3$	COPD mortality	55,341~80,280	[154]
China (2000)	1h-O_3	75.2 $\mu g/m^3$	Premature all-cause mortality[2]	70,000~150,000	[245]
China (2010)	1h-O_3	75.2 $\mu g/m^3$	Respiratory morality	300,000	[246]
Urban China (2015)	8h-O_3	50 $\mu g/m^3$	Premature all-cause mortality	70,800	[247]

1. Results from this predicted concentration in this work.
2. All-cause mortality includes all O_3-related diseases

6.3.2 Health risk contribution from emissions sources for NCP

Health risk contribution from emissions of NO_x and VOCs are shown in Figure 34, these results are from predicted O_3 concentration by using EDGAR+ which has slightly better accuracy

in matching averaged O_3 concentration in NCP. Emission-related O_3 causes ~46.5% of total premature mortality while the rest of them are due to background O_3 (53.5%). It is noted that NO_x is the major source in NCP while both NO_x and VOCs have great impacts on megacities such as Beijing, Tianjin and Shijiazhuang where have high level of both population and O_3 pollution. For major cities/provinces in NCP, total of 52,346 premature mortalities are estimated due to emissions. NO_x emissions cause 82.5% of emission-related premature mortality, correspond to 43,211 deaths. Hebei and Shandong provinces have highest premature mortality, a total of 19.16 and 19.02 thousand deaths are estimated due to emissions, a total of 5 thousand mortalities are estimated for Beijing. Source contributions to mortality are shown in Figure 35, which is associated with concentration distribution. Industry, energy and on-road emissions are major sources that cause 79% of the total emission-related mortality. Emissions from Central China, Hebei and Shandong provinces are the major sources of O_3-related premature mortality, they cause a total of 55% emission-related premature mortality. Spatial distribution of regional and sectoral emissions contributions (Figure 36) indicates that local emissions are the major health issue sources, and emissions in Hebei, Shandong and central China cause high health risk to central NCP, they cause large amount mortality in central NCP. At the meantime, high contributions from emissions from Beijing and Tianjin are also due to large population in these cities. Figure 36 also shows that industry, energy, on- and off-road emissions are major sources in central and south NCP.

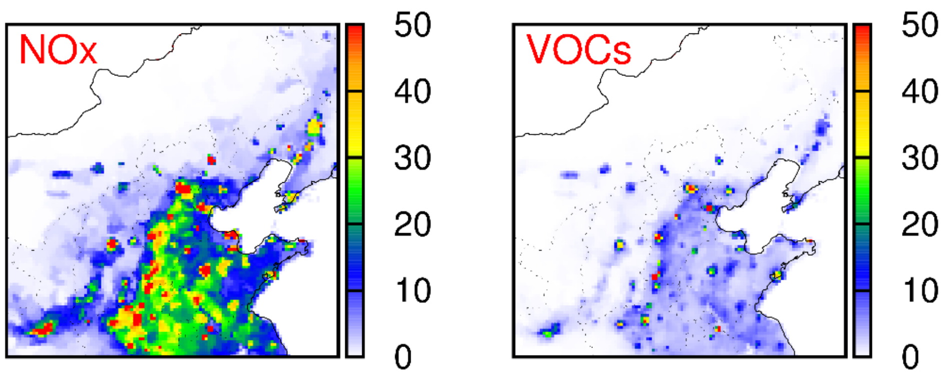

Figure 34. Spatial contributions from NO_x and VOCs emissions to premature mortality. Units are cases/grid cell.

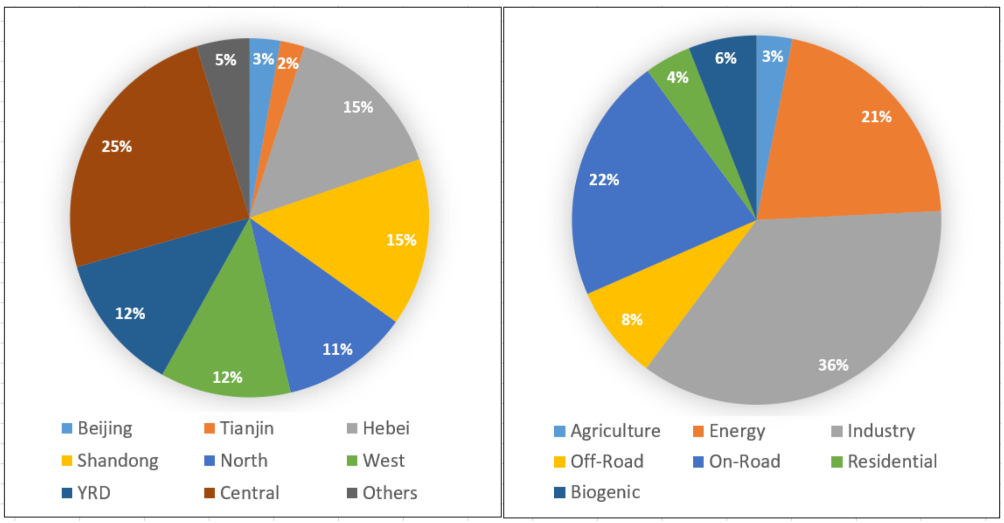

Figure 35. Regional (left) and sectoral (right) emission contribution ratios to total premature mortality.

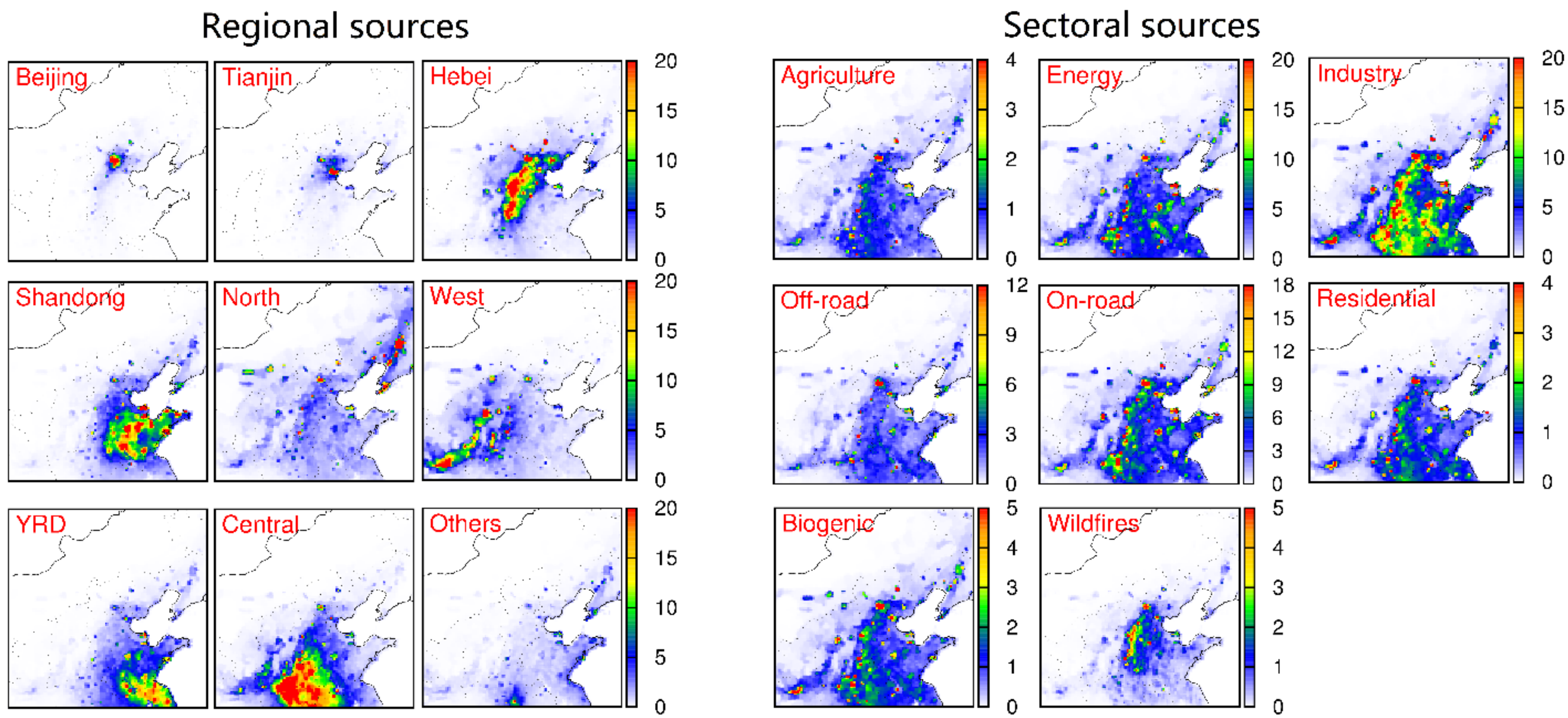

Figure 36. Spatial contribution of health impacts from regional (left) and sectoral (right) emission sources. Units are cases/grid cell.

6.3.3 Health risk analysis in SUS and comparison with NCP

O_3-related health endpoints are calculated and shown in Figure 37. All-cause mortality, respiratory mortality and cardiovascular mortality are calculated based on simulation results in chapter 5. A total of ~35 thousand all-cause mortalities are estimated due to long-term exposure to O3. Cardiovascular and respiratory diseases cause 7913 and 4605 mortalities, account for ~22% and ~13% of all-cause

mortality, respectively. High risk is estimated to associate with population density. Megacities such as Houston, Dallas, Atlanta and Orlando are estimated as high risk area, with more than 40 premature mortality cases are calculated in each grid. More than 20 thousand ER visits and 6.5 million HA are estimated in this work. These results reveal that even O_3 concentration is at a low level, it remains a great potential risk for people who is sensitive to O_3-related diseases. Contribution of O_3-related health impacts from O_3 sources are shown in Figure 38. Emissions cause a total of 12663 premature mortalities in SUS, account to 35% of total O_3-related impacts. As major sources, on-road emission cause 39% of emission-related health impact followed by emissions from energy (20%) and biogenic (14%).

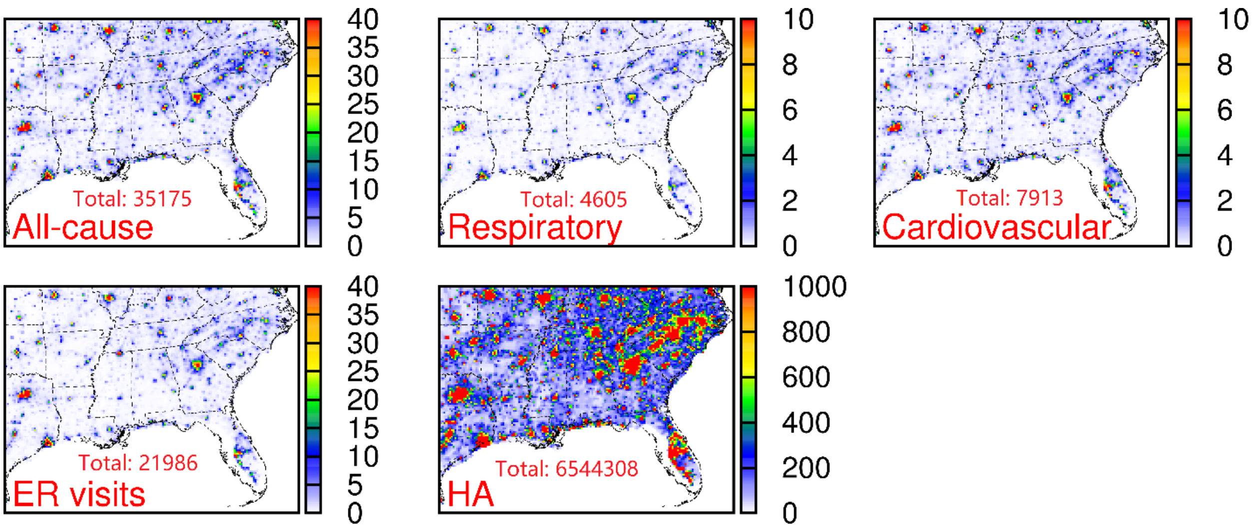

Figure 37. O_3-related health risk in SUS. First row represents the estimated premature mortality, bottom row refers to the estimated impacts cases for ER visits and HA. Units are cases/grid.

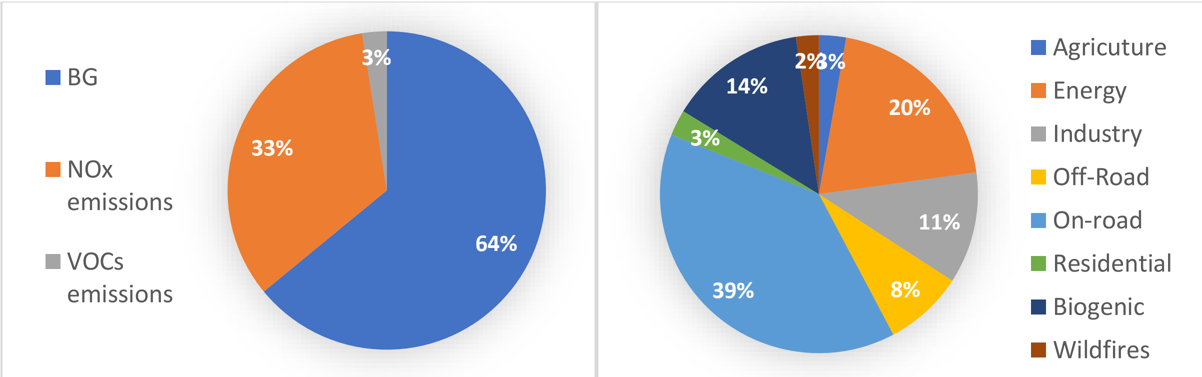

Figure 38. All-cause mortality contributions from BG and emission sources. Right panel shows the contribution of emission related impacts from emission sources.

Results in SUS are compared with health impacts in NCP. Generally, less health impacts are estimated in SUS than in NCP since lower level of both O_3 concentration. Besides, population density is another reason for this phenomenon. Population is high in big cities for both scenarios such as Houston, Dallas, Atlanta, Beijing, Tianjin and Shijiazhuang where the O_3 concentrations are also relative higher than other cities (Figure 39). But NCP has large amount population in central and south regions which refer to Hebei, Henan and Shandong provinces, where the population remains in a high level. Population in rural SUS is in a significantly lower level, which is equal to ~10% as in NCP, thus less health impacts are estimated in these regions. Different incidence rates also help to explain the differences as shown in Table 19. NCP has more than twice respiratory incidence rate than SUS and has a similar cardiovascular diseases incidence rate of mortality. However, though less people suffered from respiratory diseases, large amount people has high risk in cardiovascular diseases, which leads high mortality of CDM in SUS.

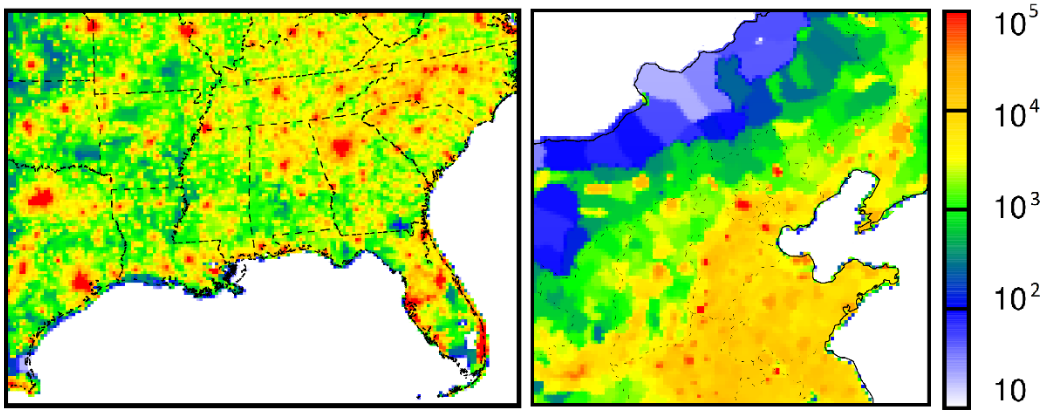

Figure 39. Population in SUS (left) and NCP (right). Population data are both for 2015.

Table 19. Incidence of mortality of respiratory (RDM) and cardiovascular (CDM) diseases. Units are cases per 100,000 people.

	SUS	NCP
RMD	18-40	~82
CMD	220-360	~78

- Incidence rates are calculated based on dataset recruited in BenMAP and GBD.

6.4 Conclusions

This chapter detailed analyzed O_3-related health risk in NCP and SUS. A total of ~ 0.11 million and 0.12 million premature mortalities are estimated by using different emission inventories in NCP. A major contribution from COPD is estimated to account for ~33.3% of total mortality. Emission-related health impacts account for ~46.5% of total mortality in NCP based on simulation from EDGAR+. Emissions from Hebei and Shandong dominate the impacts in high risk area (central NCP). Emissions from industry, energy and on-road sectors correspond to 79% of emission-related mortality in this study. Health risk analysis in SUS indicate that nature and anthropogenic emissions have less contribution to O_3-related health problems, the major source is the background O_3. In emission-related mortality, on-road emissions are the major sources followed by energy and biogenic emissions. Differences between NCP and SUS are mainly due to

different emissions, population and incidence rates. This simulation quantifies the health risk contribution from emission sources, which can be used in further estimation of economic loss and helps to deeper understand impacts from O_3 pollution.

CHAPTER 7. CONCLUSIONS

This study builds a fully understanding of current O_3 pollution in China and approaches in estimating source contributions firstly. Then a comprehensive analysis of O_3, its impact factors and source apportionment is conducted for 2017 summertime in NCP. A source apportionment analysis was also conducted for SUS for comparison with NCP. This study provides valuable results for designing O_3 controlling strategies in China. At the end, O_3-related health risk analysis in the last chapter, which helps to quantify health impacts from current O_3 pollution and their contributions from emissions sources.

Chapter 2 provides a brief overview of four major O_3 source apportionment approaches including DDM, BFM, OSAT and source-oriented methods. These methods are developed to quantify impacts from user specific sources by different ways. Each method has its own advantages and limitations. DDM has limitation in estimate contribution through high order chemical reactions, which causes significant uncertainty in tracking source contributions from secondary pollutants such as O_3. BMF can quantify effects of emission control policies in lowing O_3 but it is not a quantifying method to estimate current contribution from emissions sources. Both OSAT and O_3-oriented method are commonly used to quantify O_3 contribution from emission sources. But without the reactive tracer, OSAT misses information through O_3 forming processes and causes limitations in the result. Thus O_3-oriented method would be a better approach, which is applied in following chapters to quantify emission impacts on O_3 concentration. Overview of current O_3 source apportionment studies in China provides a clear result that China is experiencing severe O_3 pollution and the O_3 concentration is increasing in recent years. Anthropogenic emission of NO_x and VOCs and their effects on O_3 formation are commonly studied in China, but there is no a

sufficient study provides a comprehensive understanding in NCP where is one of the high O_3 risk area in China.

CTMs are a widely used method to analyze O_3 behaviors, but uncertainty remains in its sensitivity to emission inventory. To fully understand O_3 pollution in NCP, Chapter 3 simulates 2017 summertime O_3 concentration in NCP by using WRF/CMAQ system and compare the performances from using different emission inventories, this objective aims to evaluated performances from different inventories and improves simulation accuracy. In this chapter, model performances are validated, performances in EDGAR+ and MEIC are compared with each other. Statistical results reveal that EDGAR+ has an overall better performance in both regional scales and city scale while MEIC has better ability in predicting peak O_3 value. Summertime O_3 concentration are estimated higher than ~70 ppb in major cities in NCP. Significantly high concentrations are found in Beijing, Tianjin, south Hebei, west Shandong and north Henan with maximum of ~90 ppb, and these regions are classified as high risk area. O_3 analysis of diurnal and peak episodes indicates that high concentrations are always associated with slightly lower emissions under high temperature, low RH and steady wind field. Emissions could lead significant variations of O_3 predictions. Compare to MEIC, significant lower (< 200 tons/month) of NO_x and similar (difference within ±5 tons/month) VOCs emissions in EDGAR+ induce more O_3 formation; less O_3 is predicted when both NO_x and VOCs emissions are significantly lower (<200 tons/month and <10 tons/month, respectively); O_3 concentrations are barely changed (within ±10 ppb) when NO_x emissions are significantly lower (<200 tons/month) and VOCs emissions are significantly higher (>10 tons/month) in EDGAR+.

The source apportionment analysis of 2017 summertime O_3 in NCP is conducted in Chapter 4. Due to its better accuracy in matching overall O_3concentration and spatiotemporal variations,

EDGAR+ is applied in this simulation. This objective aims to deeper understand effects from emission sources. O_3 contributions from emission sources are quantified by sectoral and regional analysis. Overall, emission sources contribute ~30%-50% to total O_3 concentration in NCP, and the contributions are increased to ~50%-60% in peak episodes when O_3 concentration is higher than ~90 ppb in major cities. NO_x emissions are estimated to dominate O_3 concentrations in most NCP while VOCs emissions have significant impacts in megacities such as Tianjin and Shijiazhuang. Emissions from industry sector are the major contributors to O_3 formation followed by energy and on-road emissions, and they cause ~75% of total emission-related O_3 formation in study period. Local emissions are classified as the major contributors while impacts of emissions from surrounding regions are also important. Emissions from Hebei, Shandong and central China are the major sources of high concentration in NCP. In addition, emissions from central China have significant impacts in Beijing, central, south and southwestern NCP while Tianjin, western NCP are more associated with emissions from local and YRD especially in high concentration episodes.

Source apportionment study in SUS is conducted in Chapter 5, O_3 concentrations are predicted by using scaled EDGAR inventory. Similar analysis methods as used as in NCP scenario help to detailed analyze sectoral contribution to O_3 formation from emission sources. The results are compared to NCP to understand the differences between developing and developed countries. Both NCP and SUS have general high sensitivity to NO_x emission than to VOCs. High contributions are always found in megacities in NCP and SUS where NO_x emissions are high in these regions. It is different to NCP that anthropogenic emissions have significantly less contributions in SUS while contribution from biogenic emissions dominate the O_3 formation especially in Florida. Biogenic emissions are generally have slightly impacts in NCP. The main

reason of this phenomenon is the low anthropogenic emissions in SUS. Total NO_x and VOCs emissions in SUS are much lower than in NCP. Though most anthropogenic emissions are low, contribution from on-road emissions also cause ~5-8 ppb O_3 in SUS.

O_3-related health risk analysis are shown in Chapter 6 for both NCP and SUS and their contributions from emission sources. Generally, the health impacts are calculated associate with pollution concentration, population and baseline incidence rates. Estimating functions are from previous epidemiological studies that indicate a certain threshold of O_3 concentration, beyond which will cause additional adverse health effects. Health impacts due to emission sources are quantified. There are total of ~0.11 thousand premature mortalities due to respiratory and cardiovascular diseases estimated in NCP based on EDGAR+ while MEIC predicts slightly higher (by 0.12 thousand) mortality for same period. COPD is the major disease that causes ~40% of total premature mortality. Source contribution results are consisted with concentration results in chapter 5. NO_x emissions cause 82.5% of emission-related premature mortality, correspond to 43,211 deaths. Industry, energy and on-road emissions cause ~79% of emission-related premature mortality. Emissions from central China, Hebei and Shandong provinces are the major regional sources that cause ~55% of total death. It is noted that emissions from Beijing and Tianjin also has high contribution to local premature mortality even their contributions to concentration is not that high, the main reason is the high population in these regions. A total of 35175 all-cause mortalities are estimated in this study for SUS, which is mainly due to respiratory (4605) and cardiovascular (7913) diseases. a total of 22 thousand ER visits and 6.5 million hospital admissions indicates that even O_3 concentration is not at a high value, its impact on human health remains significantly. Health impacts in SUS are mainly from on-road, energy and biogenic emissions, which account for ~73% of total emission-related mortality.

This work details overview O_3 source apportionment methods and applies in analyzing O_3 behaviors in NCP and SUS and their source contributions. Though extensive work has been done to deeper understand O_3 in NCP and SUS, there are still uncertainties remain to be improved in future. A year-long improvement of emission inventory should be conducted to provide long-term O_3 simulation in both high and low concentration seasons and thus to increase accurate of the results from source apportionment and health risk analysis. Furthermore, to measure the long-term O_3 behavior and its impacts, simulation period should be extent to decades in cases. Historical and future potential changes would lead a deeper understanding of O_3 pollution. To comprehensive analyze current O_3 pollution in China, a national wide investigation is also needed to fully evaluate emission contributions not only in high risk regions but also in increasing developing regions such as south and southeastern China, where emissions structures are different with NCP and so as to their contributions. Finally, a further study on O_3-related impacts on economic and ecosystem should be processed to evaluate the total impacts from O_3 pollution.

REFERENCES

1. Karlsson, P. E.; Klingberg, J.; Engardt, M.; Andersson, C.; Langner, J.; Karlsson, G. P.; Pleijel, H., Past, present and future concentrations of ground-level ozone and potential impacts on ecosystems and human health in northern Europe. *Science of The Total Environment* **2017,** *576*, 22-35.
2. Feng, Z.; De Marco, A.; Anav, A.; Gualtieri, M.; Sicard, P.; Tian, H.; Fornasier, F.; Tao, F.; Guo, A.; Paoletti, E., Economic losses due to ozone impacts on human health, forest productivity and crop yield across China. *Environment International* **2019,** *131*, 104966.
3. Hubbell, B. J.; Hallberg, A.; McCubbin, D. R.; Post, E., Health-related benefits of attaining the 8-hr ozone standard. *Environmental health perspectives* **2004,** *113*, (1), 73-82.
4. Orru, H.; Andersson, C.; Ebi, K. L.; Langner, J.; Åström, C.; Forsberg, B., Impact of climate change on ozone-related mortality and morbidity in Europe. *European Respiratory Journal* **2013,** *41*, (2), 285-294.
5. Wang, Y.; Zu, Y.; Huang, L.; Zhang, H.; Wang, C.; Hu, J., Associations between daily outpatient visits for respiratory diseases and ambient fine particulate matter and ozone levels in Shanghai, China. *Environmental pollution* **2018,** *240*, 754-763.
6. Lippmann, M., Health effects of ozone a critical review. *Japca* **1989,** *39*, (5), 672-695.
7. Chuwah, C.; van Noije, T.; van Vuuren, D. P.; Stehfest, E.; Hazeleger, W., Global impacts of surface ozone changes on crop yields and land use. *Atmospheric Environment* **2015,** *106*, 11-23.
8. Sicard, P.; Anav, A.; Marco, A. D.; Paoletti, E., Projected global ground-level ozone impacts on vegetation under different emission and climate scenarios. *Atmospheric Chemistry and Physics* **2017,** *17*, (19), 12177-12196.
9. McCarthy, J. E.; Lattanzio, R. K. In *Ozone Air Quality Standards: EPA's 2015 Revision*, 2014; Library of Congress, Congressional Research Service: 2014.
10. McGlynn, D.; Mao, H.; Wu, Z.; Sive, B.; Sharac, T. J. A., Understanding long-term variations in surface ozone in United States (US) National Parks. **2018,** *9*, (4), 125.
11. Levelt, P. F.; Joiner, J.; Tamminen, J.; Veefkind, J. P.; Bhartia, P. K.; Carn, S. J. A. C.; Physics, The Ozone Monitoring Instrument: overview of 14 years in space. **2018,** *18*, 5699.
12. Wang, T.; Xue, L.; Brimblecombe, P.; Lam, Y. F.; Li, L.; Zhang, L. J. S. o. t. T. E., Ozone pollution in China: A review of concentrations, meteorological influences, chemical precursors, and effects. **2017,** *575*, 1582-1596.
13. Fann, N.; Lamson, A. D.; Anenberg, S. C.; Wesson, K.; Risley, D.; Hubbell, B. J., Estimating the national public health burden associated with exposure to ambient PM2. 5 and ozone. *Risk Analysis: An International Journal* **2012,** *32*, (1), 81-95.
14. Liu, H.; Liu, S.; Xue, B.; Lv, Z.; Meng, Z.; Yang, X.; Xue, T.; Yu, Q.; He, K. J. A. e., Ground-level ozone pollution and its health impacts in China. **2018,** *173*, 223-230.
15. Feng, Z.; Hu, E.; Wang, X.; Jiang, L.; Liu, X. J. E. P., Ground-level O3 pollution and its impacts on food crops in China: a review. **2015,** *199*, 42-48.
16. Ma, Z.; Xu, J.; Quan, W.; Zhang, Z.; Lin, W.; Xu, X., Significant increase of surface ozone at a rural site, north of eastern China. *Atmospheric Chemistry and Physics* **2016,** *16*, (6), 3969-3977.

17. Sun, L.; Xue, L.; Wang, T.; Gao, J.; Ding, A.; Cooper, O. R.; Lin, M.; Xu, P.; Wang, Z.; Wang, X., Significant increase of summertime ozone at Mount Tai in Central Eastern China. *Atmospheric Chemistry and Physics* **2016,** *16*, (16), 10637-10650.

18. Cooper, O. R.; Gao, R. S.; Tarasick, D.; Leblanc, T.; Sweeney, C., Long‐term ozone trends at rural ozone monitoring sites across the United States, 1990–2010. *Journal of Geophysical Research: Atmospheres* **2012,** *117*, (D22).

19. Lin, M.; Horowitz, L. W.; Payton, R.; Fiore, A. M.; Tonnesen, G., US surface ozone trends and extremes from 1980 to 2014: quantifying the roles of rising Asian emissions, domestic controls, wildfires, and climate. *Atmospheric Chemistry & Physics* **2017,** *17*, (4).

20. Canty, T.; Hembeck, L.; Vinciguerra, T.; Anderson, D.; Goldberg, D.; Carpenter, S.; Allen, D.; Loughner, C.; Salawitch, R.; Dickerson, R. J. A. C. P., Ozone and NOx chemistry in the eastern US: evaluation of CMAQ/CB05 with satellite (OMI) data. **2015,** *15*, (19), 10965-10982.

21. Seinfeld, J., Improving Chemical Mechanisms for Ozone and Secondary Organic Carbon. **2018**.

22. Li, J.; Pochanart, P.; Wang, Z.; Liu, Y.; Yamaji, K.; Takigawa, M.; Kanaya, Y.; Akimoto, H., Impact of chemical production and transport on summertime diurnal ozone behavior at a mountainous site in North China Plain. *Sola* **2008,** *4*, 121-124.

23. Yang, Y.; Hong, L.; Si-Jia, L., Simulated impacts of sulfate and nitrate aerosol formation on surface-layer ozone concentrations in China. *Atmospheric and Oceanic Science Letters* **2014,** *7*, (5), 441-446.

24. Hu, X.-M.; Ma, Z.; Lin, W.; Zhang, H.; Hu, J.; Wang, Y.; Xu, X.; Fuentes, J. D.; Xue, M., Impact of the Loess Plateau on the atmospheric boundary layer structure and air quality in the North China Plain: A case study. *Science of the Total Environment* **2014,** *499*, 228-237.

25. Loughner, C. P.; Follette-Cook, M. B.; Duncan, B. N.; Hains, J.; Pickering, K. E.; Moy, J.; Tzortziou, M. J. J. o. t. A.; Association, W. M., The benefits of lower ozone due to air pollution emission reductions (2002–2011) in the Eastern US during extreme heat. **2020**, 1-13.

26. Nopmongcol, U.; Jung, J.; Kumar, N.; Yarwood, G. J. A. e., Changes in US background ozone due to global anthropogenic emissions from 1970 to 2020. **2016,** *140*, 446-455.

27. Stockwell, W. R.; Lawson, C. V.; Saunders, E.; Goliff, W. S., A review of tropospheric atmospheric chemistry and gas-phase chemical mechanisms for air quality modeling. *Atmosphere* **2012,** *3*, (1), 1-32.

28. Sillman, S., Overview: Tropospheric ozone, smog and ozone-NOx-VOC sensitivity. *Treatise on Geochemistry* **2003**.

29. Chi, X.; Liu, C.; Xie, Z.; Fan, G.; Wang, Y.; He, P.; Fan, S.; Hong, Q.; Wang, Z.; Yu, X., Observations of ozone vertical profiles and corresponding precursors in the low troposphere in Beijing, China. *Atmospheric Research* **2018,** *213*, 224-235.

30. Chang, C.-Y.; Faust, E.; Hou, X.; Lee, P.; Kim, H. C.; Hedquist, B. C.; Liao, K.-J., Investigating ambient ozone formation regimes in neighboring cities of shale plays in the Northeast United States using photochemical modeling and satellite retrievals. *Atmospheric environment* **2016,** *142*, 152-170.

31. Cohan, D. S. In *Applicability of CMAQ-DDM to Source Apportionment and Control Strategy Development*, 3rd Annual CMAS Models-3 Users' Conference, RTP, NC,(October 2004), 2004; 2004.

32. Kelly, J. T.; Baker, K. R.; Napelenok, S. L.; Roselle, S. J., Examining single-source secondary impacts estimated from brute-force, decoupled direct method, and advanced plume treatment approaches. *Atmospheric Environment* **2015,** *111*, 10-19.

33. Yarwood, G.; Wilson, G.; Morris, R.; Yocke, M. J. E. I. C. r. t. t. S. C. A. Q. M. D., Diamond Bar, CA, User's Guide to the Urban Airshed Model with Ozone Source Apportionment Development. **1997**.

34. Zhang, H.; Ying, Q. J. A. e., Contributions of local and regional sources of NOx to ozone concentrations in Southeast Texas. **2011,** *45*, (17), 2877-2887.

35. Ying, Q.; Krishnan, A. J. J. o. G. R. A., Source contributions of volatile organic compounds to ozone formation in southeast Texas. **2010,** *115*, (D17).

36. Wang, P.; Chen, Y.; Hu, J.; Zhang, H.; Ying, Q. J. E. s.; technology, Attribution of Tropospheric Ozone to NO x and VOC Emissions: Considering Ozone Formation in the Transition Regime. **2018,** *53*, (3), 1404-1412.

37. Wang, X.; Liang, X.-Z.; Jiang, W.; Tao, Z.; Wang, J. X.; Liu, H.; Han, Z.; Liu, S.; Zhang, Y.; Grell, G. A. J. A. E., WRF-Chem simulation of East Asian air quality: Sensitivity to temporal and vertical emissions distributions. **2010,** *44*, (5), 660-669.

38. Wang, Y.; Zhang, Y.; Hao, J.; Luo, M. J. A. C.; Physics, Seasonal and spatial variability of surface ozone over China: contributions from background and domestic pollution. **2011,** *11*, (7), 3511.

39. Zhao, B.; Wang, P.; Ma, J.; Zhu, S.; Pozzer, A.; Li, W. J. A. C.; Discussions, P., A high-resolution emission inventory of primary pollutants for the Huabei region, China. **2011,** *11*, (7).

40. Zhang, H.; Li, J.; Ying, Q.; Yu, J. Z.; Wu, D.; Cheng, Y.; He, K.; Jiang, J. J. A. e., Source apportionment of PM2. 5 nitrate and sulfate in China using a source-oriented chemical transport model. **2012,** *62*, 228-242.

41. Ma, J.; Van Aardenne, J., Impact of different emission inventories on simulated tropospheric ozone over China: a regional chemical transport model evaluation. **2004**.

42. Su, S.; Li, B.; Cui, S.; Tao, S. J. E. s.; technology, Sulfur dioxide emissions from combustion in China: from 1990 to 2007. **2011,** *45*, (19), 8403-8410.

43. Zhao, Y.; Wang, S.; Duan, L.; Lei, Y.; Cao, P.; Hao, J. J. A. E., Primary air pollutant emissions of coal-fired power plants in China: Current status and future prediction. **2008,** *42*, (36), 8442-8452.

44. Ohara, T.; Yamaji, K.; Uno, I.; Tanimoto, H.; Sugata, S.; Nagashima, T.; Kurokawa, J.-i.; Horii, N.; Akimoto, H., Long-term simulations of surface ozone in East Asia during 1980–2020 with CMAQ and REAS inventory. In *Air Pollution Modeling and Its Application XIX*, Springer: 2008; pp 136-144.

45. Verstraeten, W. W.; Neu, J. L.; Williams, J. E.; Bowman, K. W.; Worden, J. R.; Boersma, K. F. J. N. g., Rapid increases in tropospheric ozone production and export from China. **2015,** *8*, (9), 690-695.

46. Tang, H.; Takigawa, M.; Liu, G.; Zhu, J.; Kobayashi, K. J. G. C. B., A projection of ozone‐induced wheat production loss in C hina and I ndia for the years 2000 and 2020 with exposure‐based and flux‐based approaches. **2013,** *19*, (9), 2739-2752.

47. Ma, Z.; Xu, J.; Quan, W.; Zhang, Z.; Lin, W.; Xu, X. J. A. C.; Physics, Significant increase of surface ozone at a rural site, north of eastern China. **2016,** *16*, (6).

48. Kang, M.; Guo, H.; Wang, P.; Fu, P.; Ying, Q.; Liu, H.; Zhao, Y.; Zhang, H., Characterization and source apportionment of marine aerosols over the East China Sea. *Science of the Total Environment* **2019,** *651*, 2679-2688.

49. Li, M.; Zhang, Q.; Kurokawa, J.-i.; Woo, J.-H.; He, K.; Lu, Z.; Ohara, T.; Song, Y.; Streets, D. G.; Carmichael, G. R. J. A. C.; Physics, MIX: a mosaic Asian anthropogenic emission inventory under the international collaboration framework of the MICS-Asia and HTAP. **2017,** *17*, (2).

50. Hu, J.; Li, X.; Huang, L.; Ying, Q.; Zhang, Q.; Zhao, B.; Wang, S.; Zhang, H., Ensemble prediction of air quality using the WRF/CMAQ model system for health effect studies in China. *Atmos. Chem. Phys.* **2017,** *17*, (21), 13103-13118.

51. Li, K.; Jacob, D. J.; Liao, H.; Shen, L.; Zhang, Q.; Bates, K. H. J. P. o. t. N. A. o. S., Anthropogenic drivers of 2013–2017 trends in summer surface ozone in China. **2019,** *116*, (2), 422-427.

52. Kwok, R.; Baker, K.; Napelenok, S.; Tonnesen, G., Photochemical grid model implementation and application of VOC, NO x, and O 3 source apportionment. *Geoscientific Model Development* **2015,** *8*, (1), 99-114.

53. Wang, P.; Chen, Y.; Hu, J.; Zhang, H.; Ying, Q., Attribution of Tropospheric Ozone to NO x and VOC Emissions: Considering Ozone Formation in the Transition Regime. *Environmental science & technology* **2018,** *53*, (3), 1404-1412.

54. Bloomer, B. J.; Vinnikov, K. Y.; Dickerson, R. R., Changes in seasonal and diurnal cycles of ozone and temperature in the eastern US. *Atmospheric Environment* **2010,** *44*, (21-22), 2543-2551.

55. Keiser, D.; Lade, G.; Rudik, I., Air pollution and visitation at US national parks. *Science advances* **2018,** *4*, (7), eaat1613.

56. Cooper, O. R.; Parrish, D.; Stohl, A.; Trainer, M.; Nédélec, P.; Thouret, V.; Cammas, J.-P.; Oltmans, S.; Johnson, B.; Tarasick, D., Increasing springtime ozone mixing ratios in the free troposphere over western North America. *Nature* **2010,** *463*, (7279), 344-348.

57. Nopmongcol, U.; Jung, J.; Kumar, N.; Yarwood, G., Changes in US background ozone due to global anthropogenic emissions from 1970 to 2020. *Atmospheric environment* **2016,** *140*, 446-455.

58. Verstraeten, W. W.; Neu, J. L.; Williams, J. E.; Bowman, K. W.; Worden, J. R.; Boersma, K. F., Rapid increases in tropospheric ozone production and export from China. *Nature geoscience* **2015,** *8*, (9), 690.

59. Zhang, Y.; Wang, Y., Climate-driven ground-level ozone extreme in the fall over the Southeast United States. *Proceedings of the National Academy of Sciences* **2016,** *113*, (36), 10025-10030.

60. Travis, K. R.; Jacob, D. J., Systematic bias in evaluating chemical transport models with maximum daily 8 h average (MDA8) surface ozone for air quality applications: a case study with GEOS-Chem v9. 02. *Geoscientific Model Development* **2019,** *12*, (8), 3641-3648.

61. Johnson, M.; Kuang, S.; Wang, L.; Newchurch, M., Evaluating summer-time ozone enhancement events in the southeast United States. *Atmosphere* **2016,** *7*, (8), 108.

62. Hodzic, A.; Madronich, S., Response of surface ozone over the continental United States to UV radiation declines from the expected recovery of stratospheric ozone. *npj Climate and Atmospheric Science* **2018,** *1*, (1), 35.

63. Camalier, L.; Cox, W.; Dolwick, P., The effects of meteorology on ozone in urban areas and their use in assessing ozone trends. *Atmospheric Environment* **2007,** *41*, (33), 7127-7137.

64. Li, T.; Yan, M.; Ma, W.; Ban, J.; Liu, T.; Lin, H.; Liu, Z., Short-term effects of multiple ozone metrics on daily mortality in a megacity of China. *Environmental science and pollution research* **2015,** *22*, (11), 8738-8746.

65. Xiang, J.; Weschler, C. J.; Zhang, J.; Zhang, L.; Sun, Z.; Duan, X.; Zhang, Y., Ozone in Urban China: Impact on Mortalities and Approaches for Establishing Indoor Guideline Concentrations. *Indoor air* **2019**.

66. Yim, S. H.; Wang, M.; Gu, Y.; Yang, Y.; Dong, G.; Li, Q., Effect of Urbanization on Ozone and Resultant Health Effects in the Pearl River Delta Region of China. *Journal of Geophysical Research: Atmospheres* **2019**.

67. Seltzer, K. M.; Shindell, D. T.; Malley, C. S., Measurement-based assessment of health burdens from long-term ozone exposure in the United States, Europe, and China. *Environmental Research Letters* **2018,** *13*, (10), 104018.

68. Turner, M. C.; Jerrett, M.; Pope III, C. A.; Krewski, D.; Gapstur, S. M.; Diver, W. R.; Beckerman, B. S.; Marshall, J. D.; Su, J.; Crouse, D. L., Long-term ozone exposure and mortality in a large prospective study. *American journal of respiratory and critical care medicine* **2016,** *193*, (10), 1134-1142.

69. Wang, T.; Xue, L.; Brimblecombe, P.; Lam, Y. F.; Li, L.; Zhang, L., Ozone pollution in China: A review of concentrations, meteorological influences, chemical precursors, and effects. *Science of the Total Environment* **2017,** *575*, 1582-1596.

70. Colucci, J. M.; Begeman, C. R., The Automotive Contribution to Air-Borne Polynuclear Aromatic Hydrocarbons in Detroit: Informative Report No. 6. *Journal of the Air Pollution Control Association* **1965,** *15*, (3), 113-122.

71. Hopke, P. K., Review of receptor modeling methods for source apportionment. *Journal of the Air & Waste Management Association* **2016,** *66*, (3), 237-259.

72. Prinz, B.; Stratmann, H., The possible use of factor analysis in investigating air quality. *Staub-Reinhalt Luft* **1968,** *28*, 33-39.

73. Blifford Jr, I. H.; Meeker, G. O., A factor analysis model of large scale pollution. *Atmospheric Environment (1967)* **1967,** *1*, (2), 147-157.

74. Miller, M.; Friedlander, S.; Hidy, G., A chemical element balance for the Pasadena aerosol. *Journal of Colloid and Interface Science* **1972,** *39*, (1), 165-176.

75. Winchester, J. W.; Nifong, G. D., Water pollution in Lake Michigan by trace elements from pollution aerosol fallout. *Water, Air, and Soil Pollution* **1971,** *1*, (1), 50-64.

76. Watson, J. G.; Cooper, J. A.; Huntzicker, J. J., The effective variance weighting for least squares calculations applied to the mass balance receptor model. *Atmospheric Environment (1967)* **1984,** *18*, (7), 1347-1355.

77. Dickinson, R. P.; Gelinas, R. J., Sensitivity analysis of ordinary differential equation systems—a direct method. *Journal of computational physics* **1976,** *21*, (2), 123-143.

78. Dunker, A. M., Efficient calculation of sensitivity coefficients for complex atmospheric models. *Atmospheric Environment (1967)* **1981,** *15*, (7), 1155-1161.

79. Dunker, A. M.; Yarwood, G.; Ortmann, J. P.; Wilson, G. M., Comparison of source apportionment and source sensitivity of ozone in a three-dimensional air quality model. *Environmental science & technology* **2002,** *36*, (13), 2953-2964.

80. Dunker, A. M.; Yarwood, G.; Ortmann, J. P.; Wilson, G. M. J. E. s.; technology, Comparison of source apportionment and source sensitivity of ozone in a three-dimensional air quality model. **2002,** *36*, (13), 2953-2964.

81. Kwok, R.; Baker, K.; Napelenok, S.; Tonnesen, G. J. G. M. D., Photochemical grid model implementation and application of VOC, NOx, and O3 source apportionment. **2015,** *8*, (1), 99-114.

82. Zhang, Y.; Vijayaraghavan, K.; Seigneur, C. J. J. o. G. R. A., Evaluation of three probing techniques in a three‐dimensional air quality model. **2005,** *110*, (D2).

83. Collet, S.; Minoura, H.; Kidokoro, T.; Sonoda, Y.; Kinugasa, Y.; Karamchandani, P.; Johnson, J.; Shah, T.; Jung, J.; DenBleyker, A. J. J. o. t. A.; Association, W. M., Future year ozone source attribution modeling studies for the eastern and western United States. **2014,** *64*, (10), 1174-1185.

84. Christiansen, J., Second joint conference on applications of air pollution meteorology. **1980**.

85. Dunker, A. M., The decoupled direct method for calculating sensitivity coefficients in chemical kinetics. *The Journal of chemical physics* **1984,** *81*, (5), 2385-2393.

86. Hakami, A.; Odman, M. T.; Russell, A. G., High-order, direct sensitivity analysis of multidimensional air quality models. *Environmental Science & Technology* **2003,** *37*, (11), 2442-2452.

87. Jeon, W.-B.; Lee, S.-H.; Lee, H.; Park, C.; Kim, D.-H.; Park, S.-Y., A study on high ozone formation mechanism associated with change of NOx/VOCs ratio at a rural area in the Korean Peninsula. *Atmospheric Environment* **2014,** *89*, 10-21.

88. Yang, Y.-J.; Wilkinson, J. G.; Odman, M. T.; Russell, A. G., Ozone sensitivity and uncertainty analysis using DDM-3D in a photochemical air quality model. In *Air Pollution Modeling and Its Application XIII*, Springer: 2000; pp 183-194.

89. Kim, S.; Byun, D. W.; Cohan, D., Contributions of inter-and intra-state emissions to ozone over Dallas-Fort Worth, Texas. *Civil Engineering and Environmental Systems* **2009,** *26*, (1), 103-116.

90. Cohan, D. S.; Koo, B.; Yarwood, G., Influence of uncertain reaction rates on ozone sensitivity to emissions. *Atmospheric Environment* **2010,** *44*, (26), 3101-3109.

91. Mendoza-Dominguez, A.; Wilkinson, J. G.; Yang, Y.-J.; Russell, A. G., Modeling and direct sensitivity analysis of biogenic emissions impacts on regional ozone formation in the Mexico-US border area. *Journal of the Air & Waste Management Association* **2000,** *50*, (1), 21-31.

92. Luecken, D.; Napelenok, S.; Strum, M.; Scheffe, R.; Phillips, S., Sensitivity of ambient atmospheric formaldehyde and ozone to precursor species and source types across the United States. *Environmental science & technology* **2018,** *52*, (8), 4668-4675.

93. Dunker, A. M.; Koo, B.; Yarwood, G., Ozone sensitivity to isoprene chemistry and emissions and anthropogenic emissions in central California. *Atmospheric environment* **2016,** *145*, 326-337.

94. Cohan, D. S.; Hakami, A.; Hu, Y.; Russell, A. G., Nonlinear response of ozone to emissions: Source apportionment and sensitivity analysis. *Environmental Science & Technology* **2005,** *39*, (17), 6739-6748.

95. Downey, N.; Emery, C.; Jung, J.; Sakulyanontvittaya, T.; Hebert, L.; Blewitt, D.; Yarwood, G., Emission reductions and urban ozone responses under more stringent US standards. *Atmospheric Environment* **2015,** *101*, 209-216.

96. Henneman, L. R.; Liu, C.; Hu, Y.; Mulholland, J. A.; Russell, A. G., Air quality modeling for accountability research: Operational, dynamic, and diagnostic evaluation. *Atmospheric environment* **2017,** *166*, 551-565.

97. Henneman, L. R.; Chang, H. H.; Liao, K.-J.; Lavoué, D.; Mulholland, J. A.; Russell, A. G., Accountability assessment of regulatory impacts on ozone and PM 2.5 concentrations using statistical and deterministic pollutant sensitivities. *Air Quality, Atmosphere & Health* **2017,** *10*, (6), 695-711.

98. Tang, W.; Cohan, D.; Pour-Biazar, A.; Lamsal, L.; White, A.; Xiao, X.; Zhou, W.; Henderson, B.; Lash, B., Influence of satellite-derived photolysis rates and NO x emissions on Texas ozone modeling. *Atmospheric Chemistry and Physics* **2015,** *15*, (4), 1601-1619.

99. Dunker, A. M.; Koo, B.; Yarwood, G., Source apportionment of the anthropogenic increment to ozone, formaldehyde, and nitrogen dioxide by the path-integral method in a 3D model. *Environmental science & technology* **2015,** *49*, (11), 6751-6759.

100. Itahashi, S.; Uno, I.; Kim, S., Seasonal source contributions of tropospheric ozone over East Asia based on CMAQ–HDDM. *Atmospheric environment* **2013,** *70*, 204-217.

101. Hakami, A.; Harley, R.; Milford, J.; Odman, M.; Russell, A., Regional, three-dimensional assessment of the ozone formation potential of organic compounds. *Atmospheric Environment* **2004,** *38*, (1), 121-134.

102. Wang, X.; Zhang, Y.; Hu, Y.; Zhou, W.; Zeng, L.; Hu, M.; Cohan, D. S.; Russell, A. G., Decoupled direct sensitivity analysis of regional ozone pollution over the Pearl River Delta during the PRIDE-PRD2004 campaign. *Atmospheric environment* **2011,** *45*, (28), 4941-4949.

103. Byun, D.; Schere, K. L., Review of the Governing Equations, Computational Algorithms, and Other Components of the Models-3 Community Multiscale Air Quality (CMAQ) Modeling System. *Applied Mechanics Reviews* **2006,** *59*, (2), 51-77.

104. Burr, M. J.; Zhang, Y., Source apportionment of fine particulate matter over the Eastern U.S. Part I: source sensitivity simulations using CMAQ with the Brute Force method. *Atmospheric Pollution Research* **2011,** *2*, (3), 300-317.

105. Nguyen, N. P.; Marshall, J. D., Impact, efficiency, inequality, and injustice of urban air pollution: variability by emission location. *Environmental Research Letters* **2018,** *13*, (2), 024002.

106. Tang, X.; Wang, Z.; Zhu, J.; Gbaguidi, A. E.; Wu, Q.; Li, J.; Zhu, T., Sensitivity of ozone to precursor emissions in urban Beijing with a Monte Carlo scheme. *Atmospheric Environment* **2010,** *44*, (31), 3833-3842.

107. Qu, Y.; An, J.; Li, J.; Chen, Y.; Li, Y.; Liu, X.; Hu, M., Effects of NO x and VOCs from five emission sources on summer surface O 3 over the Beijing-Tianjin-Hebei region. *Advances in Atmospheric Sciences* **2014,** *31*, (4), 787-800.

108. Zavala, M.; Lei, W.; Molina, M.; Molina, L., Modeled and observed ozone sensitivity to mobile-source emissions in Mexico City. *Atmospheric Chemistry and Physics* **2009,** *9*, (1), 39-55.

109. Zhang, R.; Cohan, A.; Biazar, A. P.; Cohan, D. S., Source apportionment of biogenic contributions to ozone formation over the United States. *Atmospheric environment* **2017,** *164*, 8-19.

110. Baker, K.; Woody, M.; Tonnesen, G.; Hutzell, W.; Pye, H.; Beaver, M.; Pouliot, G.; Pierce, T., Contribution of regional-scale fire events to ozone and PM2. 5 air quality estimated by photochemical modeling approaches. *Atmospheric Environment* **2016,** *140*, 539-554.

111. Dolwick, P.; Akhtar, F.; Baker, K. R.; Possiel, N.; Simon, H.; Tonnesen, G., Comparison of background ozone estimates over the western United States based on two separate model methodologies. *Atmospheric Environment* **2015,** *109*, 282-296.

112. Wang, X.; Carmichael, G.; Chen, D.; Tang, Y.; Wang, T., Impacts of different emission sources on air quality during March 2001 in the Pearl River Delta (PRD) region. *Atmospheric Environment* **2005,** *39*, (29), 5227-5241.

113. Minoura, H.; Chow, J. C.; Watson, J. G.; Fu, J. S.; Dong, X.; Yang, C.-E., Vertical circulation of atmospheric pollutants near mountains during a Southern California ozone episode. *Aerosol and Air Quality Research* **2016,** *16*, (10), 2396-2404.

114. Dunker, A. M.; Koo, B.; Yarwood, G. J. E. s.; technology, Source apportionment of the anthropogenic increment to ozone, formaldehyde, and nitrogen dioxide by the path-integral method in a 3D model. **2015,** *49*, (11), 6751-6759.

115. Price, J.; Yarwood, G.; Koo, B. J. C., Final Report Improved OSAT, APCA and PSAT Algorithms for CAMx. **2015,** *582*, 15-50417.

116. Li, Y.; Lau, A. H.; Fung, J. H.; Zheng, J.; Zhong, L.; Louie, P. K. K. J. J. o. G. R. A., Ozone source apportionment (OSAT) to differentiate local regional and super-regional source contributions in the Pearl River Delta region, China. **2012,** *117*, (D15).

117. Wang, X.; Li, J.; Zhang, Y.; Xie, S.; Tang, X. J. S. i. C. S. B. C., Ozone source attribution during a severe photochemical smog episode in Beijing, China. **2009,** *52*, (8), 1270-1280.

118. Zhang, R.; Cohan, A.; Biazar, A. P.; Cohan, D. S. J. A. e., Source apportionment of biogenic contributions to ozone formation over the United States. **2017,** *164*, 8-19.

119. Li, Y.; Lau, A. K.; Fung, J. C.; Ma, H.; Tse, Y. J. A. e., Systematic evaluation of ozone control policies using an Ozone Source Apportionment method. **2013,** *76*, 136-146.

120. Baker, K. R.; Emery, C.; Dolwick, P.; Yarwood, G. J. A. E., Photochemical grid model estimates of lateral boundary contributions to ozone and particulate matter across the continental United States. **2015,** *123*, 49-62.

121. Li, H.; Li, L.; Huang, C.; An, J.; Yan, R.; Huang, H.; Wang, Y.; Lu, Q.; Wang, Q.; Lou, S. J. H. J. k. X. H. K., Ozone source apportionment at urban area during a typical photochemical pollution episode in the summer of 2013 in the Yangtze River Delta. **2015,** *36*, (1), 1-10.

122. Yarwood, G.; Emery, C.; Baker, K.; Dolwick, P., Resolving and Quantifying Ozone Contributions from Boundary Conditions Within Regional Models. In *Air Pollution Modeling and its Application XXIII*, Springer: 2014; pp 445-450.

123. Lefohn, A. S.; Emery, C.; Shadwick, D.; Wernli, H.; Jung, J.; Oltmans, S. J. J. A. E., Estimates of background surface ozone concentrations in the United States based on model-derived source apportionment. **2014,** *84*, 275-288.

124. Zhang, Y.; Su, H.; Zhong, L.; Cheng, Y.; Zeng, L.; Wang, X.; Xiang, Y.; Wang, J.; Gao, D.; Shao, M. J. A. E., Regional ozone pollution and observation-based approach for analyzing ozone–precursor relationship during the PRIDE-PRD2004 campaign. **2008,** *42*, (25), 6203-6218.

125. Karamchandani, P.; Long, Y.; Pirovano, G.; Balzarini, A.; Yarwood, G. J. A. C.; Physics, Source-sector contributions to European ozone and fine PM in 2010 using AQMEII modeling data. **2017,** *17*, (9), 5643.

126. Li, L.; An, J.; Shi, Y.; Zhou, M.; Yan, R.; Huang, C.; Wang, H.; Lou, S.; Wang, Q.; Lu, Q. J. A. e., Source apportionment of surface ozone in the Yangtze River Delta, China in the summer of 2013. **2016,** *144*, 194-207.

127. Li, L.; An, J.; Huang, L.; Yan, R.; Huang, C.; Yarwood, G. J. A. e., Ozone source apportionment over the Yangtze River Delta region, China: Investigation of regional transport, sectoral contributions and seasonal differences. **2019,** *202*, 269-280.

128. Zawacki, M.; Baker, K. R.; Phillips, S.; Davidson, K.; Wolfe, P. J. A. e., Mobile source contributions to ambient ozone and particulate matter in 2025. **2018,** *188*, 129-141.

129. Nopmongcol, U.; Alvarez, Y.; Jung, J.; Grant, J.; Kumar, N.; Yarwood, G. J. A. E., Source contributions to United States ozone and particulate matter over five decades from 1970 to 2020. **2017,** *167*, 116-128.

130. Collet, S.; Kidokoro, T.; Karamchandani, P.; Jung, J.; Shah, T. J. J. o. t. A.; Association, W. M., Future year ozone source attribution modeling study using CMAQ-ISAM. **2018,** *68*, (11), 1239-1247.

131. Klemm, O.; Stockwell, W.; Schlager, H.; Krautstrunk, M., NOx or VOC limitation in East German ozone plumes? *Journal of atmospheric chemistry* **2000,** *35*, (1), 1-18.

132. Yarwood, G.; Stoeckenius, T.; Wilson, G.; Morris, R.; Yocke, M., Development of a methodology to assess geographic and temporal ozone control strategies for the South Coast Air Basin. *Prepared for South Coast Air Quality Management District, Diamond Bar, CA* **1996**.

133. Yarwood, G.; Wilson, G.; Morris, R.; Yocke, M., User's Guide to the Urban Airshed Model with Ozone Source Apportionment Development. *ENVIRON International Corporation report to the South Coast Air Quality Management District, Diamond Bar, CA* **1997**.

134. Zhang, H.; Ying, Q., Contributions of local and regional sources of NOx to ozone concentrations in Southeast Texas. *Atmospheric environment* **2011,** *45*, (17), 2877-2887.

135. Ying, Q.; Krishnan, A., Source contributions of volatile organic compounds to ozone formation in southeast Texas. *Journal of Geophysical Research: Atmospheres* **2010,** *115*, (D17).

136. Sillman, S., The use of NO y, H2O2, and HNO3 as indicators for ozone‐NO x‐hydrocarbon sensitivity in urban locations. *Journal of Geophysical Research: Atmospheres* **1995,** *100*, (D7), 14175-14188.

137. Sillman, S., The relation between ozone, NOx and hydrocarbons in urban and polluted rural environments. *Atmospheric Environment* **1999,** *33*, (12), 1821-1845.

138. Tonnesen, G. S.; Dennis, R. L., Analysis of radical propagation efficiency to assess ozone sensitivity to hydrocarbons and NO x: 1. Local indicators of instantaneous odd oxygen production sensitivity. *Journal of Geophysical Research: Atmospheres* **2000,** *105*, (D7), 9213-9225.

139. Lu, C. H.; Chang, J. S., On the indicator‐based approach to assess ozone sensitivities and emissions features. *Journal of Geophysical Research: Atmospheres* **1998,** *103*, (D3), 3453-3462.

140. Martin, R. V.; Fiore, A. M.; Van Donkelaar, A., Space‐based diagnosis of surface ozone sensitivity to anthropogenic emissions. *Geophysical Research Letters* **2004,** *31*, (6).

141. Zhang, Y.; Wen, X. Y.; Wang, K.; Vijayaraghavan, K.; Jacobson, M. Z., Probing into regional O3 and particulate matter pollution in the United States: 2. An examination of formation mechanisms through a process analysis technique and sensitivity study. *Journal of Geophysical Research: Atmospheres* **2009,** *114*, (D22).

142. Wang, X.; Li, J.; Zhang, Y.; Xie, S.; Tang, X., Ozone source attribution during a severe photochemical smog episode in Beijing, China. *Science in China Series B: Chemistry* **2009,** *52*, (8), 1270-1280.

143. Gao, J.; Zhu, B.; Xiao, H.; Kang, H.; Hou, X.; Yin, Y.; Zhang, L.; Miao, Q., Diurnal variations and source apportionment of ozone at the summit of Mount Huang, a rural site in Eastern China. *Environmental pollution* **2017,** *222*, 513-522.

144. Nagashima, T.; Sudo, K.; Akimoto, H.; Kurokawa, J.; Ohara, T., Long-term change in the source contribution to surface ozone over Japan. *Atmospheric Chemistry and Physics* **2017,** *17*, (13), 8231-8246.

145. Li, L.; An, J.; Huang, L.; Yan, R.; Huang, C.; Yarwood, G., Ozone source apportionment over the Yangtze River Delta region, China: Investigation of regional transport, sectoral contributions and seasonal differences. *Atmospheric environment* **2019,** *202*, 269-280.

146. Li, L.; An, J.; Shi, Y.; Zhou, M.; Yan, R.; Huang, C.; Wang, H.; Lou, S.; Wang, Q.; Lu, Q., Source apportionment of surface ozone in the Yangtze River Delta, China in the summer of 2013. *Atmospheric environment* **2016,** *144*, 194-207.

147. Li, Y.; Lau, A. H.; Fung, J. H.; Zheng, J.; Zhong, L.; Louie, P., Ozone source apportionment (OSAT) to differentiate local regional and super‐regional source contributions in the Pearl River Delta region, China. *Journal of Geophysical Research: Atmospheres* **2012,** *117*, (D15).

148. Wang, P.; Chen, Y.; Hu, J.; Zhang, H.; Ying, Q., Source apportionment of summertime ozone in China using a source-oriented chemical transport model. *Atmospheric Environment* **2019,** *211*, 79-90.

149. Luo, C.; St. John, J.; Xiuji, Z.; Lam, K.; Wang, T.; Chameides, W. J. J. o. G. R. A., A nonurban ozone air pollution episode over eastern China: Observations and model simulations. **2000,** *105*, (D2), 1889-1908.

150. Ma, J.; Zhou, X.; Hauglustaine, D. J. J. o. G. R. A., Summertime tropospheric ozone over China simulated with a regional chemical transport model 2. Source contributions and budget. **2002,** *107*, (D22), ACH 2-1-ACH 2-11.

151. Liu, X.-H.; Zhang, Y.; Xing, J.; Zhang, Q.; Wang, K.; Streets, D. G.; Jang, C.; Wang, W.-X.; Hao, J.-M. J. A. E., Understanding of regional air pollution over China using CMAQ, part II. Process analysis and sensitivity of ozone and particulate matter to precursor emissions. **2010,** *44*, (30), 3719-3727.

152. Wang, Y.; Shen, L.; Wu, S.; Mickley, L.; He, J.; Hao, J., Sensitivity of surface ozone over China to 2000–2050 global changes of climate and emissions. *Atmospheric Environment* **2013,** *75*, 374-382.

153. Wang, S.; Hao, J. J. J. o. E. S., Air quality management in China: Issues, challenges, and options. **2012,** *24*, (1), 2-13.

154. Liu, H.; Liu, S.; Xue, B.; Lv, Z.; Meng, Z.; Yang, X.; Xue, T.; Yu, Q.; He, K., Ground-level ozone pollution and its health impacts in China. *Atmospheric Environment* **2018,** *173*, 223-230.

155. Wang, S.; Zhao, M.; Xing, J.; Wu, Y.; Zhou, Y.; Lei, Y.; He, K.; Fu, L.; Hao, J. J. E. s.; technology, Quantifying the air pollutants emission reduction during the 2008 Olympic Games in Beijing. **2010,** *44*, (7), 2490-2496.

156. Shu, L.; Wang, T.; Xie, M.; Li, M.; Zhao, M.; Zhang, M.; Zhao, X. J. A. e., Episode study of fine particle and ozone during the CAPUM-YRD over Yangtze River Delta of China: Characteristics and source attribution. **2019,** *203*, 87-101.

157. Wu, J.; Wang, Q.; Chen, H.; Zhang, Y.; Wild, O. J. A.; Research, A. Q., On the origin of surface ozone episode in Shanghai over Yangtze River Delta during a prolonged heat wave. **2017,** *17*, (11), 2804-2815.

158. Liu, Y.; Li, L.; An, J.; Huang, L.; Yan, R.; Huang, C.; Wang, H.; Wang, Q.; Wang, M.; Zhang, W. J. A. E., Estimation of biogenic VOC emissions and its impact on ozone formation over the Yangtze River Delta region, China. **2018,** *186*, 113-128.

159. Han, Z.; Ueda, H.; Matsuda, K. J. T. B. C.; Meteorology, P., Model study of the impact of biogenic emission on regional ozone and the effectiveness of emission reduction scenarios over eastern China. **2005,** *57*, (1), 12-27.

160. Shen, J.; Zhang, Y.; Wang, X.; Li, J.; Chen, H.; Liu, R.; Zhong, L.; Jiang, M.; Yue, D.; Chen, D. J. A. E., An ozone episode over the Pearl River Delta in October 2008. **2015,** *122*, 852-863.

161. Zheng, J.; Zhong, L.; Wang, T.; Louie, P. K.; Li, Z. J. A. E., Ground-level ozone in the Pearl River Delta region: Analysis of data from a recently established regional air quality monitoring network. **2010,** *44*, (6), 814-823.

162. Zheng, J.; Shao, M.; Che, W.; Zhang, L.; Zhong, L.; Zhang, Y.; Streets, D. J. E. s.; technology, Speciated VOC emission inventory and spatial patterns of ozone formation potential in the Pearl River Delta, China. **2009,** *43*, (22), 8580-8586.

163. Shao, M.; Zhang, Y.; Zeng, L.; Tang, X.; Zhang, J.; Zhong, L.; Wang, B. J. J. o. E. M., Ground-level ozone in the Pearl River Delta and the roles of VOC and NOx in its production. **2009,** *90*, (1), 512-518.

164. Cheng, H.; Guo, H.; Saunders, S.; Lam, S.; Jiang, F.; Wang, X.; Simpson, I.; Blake, D.; Louie, P.; Wang, T. J. A. E., Assessing photochemical ozone formation in the Pearl River Delta with a photochemical trajectory model. **2010,** *44*, (34), 4199-4208.

165. Yang, W.; Chen, H.; Wang, W.; Wu, J.; Li, J.; Wang, Z.; Zheng, J.; Chen, D. J. E. P., Modeling study of ozone source apportionment over the Pearl River Delta in 2015. **2019,** *253*, 393-402.

166. Han, X.; Zhu, L.; Wang, S.; Meng, X.; Zhang, M.; Hu, J., Modeling study of impacts on surface ozone of regional transport and emissions reductions over North China Plain in summer 2015. *Atmospheric Chemistry and Physics* **2018**, 12207.

167. Wang, T.; Ding, A.; Gao, J.; Wu, W. S., Strong ozone production in urban plumes from Beijing, China. In 2006; Vol. 33.

168. Fu, J. S.; Streets, D. G.; Jang, C. J.; Jiming, H.; Kebin, H.; Litao, W.; Qiang, Z., Modeling Regional/Urban Ozone and Particulate Matter in Beijing, China. *Journal of the Air & Waste Management Association (Air & Waste Management Association)* **2009,** *59*, (1), 37-44.

169. Wang, X.; Li, J.; Zhang, Y.; Xie, S.; Tang, X., Ozone source attribution during a severe photochemical smog episode in Beijing, China. In 2009; Vol. 52, pp 1270-1280.

170. Liu, H.; Zhang, M.; Han, X.; Li, J.; Chen, L., Episode analysis of regional contributions to tropospheric ozone in Beijing using a regional air quality model. *Atmospheric Environment* **2019,** *199*, 299-312.

171. Guo, B.; Chen, F.; Deng, Y.; Zhang, H.; Qiao, X.; Qiao, Z.; Ji, K.; Zeng, J.; Luo, B.; Zhang, W., Using rush hour and daytime exposure indicators to estimate the short-term mortality effects of air pollution: A case study in the Sichuan Basin, China. *Environmental Pollution* **2018,** *242*, 1291-1298.

172. Xie, Y.; Dai, H.; Zhang, Y.; Hanaoka, T.; Masui, T., Health and economic impacts of ozone pollution in China: a provincial level analysis. *Atmos. Chem. Phys. Discuss.* **2017**, 1-63.

173. Weihan, S.; Wenzhi, S.; Chao, L.; Qiupeng, Z.; Wilson, Y. J. T. E. M. C. W., OZONE POLLUTION IN BEIJING-TIANJIN AREA. *Acta Scientiae Circumstantiae* **1987**, (4), 15.

174. Wang, T.; Ding, A.; Gao, J.; Wu, W. S., Strong ozone production in urban plumes from Beijing, China. *Geophysical Research Letters* **2006,** *33*, (21).

175. Wang, W.-N.; Cheng, T.-H.; Gu, X.-F.; Chen, H.; Guo, H.; Wang, Y.; Bao, F.-W.; Shi, S.-Y.; Xu, B.-R.; Zuo, X., Assessing spatial and temporal patterns of observed ground-level ozone in China. *Scientific reports* **2017,** *7*, (1), 3651.

176. Appel, K.; Pouliot, G.; Simon, H.; Sarwar, G.; Pye, H.; Napelenok, S.; Akhtar, F.; Roselle, S., Evaluation of dust and trace metal estimates from the Community Multiscale Air Quality (CMAQ) model version 5.0. *Geoscientific Model Development* **2013,** *6*, 1859-1899.

177. Hu, J.; Chen, J.; Ying, Q.; Zhang, H., One-year simulation of ozone and particulate matter in China using WRF/CMAQ modeling system. *1foldr Import 2019-10-08 Batch 1* **2016**.

178. Language, N. C., The NCAR Command Language (Version 6.3. 0)[Software]. **2016**.

179. Binkowski, F. S.; Roselle, S. J., Models‐3 Community Multiscale Air Quality (CMAQ) model aerosol component 1. Model description. *Journal of geophysical research: Atmospheres* **2003,** *108*, (D6).

180. Hu, J.; Li, X.; Huang, L.; Qi, Y.; Zhang, Q.; Zhao, B.; Wang, S.; Zhang, H., Ensemble prediction of air quality using the WRF/CMAQ model system for health effect studies in China. *Atmospheric Chemistry and Physics* **2017,** *17*, (21), 13103.

181. NCEP FNL Operational Model Global Tropospheric Analyses, continuing from July 1999. In Research Data Archive at the National Center for Atmospheric Research, Computational and Information Systems Laboratory: Boulder, CO, 2000.

182. Liu, S.; Xing, J.; Zhang, H.; Ding, D.; Zhang, F.; Zhao, B.; Sahu, S. K.; Wang, S., Climate-driven trends of biogenic volatile organic compound emissions and their impacts on summertime ozone and secondary organic aerosol in China in the 2050s. *Atmospheric Environment* **2019,** *218*, 117020.

183. Ran, L.; Loughlin, D. H.; Yang, D.; Adelman, Z.; Baek, B. H.; Nolte, C. G., ESP v2.0: enhanced method for exploring emission impacts of future scenarios in the United States – addressing spatial allocation. *Geoscientific Model Development* **2015,** *8*, (6), 1775-1787.

184. Guenther, A.; Jiang, X.; Heald, C.; Sakulyanontvittaya, T.; Duhl, T.; Emmons, L.; Wang, X., The Model of Emissions of Gases and Aerosols from Nature version 2.1 (MEGAN2. 1): an extended and updated framework for modeling biogenic emissions. **2012,** *5*, (6), 1471-1492.

185. Wiedinmyer, C.; Akagi, S.; Yokelson, R.; Emmons, L.; Al-Saadi, J.; Orlando, J.; Soja, A., The Fire INventory from NCAR (FINN)–a high resolution global model to estimate the emissions from open burning. *Geoscientific Model Development Discussions* **2010,** *3*, (4), 2439-2476.

186. Janssens-Maenhout, G.; Pagliari, V.; Guizzardi, D.; Muntean, M., Global emission inventories in the Emission Database for Global Atmospheric Research (EDGAR)–Manual (I). *Gridding: EDGAR emissions distribution on global gridmaps, Publications Office of the European Union, Luxembourg* **2013**.

187. Wang, S.; Xing, J.; Chatani, S.; Hao, J.; Klimont, Z.; Cofala, J.; Amann, M. J. A. E., Verification of anthropogenic emissions of China by satellite and ground observations. **2011,** *45*, (35), 6347-6358.

188. Ding, J.; Mijling, B.; Levelt, P. F. J. A. M. T., Space-based NO x emission estimates over remote regions improved in DECSO. **2017,** *10*, (3), 925-938.

189. Qi, J.; Zheng, B.; Li, M.; Yu, F.; Chen, C.; Liu, F.; Zhou, X.; Yuan, J.; Zhang, Q.; He, K., A high-resolution air pollutants emission inventory in 2013 for the Beijing-Tianjin-Hebei region, China. *Atmospheric Environment* **2017,** *170*, 156-168.

190. Wang, X.; Wang, W.; Yang, L.; Gao, X.; Nie, W.; Yu, Y.; Xu, P.; Zhou, Y.; Wang, Z., The secondary formation of inorganic aerosols in the droplet mode through heterogeneous aqueous reactions under haze conditions. *Atmospheric Environment* **2012,** *63*, 68-76.

191. Lei, Y.; Zhang, Q.; Nielsen, C.; He, K., An inventory of primary air pollutants and CO2 emissions from cement production in China, 1990–2020. *Atmospheric Environment* **2011,** *45*, (1), 147-154.

192. Saikawa, E.; Kim, H.; Zhong, M.; Avramov, A.; Zhao, Y.; Janssens-Maenhout, G.; Jurokawa, J.; Klimont, Z.; Wagner, F.; Naik, V., Comparison of emissions inventories of anthropogenic air pollutants and greenhouse gases in China. *Atmospheric Chemistry and Physics* **2017,** *17*, (10), 6393-6421.

193. Zhao, Y.; Xia, Y.; Zhou, Y., Assessment of a high-resolution NOX emission inventory using satellite observations: A case study of southern Jiangsu, China. *Atmospheric Environment* **2018,** *190*, 135-145.

194. Emery, C.; Tai, E.; Yarwood, G., Enhanced meteorological modeling and performance evaluation for two Texas ozone episodes. *Prepared for the Texas natural resource conservation commission, by ENVIRON International Corporation* **2001**.

195. Kota, S. H.; Guo, H.; Myllyvirta, L.; Hu, J.; Sahu, S. K.; Garaga, R.; Ying, Q.; Gao, A.; Dahiya, S.; Wang, Y.; Zhang, H., Year-long simulation of gaseous and particulate air pollutants in India. *Atmospheric Environment* **2018,** *180*, 244-255.

196. Guo, H.; Chen, K.; Wang, P.; Hu, J.; Ying, Q.; Gao, A.; Zhang, H., Simulation of summer ozone and its sensitivity to emission changes in China. *Atmospheric Pollution Research* **2019,** *10*, (5), 1543-1552.

197. Wang, P.; Guo, H.; Hu, J.; Kota, S. H.; Ying, Q.; Zhang, H., Responses of PM2. 5 and O3 concentrations to changes of meteorology and emissions in China. *Science of the Total Environment* **2019,** *662*, 297-306.

198. USEPA, O. *Guidance on the Use of Models and Other Analyses in Attainment Demonstrations for the 8-hour Ozone NAAQS*; US EPA Report No. EPA-454/R-05-002. Office of Air Quality Planning and Standards, Research Triangle Park, North Carolina, US, 2005.: 2005.

199. Meehl, G. A.; Hu, A.; Santer, B. D.; Xie, S.-P., Contribution of the Interdecadal Pacific Oscillation to twentieth-century global surface temperature trends. *Nature Climate Change* **2016,** *6*, (11), 1005-1008.

200. EPA, U., Guidance on the use of models and other analyses for demonstrating attainment of air quality goals for ozone, PM2. 5, and regional haze. *US Environmental Protection Agency, Office of Air Quality Planning and Standards* **2007**.

201. Wei, W.; Lv, Z. F.; Li, Y.; Wang, L. T.; Cheng, S.; Liu, H., A WRF-Chem model study of the impact of VOCs emission of a huge petro-chemical industrial zone on the summertime ozone in Beijing, China. *Atmospheric Environment* **2018,** *175*, 44-53.

202. Shao, M.; Tang, X.; Zhang, Y.; Li, W., City clusters in China: air and surface water pollution. *Frontiers in Ecology and the Environment* **2006,** *4*, (7), 353-361.

203. Ma, Z.; Xu, J.; Quan, W.; Zhang, Z.; Lin, W.; Xu, X. J. A. C.; Physics, Significant increase of surface ozone at a rural site, north of eastern China. **2016,** *16*, (6), 3969-3977.

204. Bell, M. L.; McDermott, A.; Zeger, S. L.; Samet, J. M.; Dominici, F., Ozone and short-term mortality in 95 US urban communities, 1987-2000. *Jama* **2004,** *292*, (19), 2372-2378.

205. Yan, M.; Liu, Z.; Liu, X.; Duan, H.; Li, T., Meta-analysis of the Chinese studies of the association between ambient ozone and mortality. *Chemosphere* **2013,** *93*, (6), 899-905.

206. Zhang, Y.; Huang, W.; London, S. J.; Song, G.; Chen, G.; Jiang, L.; Zhao, N.; Chen, B.; Kan, H., Ozone and daily mortality in Shanghai, China. *Environmental health perspectives* **2006,** *114*, (8), 1227-1232.

207. Hu, J.; Chen, J.; Ying, Q.; Zhang, H., One-year simulation of ozone and particulate matter in China using WRF/CMAQ modeling system. *Atmospheric Chemistry & Physics* **2016,** *16*, (16), 10333-10350.

208. Mysliwiec, M. J.; Kleeman, M. J., Source apportionment of secondary airborne particulate matter in a polluted atmosphere. *Environmental science & technology* **2002,** *36*, (24), 5376-5384.

209. Hu, J.; Jathar, S.; Zhang, H.; Ying, Q.; Chen, S.-H.; Cappa, C. D.; Kleeman, M. J., Long-term particulate matter modeling for health effect studies in California–Part 2: Concentrations and sources of ultrafine organic aerosols. *Atmospheric Chemistry and Physics* **2017,** *17*, (8), 5379-5391.

210. Qiao, X.; Guo, H.; Wang, P.; Tang, Y.; Ying, Q.; Zhao, X.; Deng, W.; Zhang, H., Fine Particulate Matter and Ozone Pollution in the 18 Cities of the Sichuan Basin in Southwestern China: Model Performance and Characteristics. *Aerosol and Air Quality Research* **2019,** *19*, 2308-2319.

211. Gong, X.; Hong, S.; Jaffe, D. A., Ozone in China: Spatial distribution and leading meteorological factors controlling O3 in 16 Chinese cities. *Aerosol Air Qual. Res* **2018,** *18*, 2287-2300.

212. Wu, Y.; Zhang, S.; Hao, J.; Liu, H.; Wu, X.; Hu, J.; Walsh, M. P.; Wallington, T. J.; Zhang, K. M.; Stevanovic, S., On-road vehicle emissions and their control in China: A review and outlook. *Science of the Total Environment* **2017,** *574*, 332-349.

213. 600/R-10/076F, U. E. P. A. J. E., Integrated science assessment for ozone and related photochemical oxidants. **2013**.

214. Parrish, D. D.; Ennis, C. A. J. A. C.; Physics, Estimating background contributions and US anthropogenic enhancements to maximum ozone concentrations in the northern US. **2019,** *19*, (19), 12587-12605.

215. Lin, M.; Horowitz, L. W.; Payton, R.; Fiore, A. M.; Tonnesen, G. J. A. C.; Physics, US surface ozone trends and extremes from 1980 to 2014: quantifying the roles of rising Asian emissions, domestic controls, wildfires, and climate. **2017,** *17*, (4).

216. Baublitz, C.; Fiore, A. M.; Clifton, O.; Mao, J.; Li, J.; Horowitz, L. W.; Paulot, F.; Correa, G. J. J. A., The sensitivity of Southeast US ozone abundance and production to dry deposition. **2019,** *2019*, A31C-03.

217. Jing, P.; Lu, Z.; Steiner, A. L. J. A. E., The ozone-climate penalty in the Midwestern US. **2017,** *170*, 130-142.

218. Archer, C. L.; Brodie, J. F.; Rauscher, S. A. J. J. o. A. M.; Climatology, Global warming will aggravate ozone pollution in the US Mid-Atlantic. **2019,** *58*, (6), 1267-1278.

219. Parrish, D. D.; Young, L. M.; Newman, M. H.; Aikin, K. C.; Ryerson, T. B. J. J. o. G. R. A., Ozone design values in Southern California's air basins: Temporal evolution and US background contribution. **2017,** *122*, (20), 11,166-11,182.

220. Simon, H.; Reff, A.; Wells, B.; Xing, J.; Frank, N. J. E. s.; technology, Ozone trends across the United States over a period of decreasing NOx and VOC emissions. **2015,** *49*, (1), 186-195.

221. Fiore, A. M.; Horowitz, L. W.; Purves, D. W.; Levy, H.; Evans, M. J.; Wang, Y.; Li, Q.; Yantosca, R. M. J. J. o. G. R. A., Evaluating the contribution of changes in isoprene emissions to surface ozone trends over the eastern United States. **2005,** *110*, (D12).

222. Cao, T.; Lin, C. J.; Yang, W.; Huang, S.; Chu, H.-w.; Ho, T. C. In *Application of ABaCAS-TX for ozone non-attainment in Southeast Texas*, 16th Annual CMAS Conference, Chapel Hill, NC, USA, 2017; 2017; pp 23-25.

223. Zhang, Y.; Wang, Y. J. P. o. t. N. A. o. S., Climate-driven ground-level ozone extreme in the fall over the Southeast United States. **2016,** *113*, (36), 10025-10030.

224. Liu, B.; Xue, Z.; Zhu, X.; Jia, C. J. E. p., Long-term trends (1990–2014), health risks, and sources of atmospheric polycyclic aromatic hydrocarbons (PAHs) in the US. **2017,** *220*, 1171-1179.

225. McDonald, B. C.; McKeen, S. A.; Cui, Y. Y.; Ahmadov, R.; Kim, S.-W.; Frost, G. J.; Pollack, I. B.; Peischl, J.; Ryerson, T. B.; Holloway, J. S. J. E. s.; technology, Modeling ozone in the eastern US using a fuel-based mobile source emissions inventory. **2018,** *52*, (13), 7360-7370.

226. Lefohn, A. S.; Malley, C. S.; Simon, H.; Wells, B.; Xu, X.; Zhang, L.; Wang, T. J. A. e., Responses of human health and vegetation exposure metrics to changes in ozone concentration distributions in the European Union, United States, and China. **2017,** *152*, 123-145.

227. Yari, A. R.; Goudarzi, G.; Geravandi, S.; Dobaradaran, S.; Yousefi, F.; Idani, E.; Jamshidi, F.; Shirali, S.; Khishdost, M.; Mohammadi, M. J. J. T. r., Study of ground-level ozone and its health risk assessment in residents in Ahvaz City, Iran during 2013. **2016,** *35*, (3-4), 201-206.

228. Bylin, G.; Cotgreave, I.; Gustafsson, L.; Nyberg, F.; Pershagen, G.; Sundell, J.; Victorin, K.; Zuber, A. J. S. J. o. W., Environment; Health, Health risk evaluation of ozone. **1996**, 1-102.

229. Lelieveld, J.; Evans, J. S.; Fnais, M.; Giannadaki, D.; Pozzer, A. J. N., The contribution of outdoor air pollution sources to premature mortality on a global scale. **2015,** *525*, (7569), 367-371.

230. Anenberg, S. C.; Henze, D. K.; Tinney, V.; Kinney, P. L.; Raich, W.; Fann, N.; Malley, C. S.; Roman, H.; Lamsal, L.; Duncan, B. J. E. h. p., Estimates of the global burden of ambient PM 2.5, ozone, and NO 2 on asthma incidence and emergency room visits. **2018,** *126*, (10), 107004.

231. Maji, K. J.; Ye, W.-F.; Arora, M.; Nagendra, S. S. J. E. p., Ozone pollution in Chinese cities: Assessment of seasonal variation, health effects and economic burden. **2019,** *247*, 792-801.

232. Feng, Z.; De Marco, A.; Anav, A.; Gualtieri, M.; Sicard, P.; Tian, H.; Fornasier, F.; Tao, F.; Guo, A.; Paoletti, E. J. E. i., Economic losses due to ozone impacts on human health, forest productivity and crop yield across China. **2019,** *131*, 104966.

233. Yim, S. H. L.; Wang, M.; Gu, Y.; Yang, Y.; Dong, G.; Li, Q. J. J. o. G. R. A., Effect of urbanization on ozone and resultant health effects in the Pearl River Delta region of China. **2019,** *124*, (21), 11568-11579.

234. Yin, P.; Chen, R.; Wang, L.; Meng, X.; Liu, C.; Niu, Y.; Lin, Z.; Liu, Y.; Liu, J.; Qi, J., Ambient ozone pollution and daily mortality: a nationwide study in 272 Chinese cities. *Environmental health perspectives* **2017,** *125*, (11), 117006.

235. Berman, J. D.; Fann, N.; Hollingsworth, J. W.; Pinkerton, K. E.; Rom, W. N.; Szema, A. M.; Breysse, P. N.; White, R. H.; Curriero, F. C., Health benefits from large-scale ozone reduction in the United States. *Environmental health perspectives* **2012,** *120*, (10), 1404-1410.

236. Bell, M. L.; Goldberg, R.; Hogrefe, C.; Kinney, P. L.; Knowlton, K.; Lynn, B.; Rosenthal, J.; Rosenzweig, C.; Patz, J. A., Climate change, ambient ozone, and health in 50 US cities. *Climatic Change* **2007,** *82*, (1-2), 61-76.

237. Jerrett, M.; Burnett, R. T.; Pope III, C. A.; Ito, K.; Thurston, G.; Krewski, D.; Shi, Y.; Calle, E.; Thun, M. J. N. E. J. o. M., Long-term ozone exposure and mortality. **2009,** *360*, (11), 1085-1095.

238. Bates, D. V. J. E., Ambient ozone and mortality. **2005,** *16*, (4), 427-429.

239. Anderson, H. R.; Atkinson, R. W.; Peacock, J.; Marston, L.; Konstantinou, K.; Organization, W. H. *Meta-analysis of time-series studies and panel studies of particulate matter (PM) and ozone (O3): report of a WHO task group*; Copenhagen: WHO Regional Office for Europe: 2004.

240. Xiang, J.; Weschler, C. J.; Zhang, J.; Zhang, L.; Sun, Z.; Duan, X.; Zhang, Y. J. I. a., Ozone in urban China: Impact on mortalities and approaches for establishing indoor guideline concentrations. **2019,** *29*, (4), 604-615.

241. Yan, M.; Liu, Z.; Liu, X.; Duan, H.; Li, T. J. C., Meta-analysis of the Chinese studies of the association between ambient ozone and mortality. **2013,** *93*, (6), 899-905.

242. Gu, Y.; Wong, T.; Law, C.; Dong, G.; Ho, K.; Yang, Y.; Yim, S., Impacts of sectoral emissions in China and the implications: air quality, public health, crop production, and economic costs. *Environmental Research Letters* **2018,** *13*, (8), 084008.

243. Gu, Y.; Yim, S. H. L., *The air quality and health impacts of domestic trans-boundary pollution in various regions of China*. 2016; Vol. 97.

244. Maji, K. J.; Ye, W.-F.; Arora, M.; Nagendra, S. S., Ozone pollution in Chinese cities: Assessment of seasonal variation, health effects and economic burden. *Environmental pollution* **2019,** *247*, 792-801.

245. Anenberg, S. C.; Horowitz, L. W.; Tong, D. Q.; West, J. J., An estimate of the global burden of anthropogenic ozone and fine particulate matter on premature human mortality using atmospheric modeling. *Environmental health perspectives* **2010,** *118*, (9), 1189-1195.

246. Malley, C. S.; Henze, D. K.; Kuylenstierna, J. C.; Vallack, H. W.; Davila, Y.; Anenberg, S. C.; Turner, M. C.; Ashmore, M. R., Updated global estimates of respiratory mortality in adults ≥ 30 years of age attributable to long-term ozone exposure. *Environmental health perspectives* **2017,** *125*, (8), 087021.

247. Xiang, J.; Weschler, C. J.; Zhang, J.; Zhang, L.; Sun, Z.; Duan, X.; Zhang, Y., Ozone in urban China: Impact on mortalities and approaches for establishing indoor guideline concentrations. *Indoor air* **2019,** *29*, (4), 604-615.

VITA

Kaiyu Chen was born in 1991 in Fujian Province, People's Republic of China. He graduated with a Bachelor of Science in Environmental Engineering in 2014 from China University of Mining and Technology, Beijing, China. He received his Master of Science in Environmental Engineering in 2017 from China University of Mining and Technology, Beijing, China and his thesis was entitled "*Tracking the traces of invasive plant species in China*".